

1980

Fatigue tests of curved box girder assemblies, April 1980 (DOT-FH-11.8198.4) (80-20)

R. P. Batcheler

J. H. Daniels

Follow this and additional works at: <http://preserve.lehigh.edu/engr-civil-environmental-fritz-lab-reports>

Recommended Citation

Batcheler, R. P. and Daniels, J. H., "Fatigue tests of curved box girder assemblies, April 1980 (DOT-FH-11.8198.4) (80-20)" (1980). *Fritz Laboratory Reports*. Paper 480.
<http://preserve.lehigh.edu/engr-civil-environmental-fritz-lab-reports/480>

This Technical Report is brought to you for free and open access by the Civil and Environmental Engineering at Lehigh Preserve. It has been accepted for inclusion in Fritz Laboratory Reports by an authorized administrator of Lehigh Preserve. For more information, please contact preserve@lehigh.edu.

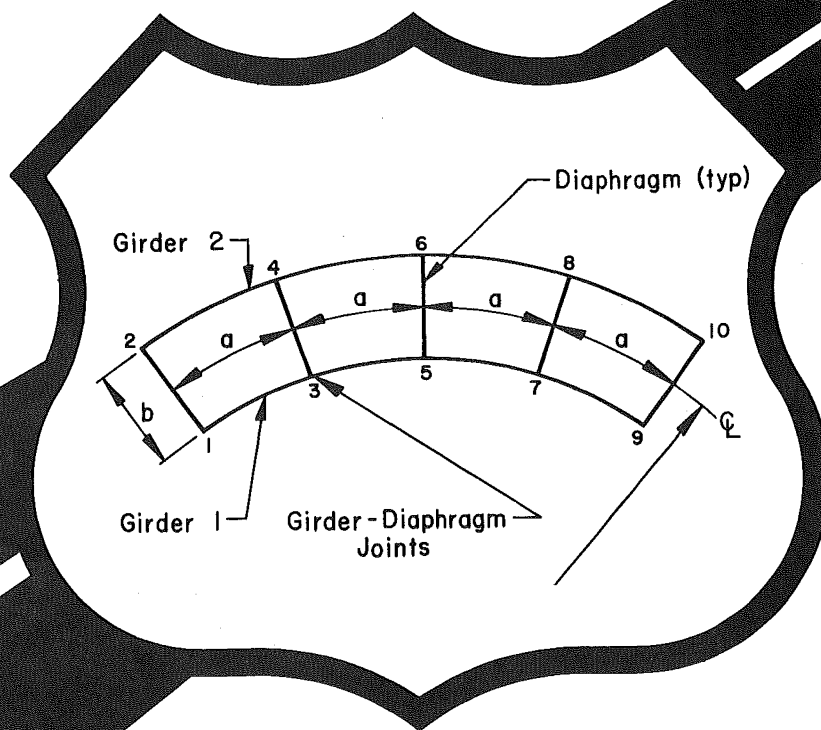
FATIGUE OF CURVED STEEL BRIDGE ELEMENTS

FRITZ ENGINEERING
LABORATORY LIBRARY

Fatigue Tests of Curved Box Girders

April 1980

Interim Report



Document is available to the public through
the National Technical Information Service,
Springfield, Virginia 22161

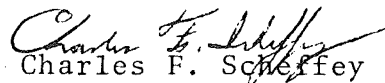


Prepared for
FEDERAL HIGHWAY ADMINISTRATION
Offices of Research & Development
Structures & Applied Mechanics Division
Washington, D.C. 20590

FOREWORD

Horizontally curved steel plate and box girders are being used more frequently for highway structures, sometimes because of increased economy, and because of their esthetic appearance. The design of curved girders differs from that of straight girders in that torsional effects, including nonuniform torsion, must be considered. The resulting use of lateral bracing between curved plate girders and internal bracing and stiffening of curved box girders gives rise to complicated states of stress and to details which can be sensitive to repetitive loads. This situation prompted the FHWA to sponsor this research, the primary objective of which is to establish fatigue design guidelines for curved girder highway bridges in the form of simplified equations or charts.

This report is one in a series of eight on the results of the research and is being distributed to the Washington and field offices of the Federal Highway Administration, State highway agencies, and interested researchers.



Charles F. Schreffey
Director, Office of Research
Federal Highway Administration

NOTICE

This document is disseminated under the sponsorship of the Department of Transportation in the interest of information exchange. The United States Government assumes no liability for its contents or use thereof. The contents of this report reflect the views of the contractor, who is responsible for the accuracy of the data presented herein. The contents do not necessarily reflect the official views or policy of the Department of Transportation. This report does not constitute a standard, specification, or regulation.

The United States Government does not endorse products or manufacturers. Trade or manufacturers' names appear herein only because they are considered essential to the object of this document.

1. Report No. FHWA-RD-79-134		2. Government Accession No.		3. Recipient's Catalog No.	
4. Title and Subtitle FATIGUE OF CURVED STEEL BRIDGE ELEMENTS - Fatigue Tests of Curved Box Girders				5. Report Date April 1980	
				6. Performing Organization Code	
7. Author(s) J. Hartley Daniels and R. P. Batcheler				8. Performing Organization Report No. Fritz Engineering Lab Report No. 398.4	
9. Performing Organization Name and Address Fritz Engineering Laboratory, Bldg. #13 Lehigh University Bethlehem, PA 18015				10. Work Unit No. (TRAIS) 35F2-052	
				11. Contract or Grant No. DOT-FH-11-8198	
12. Sponsoring Agency Name and Address U.S. Department of Transportation Federal Highway Administration Washington, DC 20590				13. Type of Report and Period Covered Interim Jan. 1977 - Jan. 1978	
				14. Sponsoring Agency Code	
15. Supplementary Notes FHWA Contract Manager Jerar Nishanian, HRS-11					
16. Abstract <p>Eight types of welded details representing AASHTO Categories B, C, D, and E are selected for placement on three full-scale curved steel box girders. The fatigue behavior of the welded details is monitored while subjecting the box girders to approximately two million constant amplitude load cycles.</p> <p>Primary fatigue crack growth due to the longitudinal normal stress ranges caused by bending and warping torsion was observed. Secondary fatigue crack growth was also observed and was due to transverse forces in the diaphragms and the introduction of out-of-plane forces and displacements into the webs and flanges.</p> <p>The observation of primary fatigue crack growth at the welded details indicates that their fatigue behavior is adequately described by the present AASHTO Categories B, C, D, and E which are applicable to straight girders.</p> <p>The observed patterns of secondary fatigue crack growth are described in detail. Several modifications of the assemblies to improve their resistance to secondary fatigue crack growth were made and their effectiveness is described.</p> <p>The report closes with an itemized summary of significant conclusions and recommendations for further study.</p>					
17. Key Words Bridges (structures), design, fatigue, girder bridges, structural engineering, testing, torsion, welding.			18. Distribution Statement Document is available to the public through the National Technical Information Service, Springfield, VA 22161		
19. Security Classif. (of this report) Unclassified		20. Security Classif. (of this page) Unclassified		21. No. of Pages 133	22. Price

ACKNOWLEDGMENTS

The investigation reported herein was conducted at Fritz Engineering Laboratory, Lehigh University, Bethlehem, Pennsylvania. Dr. Lynn S. Beedle is the Director of Fritz Laboratory and Dr. David A. VanHorn is the Chairman of the Department of Civil Engineering.

The work was a part of Fritz Laboratory Research Project 398, "Fatigue of Curved Steel Bridge Elements" sponsored by the Federal Highway Administration (FHWA) of the United States Department of Transportation. The FHWA Project Manager is Mr. Jerar Nishanian. The Advisory Panel members are Mr. A. P. Cole, Dr. Charles G. Culver, Mr. Richard S. Fountain, Mr. Gerald Fox, Dr. Theodore V. Galambos, Mr. Andrew Lally, Mr. Frank D. Sears, and Dr. Ivan M. Viest.

The following members of the faculty and staff of Lehigh University made major contributions in the conduct of this work: Dr. John W. Fisher, Dr. B. T. Yen, Dr. R. G. Slutter and W. C. Herbein.

Mr. Kenneth Harpel and Mr. Robert Dales assisted in executing the test program. Ms. Shirley Matlock typed the manuscript. Ms. Mary Snyder and Mr. Marc Marzullo assisted with organization of the manuscript. The figures were prepared by Mr. John Gera and his staff. Mr. R. N. Sopko provided the photographs.

TABLE OF CONTENTS

	<u>Page</u>
1. INTRODUCTION	1
1.1 Background	1
1.2 Objectives and Scope	2
1.3 Research Approach	2
2. DESIGN AND FABRICATION OF BOX GIRDERS	11
2.1 Analysis and Design of Box Girders	11
2.2 Design of Welded Details	13
2.3 Fabrication of Box Girders	18
3. ERECTION AND INSTRUMENTATION OF BOX GIRDERS	21
3.1 Erection	21
3.2 Instrumentation	31
4. INITIAL STATIC AND CYCLIC LOAD TESTS	42
4.1 Initial Static Load Test	42
4.2 Initial Cyclic Load Test	50
5. FATIGUE TESTING	60
5.1 General Procedure	60
5.2 Crack Detection and Repair	64
6. RESULTS OF FATIGUE TESTS	66
6.1 Primary Fatigue Crack Growth	66
6.2 Secondary Fatigue Crack Growth	70
7. DISCUSSION OF TEST RESULTS	95
7.1 Primary Fatigue Crack Growth	95
7.1.1 Type I ^{ca} and I ^{cb} Details	95
7.1.2 Type II ^{ca} Details ^{cb}	97
7.1.3 Type III ^{ca} and III ^{cb} Details	97
7.1.4 Type IV ^{ca} and IV ^{cb} Details	101
7.1.5 Type V ^{ca} Details ^{cb}	102
7.1.6 Type VI ^{ca} and VI ^{cb} Details	104
7.1.7 Type VII ^{ca} and VII ^{cb} Details	104
7.1.8 Type VIII ^{ca} Details ^{cb}	108
7.2 Secondary Fatigue Crack Growth	108

8. SUMMARY AND CONCLUSIONS	111
9. RECOMMENDATIONS FOR FURTHER STUDY	112
10. REFERENCES	113
APPENDIX A: STATEMENT OF WORK	115
APPENDIX B: LIST OF REPORTS PRODUCED UNDER DOT-FH-11-8198	118
APPENDIX C: FATIGUE CRACK REPAIR	119

LIST OF ABBREVIATIONS AND SYMBOLS

- a,aa,b,bb,etc. = designations used to identify detail locations (see Figs. 44-46)
- a,b,c,d = arbitrary constants used to simplify dimensioning in Table 1
- n = exponent in fatigue life equation for given material and environmental conditions (see Appendix C)
- A = coefficient in fatigue life equation reflecting effects of detail geometry, material properties, expected initial flaw sizes, etc. (see Appendix C)
- CA = clip angle (see Table 1)
- F = flange (see Table 1)
- LS = longitudinal stiffener (see Table 1)
- L = centerline span length of box girder assembly (feet)
- N = number of cycles to a specified crack condition (millions of cycles)
- S_r = nominal stress range (ksi)
- TS = transverse stiffener (see Table 1)
- X = position of a point along the length of the box girder assembly expressed with reference to the centerline distance (feet)
- W = web (see Table 1)
- $I_{ca}, I_{cb}, II_c,$
etc. = designations used to identify detail types and subtypes (see Table 1)
- Joints 1,2,3,
etc. = designation used to identify web-diaphragm joints and locations of Group 1 details (see Fig. 1)

- F = friction force (kips) at faying surfaces of bolted friction connections (see Appendix C)
- P = total force (kips) acting to close the fatigue crack (see Appendix C)
- α = static coefficient of friction (see Appendix C)
- P_b = total force (kips) in the bolt (see Appendix C)
- ΔK = the range of the stress intensity (ksi/in)
- p = the uniform crack surface traction (ksi) acting to close the fatigue crack (see Appendix C)
- a = crack length (see Appendix C) (inches)
- b, c = variables describing the location of the high-strength bolts

U.S. Customary-SI Conversion Factors

To convert	To	Multiply by
inches (in)	millimeters (mm)	25.40
inches (in)	centimeters (cm)	2.540
inches (in)	meters (m)	0.0254
feet (ft)	meters (m)	0.305
miles (miles)	kilometers (km)	1.61
yards (yd)	meters (m)	0.91
square inches (sq in)	square centimeters (cm ²)	6.45
square feet (sq ft)	square meters (m ²)	0.093
square yards (sq yd)	square meters (m ²)	0.836
acres (acre)	square meters (m ²)	4047
square miles (sq miles)	square kilometers (km ²)	2.59
cubic inches (cu in)	cubic centimeters (cm ³)	16.4
cubic feet (cu ft)	cubic meters (m ³)	0.028
cubic yards (cu yd)	cubic meters (m ³)	0.765
pounds (lb)	kilograms (kg)	0.453
tons (ton)	kilograms (kg)	907.2
one pound force (lbf)	newtons (N)	4.45
one kilogram force (kgf)	newtons (N)	9.81
pounds per square foot (psf)	newtons per square meter (N/m ²)	47.9
pounds per square inch (psi)	kilonewtons per square meter (kN/m ²)	6.9
gallons (gal)	cubic meters (m ³)	0.0038
acre-feet (acre-ft)	cubic meters (m ³)	1233
gallons per minute (gal/min)	cubic meters per minute (m ³ /min)	0.0038
newtons per square meter (N/m ²)	pascals (Pa)	1.00

1. INTRODUCTION

1.1 Background

The increased utilization of horizontally curved steel girders in highway bridges has prompted the initiation of several research projects on curved girder bridges, (1,2,3,4,5,6) The research has been aimed at producing expanded design guidelines or specifications for curved girders.

In 1969 the Federal Highway Administration (FHWA) of the U.S. Department of Transportation (U.S. DOT), with the sponsorship of 25 participating state highway departments, commenced a large research project on curved girder bridges. (7) The project involved four universities (Carnegie-Mellon, Pennsylvania, Rhode Island, and Syracuse) and was commonly referred to as the CURT (Consortium of University Research Teams) Project. All of the work was directed towards the development of specific curved steel girder design guidelines for inclusion in the AASHTO (American Association of State Highway and Transportation Officials) bridge design specifications. The curved girder studies included both open (plate girder) and closed (box girder) cross sections. The CURT program did not include a study of the fatigue behavior of horizontally curved steel bridges.

It has long been recognized that fatigue problems in steel bridges are most probable at details associated with bolted and welded connections in tensile stress range regions. Straight girder research has shown that welded details are more fatigue sensitive than bolted details. Modern bridge structures rely heavily on welded connections in the construction of main members and for securing attachments such as stiffeners and gusset plates.

The research reported herein is part of a multiphase investigation of curved girder fatigue at Lehigh University entitled "Fatigue of Curved Steel Bridge Elements", and is sponsored by the FHWA. This investigation is broken down into five tasks as shown in Appendix A.

1.2 Objectives and Scope

This report presents the results of constant amplitude fatigue tests of three large-scale, horizontally curved box girders. The fatigue tests were undertaken as part of Task 3 which is described in Appendix A. A list of all project reports is given in Appendix B. A discussion of the methods used to arrest fatigue crack growth during the fatigue tests, and the results obtained are presented in Appendix C.

The objectives of the research reported herein are: (1) to establish the fatigue behavior of welded details on horizontally curved steel box girder bridges, and (2) to compare the fatigue behavior of curved steel box girders with straight girder performance to determine if revisions to the current AASHTO bridge specifications are required.

1.3 Research Approach

As noted in Art. 1.1, this investigation centers upon the fatigue behavior of welded details on horizontally curved box girder bridges. The welded details shown in Table 1 were chosen for experimental study.⁽⁸⁾ In light of the number of details to be tested and the desired test replication, three large-scale, horizontally curved box girders were designed and fabricated. These girders provide stress and deflection conditions typical of actual curved box girder bridges at the details under study.

The three curved box girders are shown in Figs. 1 through 4. Each test girder consists of two curved web plates welded to the bottom flange. A heavy steel top flange is bolted to the webs to simulate the composite concrete deck typically used in highway bridges. Five diaphragms are spaced equally along the length of the girders as shown in Fig. 1. The three girders differ primarily in the type of diaphragm used at the quarter- and mid-points. The three types of interior diaphragms used in box girders 1, 2, and 3 are shown in Figs. 2, 3, and 4, respectively.

Each test girder was subjected to approximately 2 million constant amplitude load cycles by hydraulic jack loads positioned directly over the inner (nearest the center of curvature) web at the quarter-point diaphragms (Fig. 1).

Table 1 Summary of Welded Details under Study

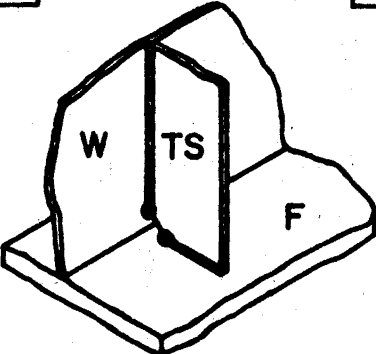
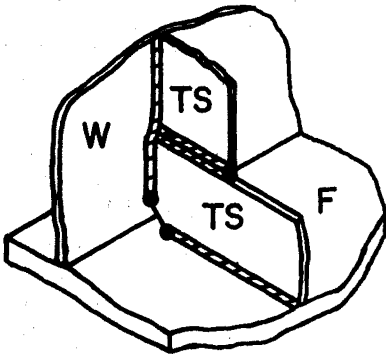
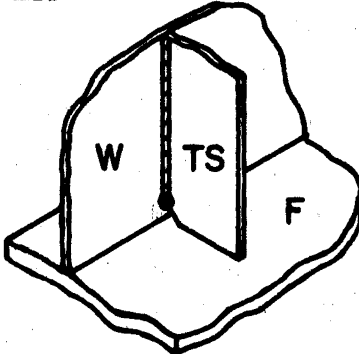
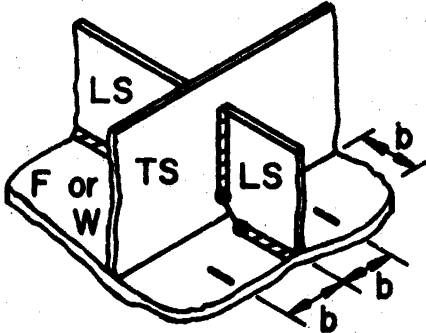
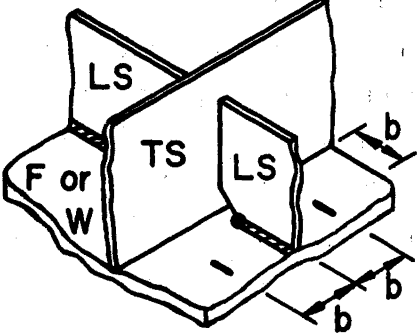
<p>I_{ca}</p> 	<p>C 13</p>	<p>I_{cb}</p> 	<p>C 13</p>
<p>II_c</p> 	<p>C 13</p>		
<p>III_{ca}</p> 	<p>C-D 13-10</p>	<p>III_{cb}</p> 	<p>E 8</p>

Table 1 (Continued)

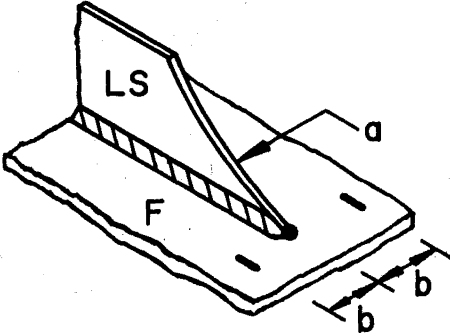
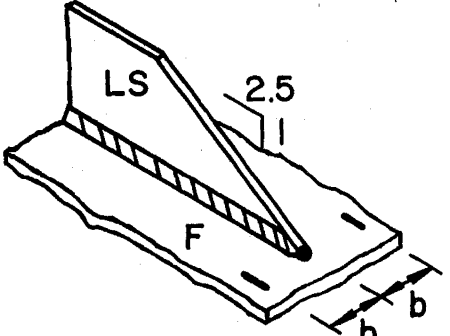
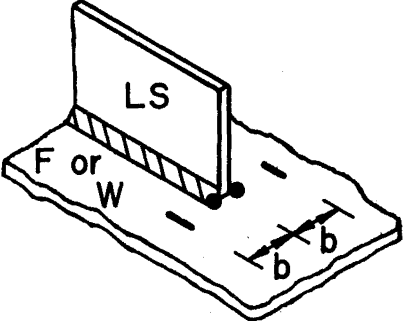
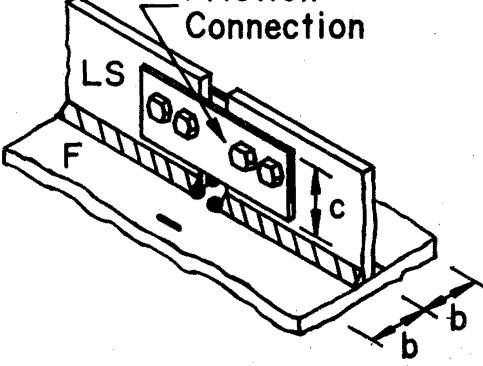
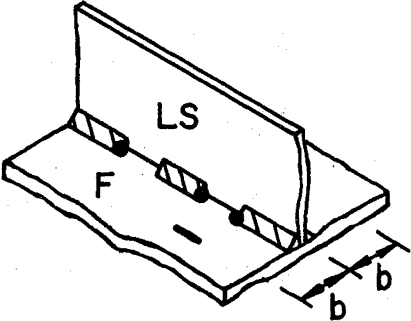
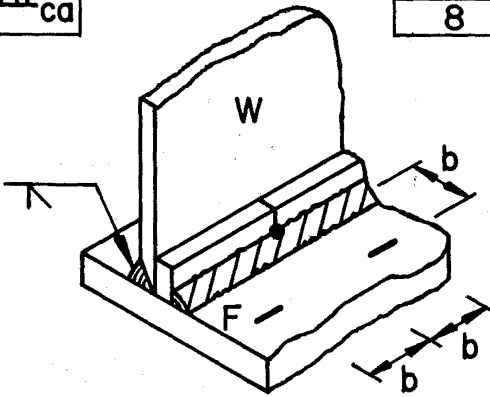
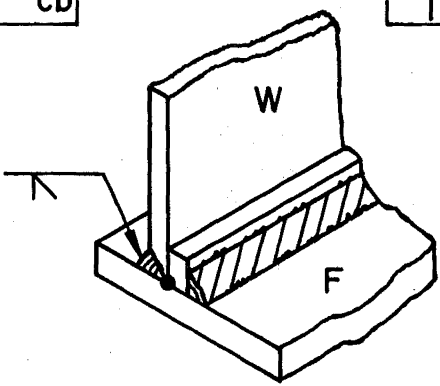
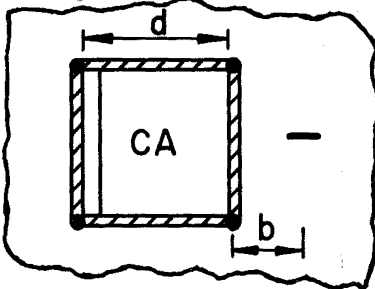
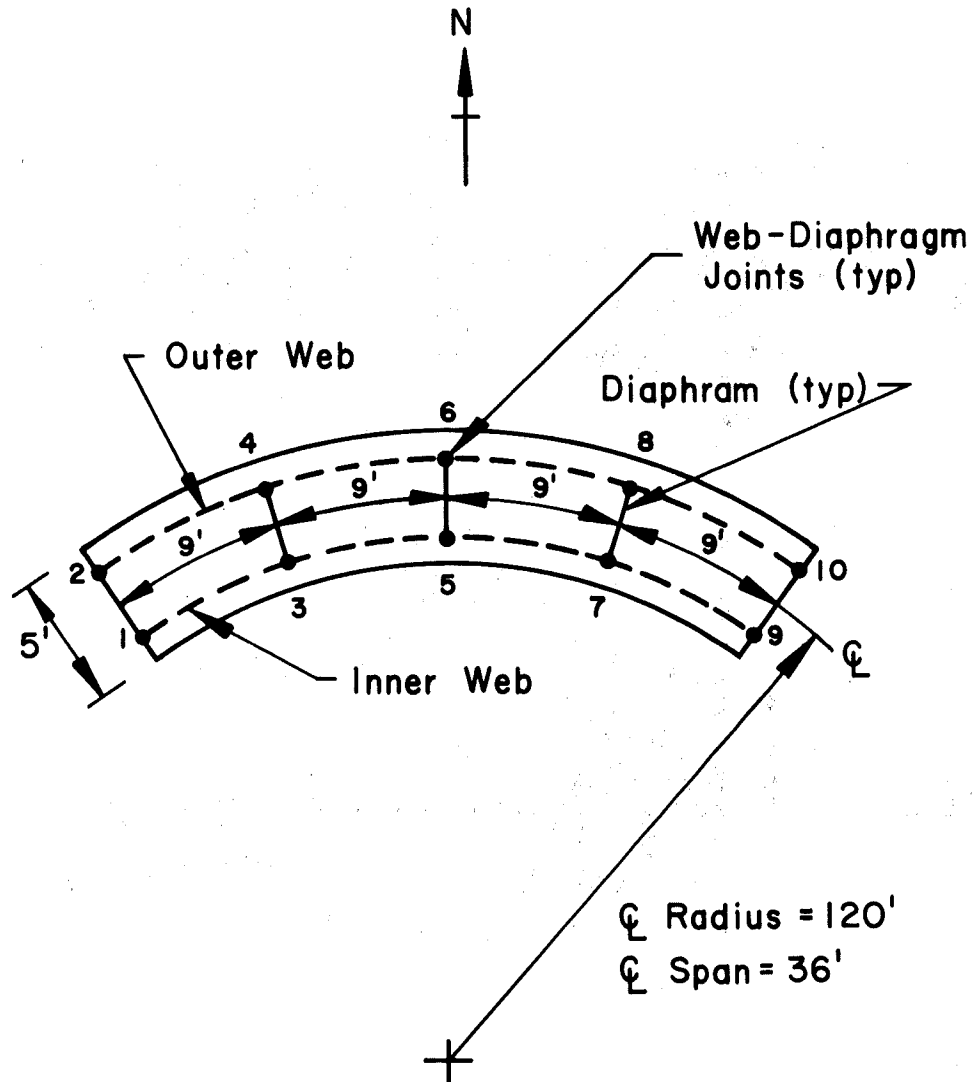
IV_{ca}	$\frac{C}{13}$	IV_{cb}	$\frac{C}{13}$
			
V_c	$\frac{E}{8}$		
			
VI_{ca}	$\frac{C-D}{13-10}$	VI_{cb}	$\frac{C-D}{13-10}$
			

Table 1 (Continued)

<div style="display: flex; justify-content: space-between;"> VII_{ca} <table border="1" style="border-collapse: collapse;"> <tr><td style="text-align: center;">E</td></tr> <tr><td style="text-align: center;">8</td></tr> </table> </div> 	E	8	<div style="display: flex; justify-content: space-between;"> VII_{cb} <table border="1" style="border-collapse: collapse;"> <tr><td style="text-align: center;">B</td></tr> <tr><td style="text-align: center;">18</td></tr> </table> </div> 	B	18						
E											
8											
B											
18											
<div style="display: flex; justify-content: space-between;"> VIII_c <table border="1" style="border-collapse: collapse;"> <tr><td style="text-align: center;">D</td></tr> <tr><td style="text-align: center;">10</td></tr> </table> </div> 	D	10									
D											
10											
<table style="width: 100%; border-collapse: collapse;"> <tr> <td style="width: 50%; vertical-align: top;"> <p>W - Web</p> <p>F - Flange</p> <p>TS - Transverse Stiffener</p> <p>LS - Longitudinal Stiffener</p> <p>CA - Clip Angle</p> <p>— Linear Strain Gage</p> </td> <td style="width: 50%; vertical-align: top;"> <p>• Predicted Crack Location</p> <p style="text-align: right;">inches</p> <table style="width: 100%; border-collapse: collapse;"> <tr> <td style="width: 100px;">a</td> <td style="text-align: right;">6</td> </tr> <tr> <td>b</td> <td style="text-align: right;">3</td> </tr> <tr> <td>c</td> <td style="text-align: right;">2</td> </tr> <tr> <td>d</td> <td style="text-align: right;">4</td> </tr> </table> </td> </tr> </table>		<p>W - Web</p> <p>F - Flange</p> <p>TS - Transverse Stiffener</p> <p>LS - Longitudinal Stiffener</p> <p>CA - Clip Angle</p> <p>— Linear Strain Gage</p>	<p>• Predicted Crack Location</p> <p style="text-align: right;">inches</p> <table style="width: 100%; border-collapse: collapse;"> <tr> <td style="width: 100px;">a</td> <td style="text-align: right;">6</td> </tr> <tr> <td>b</td> <td style="text-align: right;">3</td> </tr> <tr> <td>c</td> <td style="text-align: right;">2</td> </tr> <tr> <td>d</td> <td style="text-align: right;">4</td> </tr> </table>	a	6	b	3	c	2	d	4
<p>W - Web</p> <p>F - Flange</p> <p>TS - Transverse Stiffener</p> <p>LS - Longitudinal Stiffener</p> <p>CA - Clip Angle</p> <p>— Linear Strain Gage</p>	<p>• Predicted Crack Location</p> <p style="text-align: right;">inches</p> <table style="width: 100%; border-collapse: collapse;"> <tr> <td style="width: 100px;">a</td> <td style="text-align: right;">6</td> </tr> <tr> <td>b</td> <td style="text-align: right;">3</td> </tr> <tr> <td>c</td> <td style="text-align: right;">2</td> </tr> <tr> <td>d</td> <td style="text-align: right;">4</td> </tr> </table>	a	6	b	3	c	2	d	4		
a	6										
b	3										
c	2										
d	4										



Load Positioned Over Joints 3 & 7

Fig. 1 Schematic Plan View of Typical Curved Box Girder

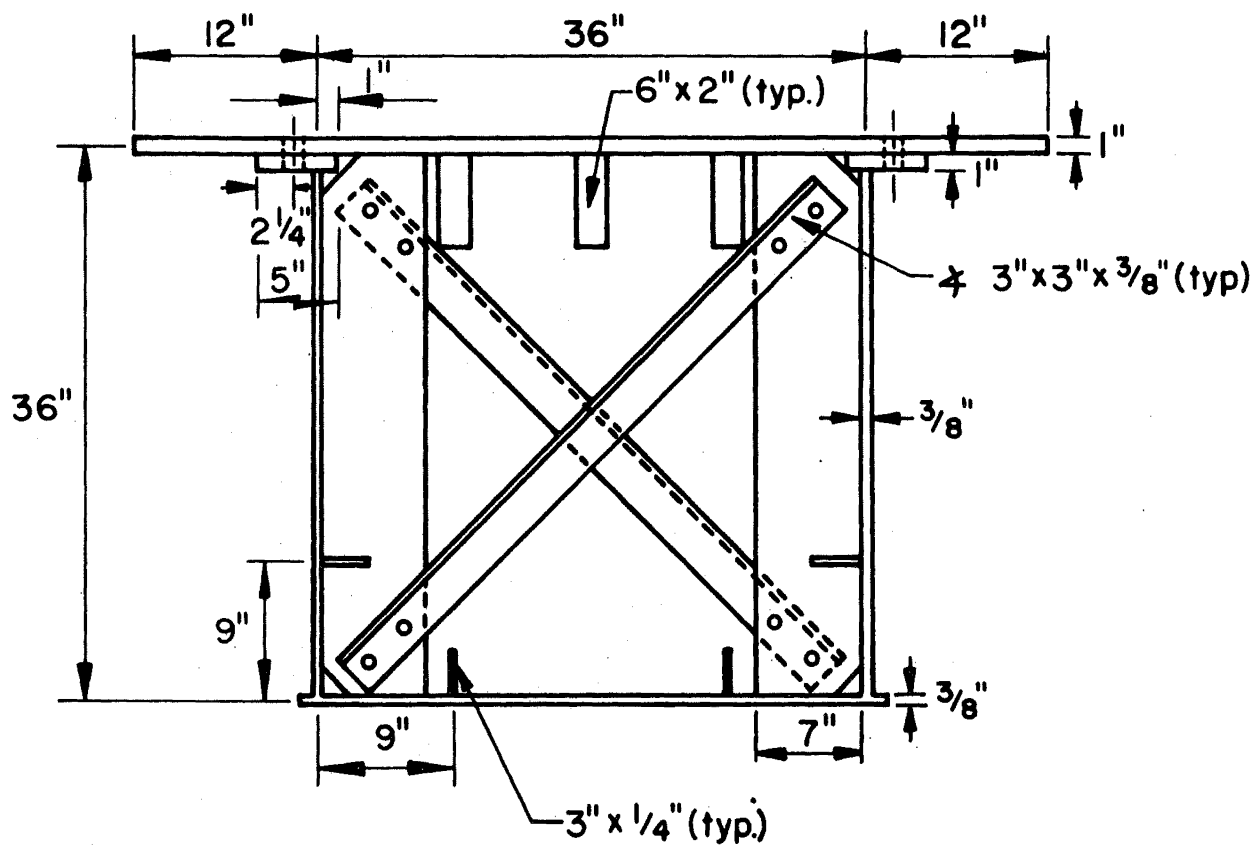


Fig. 2 Box Girder 1
 Cross Section at Interior Diaphragms

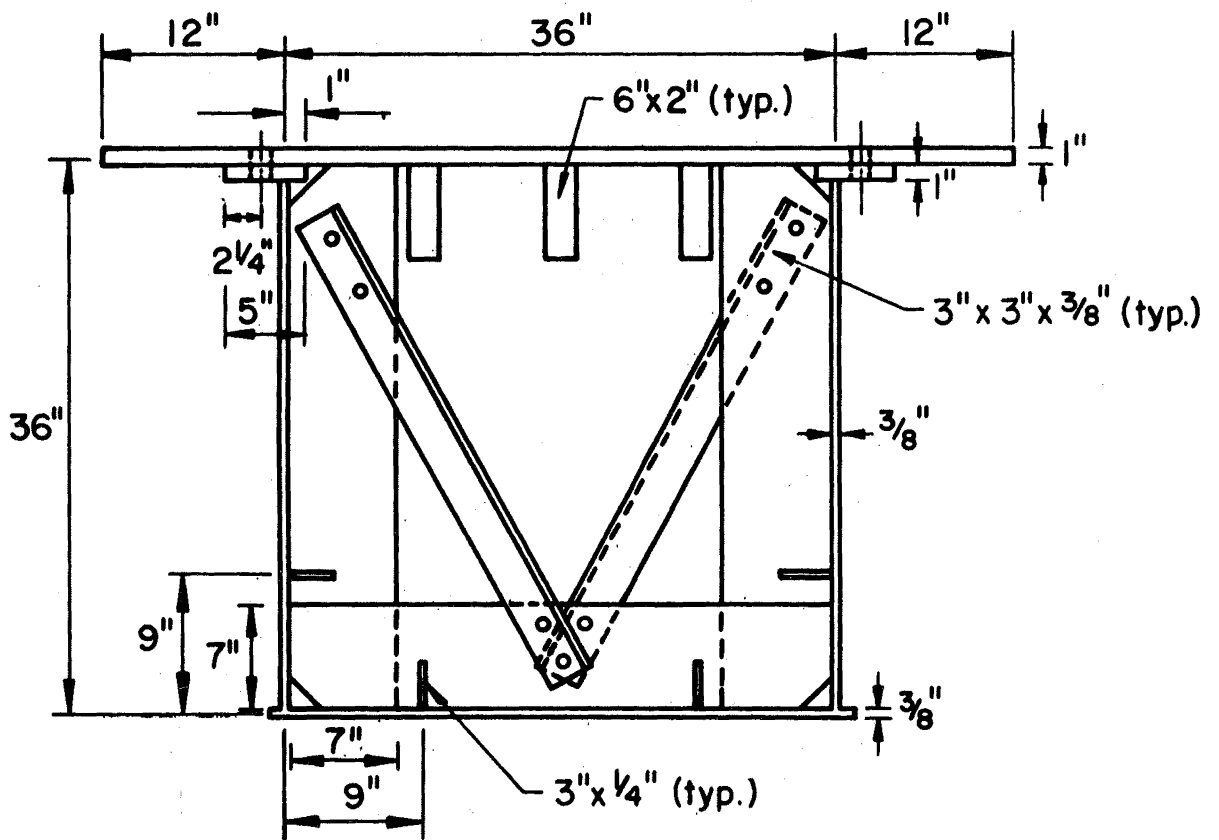


Fig. 3 Box Girder 2
Cross Section at Interior Diaphragms

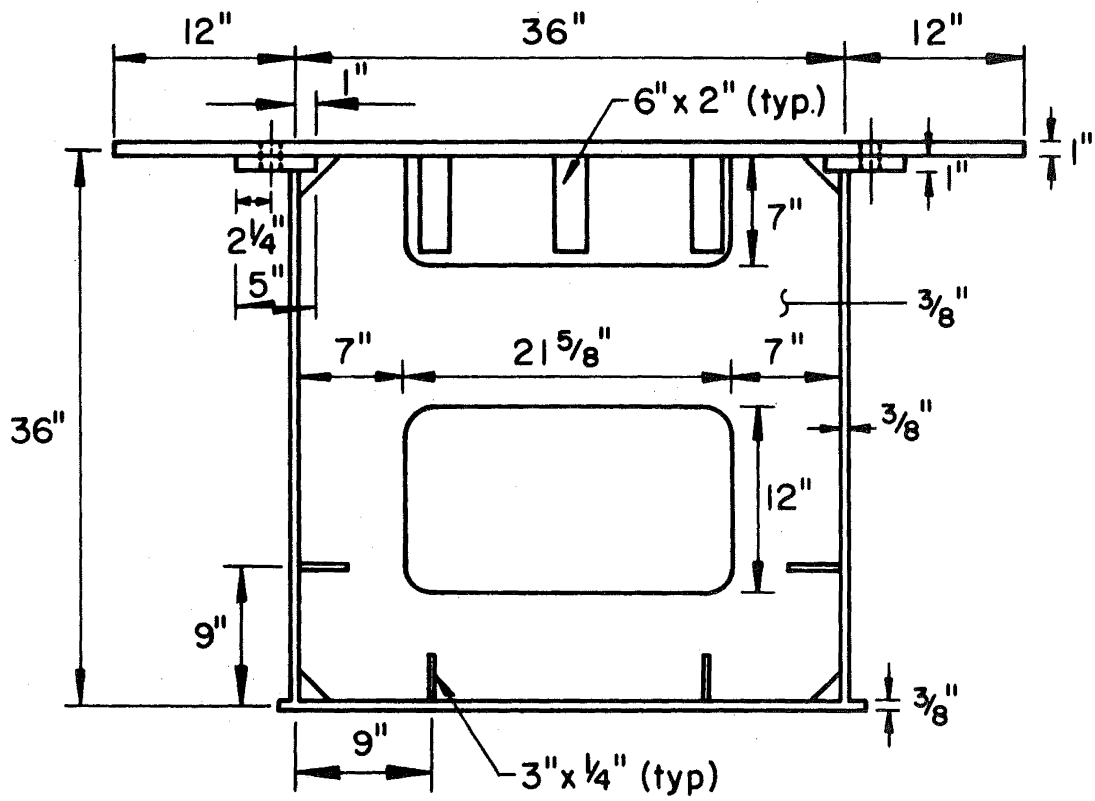


Fig. 4 Box Girder 3
 Cross Section at Interior Diaphragms

Fatigue crack growth was monitored by periodic inspection of the box girders. Records of visible and through-thickness cracks were maintained. The stress ranges (maximum stress minus minimum stress) at all details were recorded using electrical resistance strain gages and a 12-channel ultraviolet recording oscillograph.

Fatigue crack growth occurred at a number of locations on each girder. The observed fatigue crack growth can be classified into two main types, primary and secondary. Primary fatigue crack growth is due to the longitudinal normal stress range caused by bending and warping torsion. Secondary fatigue crack growth usually occurs at the interior diaphragms and is due to the introduction of out-of-plane forces into the web and other displacement-induced effects at the diaphragms.

The results of the fatigue tests are compared with the results of previous fatigue tests of straight girders and the current AASHTO fatigue provisions to determine their applicability to horizontally curved box girder bridges.

2. DESIGN AND FABRICATION OF BOX GIRDERS

2.1 Analysis and Design of Box Girders

A thorough description of the analysis and design of the curved box girders is provided in Ref. 8. A brief summary is given here.

Since the research effort is centered on fatigue crack propagation at welded details, the type and number of details to be investigated has an influence on the design of the girders. In view of the number of details to be tested and the desired replication, three horizontally curved box girders were designed to provide stress and deflection conditions typical of actual bridges at the details to be tested. The design of all girders is in accordance with the AASHTO specifications except where modified by the CURT tentative design recommendations.^(7,9,10)

The design of the box girders was subject to several constraints. First, the stress conditions at the various details must be typical of those present at welded details in service on actual curved box girder bridges. Second, the fatigue testing equipment in Fritz Laboratory has a maximum dynamic capacity of 110 kips from each hydraulic jack. The hydraulic jacks at their maximum dynamic capacity are also limited to a maximum usable stroke of approximately 0.35 inches. Third, the available loading frames in Fritz Laboratory and the layout of the dynamic test bed limit the maximum length and width and the minimum radius of the curvature of the test assemblies. Within these constraints the largest possible box girders were designed so that full size plates, details, welding, etc. would be used.

Initial preliminary designs of the box girders were obtained by a simplified analysis based on a strength of materials approach. The preliminary designs were then refined by successive cycles of analysis and design using SAP IV, a computer program for the finite element analysis of linear, elastic structures.⁽¹¹⁾ The results of the SAP IV analyses were checked using CURDI, a computer program for the analysis of curved box girder bridges based on the finite strip approach.⁽¹²⁾ Agreement between the results of both methods of analysis was observed to be within about 15 to 20%.

The final configurations of the three box girders are shown in Figs. 1 through 4. All three girders have a centerline span length of 36 ft, a diaphragm spacing of 9 ft and a radius of 120 ft (Fig. 1). The cross-section view of each girder at the interior diaphragms is shown in Figs. 2, 3, and 4. The diaphragm configurations for box girders 1, 2, and 3 are referred to as X-type, V-type, and plate-type diaphragms, respectively. The selection of three typical diaphragm configurations for the girders permits an evaluation of the effects of varying diaphragm rigidity on the fatigue behavior.

The cross-sectional dimensions of the box girders are also shown in Figs. 2, 3, and 4. The web and bottom flange thicknesses are 3/8 in. for all three girders. The box girders are 36 in. deep. The webs are 36 in. apart, center-to-center, and the bottom flange is 38 in. wide. The top flange is 60 in. wide and 1 in. thick with three stiffeners measuring 2 in. by 6 in. each. The top flange is removable, and is secured to the lower portion of the girders by A325 high-strength bolts.

Although a reinforced concrete deck would be more typical of an actual highway bridge, the removable steel top flange holds three significant advantages: (1) The top flange is interchangeable among box girders 1, 2, and 3. Using the same top flange for all three girders provides substantial savings in fabrication costs compared to forming and pouring concrete decks; (2) The capability of removing the top flange for access to the interior of the girder is vital if major repairs are required in the course of the fatigue tests; and (3) Accuracy of prediction of stress range is necessary in order to meet the objectives of the research. It was felt that greater accuracy would be obtained if a steel plate rather than a concrete slab were used. The connection of the top flange to the lower portion of the girder was designed as a friction connection to ensure composite action of the top flange and the lower portion of the girder. Adding the three massive stiffeners shown in Figs. 2, 3, and 4 raised the neutral axis of the girders, thereby providing a more realistic stress gradient through the depth of the assembly.

2.2 Design of Welded Details

Table 1 summarizes the welded details selected for investigation. There are eight basic types (I_c to $VIII_c$) with subtypes for all but types II_c , V_c and $VIII_c$. The detail type is shown by a Roman numeral in the upper left hand corner of each drawing. The first subscript, c, refers to closed (box) section. A second subscript, a or b, is given when there are subtypes. The corresponding straight girder category, relating to the 1977 AASHTO Specifications, Table 1.7.2A1, is shown by the capital letter in the upper right-hand corner of each drawing in Table 1.⁽⁹⁾ As far as box girders are concerned most details of interest are either Categories C, D or E. There are three details however (III_{ca} , VI_{ca} and VI_{cb}) for which the exact categories were not known at the time the girders were designed. These details were expected to be in the range of Category C to Category D. One additional detail (VII_{cb}) is Category B. Below the category letter is the corresponding allowable stress range (ksi) for straight girders which represents the 95% confidence limit for 95% survival at two million cycles of constant amplitude stress range.

In all drawings in Table 1 a solid dot defines the location of the predicted fatigue crack. Often two or more such locations are possible depending on stress distribution and/or initial flaw size. Only the welds relating to the details studied are shown. Groove welds are specifically identified. All welds shown without marking symbol are of the fillet type. Other welds such as those connecting webs to flanges are not shown for clarity. For any weld not shown in the drawings it can be assumed that the flaws and stress concentration associated therewith are not critical relative to those of the welds shown. Therefore, fatigue crack growth in these welds, although likely present, is not expected to limit the detail life.

Fabrication of each box girder requires the complete specification of the cross section plus all information pertaining to the diaphragms including connections to the flanges and to the web plates. All major design work therefore focused on the welded details located at diaphragm connections in the tensile region of the box girders. Because no room for error exists once fabrication is complete, the stress conditions at these locations must be known as accurately as possible prior to fabrication and testing. It is

possible to place many additional details between the internal diaphragms and on the exterior surfaces of the box girders. These details could be located, as was done in the plate girder studies, by first determining actual stress ranges under load. However, the removal and replacing of the bolted top flange made this procedure undesirable since it was anticipated that the top flange would have to be removed at least twice and possibly three or four times before the details were properly located and welded in place. A decision was therefore made to place all of the additional welded details on the box girders during their fabrication.

The welded details shown in Table 1 are also divided into four basic groups depending on the type of transverse or longitudinal attachment with which they are associated.

Group 1 welded details are associated with the type of interior diaphragm. Three diaphragm types were selected in order to examine the effect of diaphragm rigidity and cross section distortion on the fatigue behavior of the box girders. If only transverse web stiffeners plus cross bracing (no transverse flange stiffeners) are used as diaphragms the influence of relatively high distortions on fatigue strength can be examined. With reference to Table 1, details I_{ca} and II_c are associated with this type of diaphragm. Because the web distortions may seriously impair the fatigue strength, a second type of diaphragm consisting of both transverse web and flange stiffeners plus cross bracing is also provided. The type I_{cb} detail is associated with this diaphragm configuration. The stress at the flange surface may increase slightly with this type of diaphragm. However, this increase should be more than offset by a reduction in stress due to smaller distortion at the stiffener-to-web connection. The third type of diaphragm is essentially a plate type which is expected to provide the greatest diaphragm rigidity. Detail I_{cb} is also associated with this diaphragm. Because the internal diaphragms in curved box girders are subjected to higher forces than those in straight box girders the significance of the distortional effects on the fatigue strength is evaluated by looking for cracks that are expected to form either in the web when the transverse web stiffener is touching (not welded to) the bottom flange (detail II_c) or in the flange when the transverse web and flange stiffener or the plate type diaphragm is welded to the bottom flange surface (details

I_{ca} and I_{cb}). The details at the diaphragm locations are expected to govern the overall fatigue strength of curved box girder bridges. For this reason they are of primary interest to designers.

Group 2 welded details are associated with the connections of longitudinal stiffeners to the flanges and webs of the curved box girder. Referring to Table 1, detail types III_c , IV_c , V_c , and VI_c are contained in this group. There are no experimental fatigue results directly available on either straight or curved elements for these types of details. Simulated beam specimens have indicated that a severe AASHTO Category E detail may be expected when a longitudinal stiffener is abruptly discontinued such as shown in details III_{cb} and V_c of Table 1. Because a substantial reduction in fatigue strength is expected, possible improvements are examined for a modified V_c detail in the form of a curved radius transition (6" radius) at the weld toe termination shown as detail IV_{ca} , or a 1:2.5 sloped transition shown as detail IV_{cb} . Because longitudinal stiffeners are likely to occur in box girders, the application of the radius or straight transition appears to be reasonable for application to both straight and curved box girder configurations. An improvement in the III_{cb} detail is shown as detail III_{ca} where the longitudinal stiffener is welded to the transverse stiffener, providing continuity. Other variations of detail V_c such as details VI_{ca} and VI_{cb} are also examined to determine the influence of weld terminations with a bolted splice to reduce the stress concentration effect, and the influence of intermittent welds.

Group 3 welded details are associated with the continuous longitudinal web-to-flange welds. Both fillet and single beveled groove welds are examined as shown in details VII_{ca} and VII_{cb} of Table 1. These welds are not unique to curved girders but an excellent opportunity is provided to examine the influence of both continuous and discontinuous back-up bars with continuous fillet welds. These details were and are being used yet little information is presently available on their fatigue behavior. These studies are expected to be equally applicable to both curved and straight box girder configurations.

Group 4 welded details are short exterior attachments used for connecting exterior (between box) diaphragms. A clip angle, as shown in detail VIII_c of Table 1 was selected for study.

In order to reduce testing time and the problems associated with extensive fatigue crack repair, all details on the box girders were designed to fail at approximately two million cycles under the predicted nominal stress ranges at the details. Two million cycles represents the desired fatigue life for many bridges and is often considered a benchmark figure in fatigue testing. Fatigue failure of the welded details at approximately two million cycles is achieved by locating each detail on the assemblies so the detail is subjected to a design stress range estimated to produce the desired cycle life.

The design stress ranges used for the details under study are based on the AASHTO detail classification system. Allowable stress ranges of 18 ksi, 13 ksi, 10 ksi, and 8 ksi, respectively (see Table 1), represent the 95% confidence limit for 95% survival of Category B, C, D, and E details at two million cycles. Design stress ranges from 1 to 2 ksi higher than those recommended in AASHTO were selected for the fatigue tests to ensure the formation of visible fatigue cracks by two million cycles and to allow for a margin of error between calculated and measured stress ranges. For this reason a design stress range of 19 ksi was selected for all Category B details. Similarly, design stress ranges of 15 ksi, 10 to 12 ksi, and 10 ksi were selected for all Category C, D and E details, respectively.

Given the design stress ranges for the various details under study, predicted stress range profiles based on the finite element analyses (Art. 2.1) were used to locate all Group 2, 3, and 4 details. Group 1 details were located at the diaphragms. The design stress ranges at Group 1 details governed the final design of the box girders.

Table 2 summarizes the number and types of details placed on each girder. The numbers in parentheses represent Group 1 and 2 details associated with the interior diaphragms at which the predicted stress range is substantially below the design stress range for the given detail. Significant fatigue crack growth is not expected at these details.

Table 2 Summary of Number and Types of Details under Study

Detail	Girder	Number	Total
I _{ca}	1	3 (3)	3 (3)
	2	-	
	3	-	
I _{cb}	1	-	4 (4)
	2	3 (3)	
	3	1 (1)	
II _c	1	-	2 (2)
	2	-	
	3	2 (2)	
III _{ca}	1	1	2 (4)
	2	(2)	
	3	1 (2)	
III _{cb}	1	1 (2)	3 (8)
	2	1 (3)	
	3	1 (3)	
IV _{ca}	1	2	2
	2	-	
	3	-	
IV _{cb}	1	-	4
	2	2	
	3	2	
V _c	1	10	20
	2	6	
	3	4	
VI _{ca}	1	4	8
	2	2	
	3	2	
VI _{cb}	1	-	4
	2	2	
	3	2	
VII _{ca}	1	-	4
	2	-	
	3	4	
VII _{cb}	1	-	4
	2	-	
	3	4	
VIII _c	1	3	9
	2	3	
	3	3	
TOTAL			69 (21)

2.3 Fabrication of Box Girders

The three curved box girders were fabricated and assembled by Bethlehem Fabricators, Inc., Bethlehem, PA, and delivered to Fritz Engineering Laboratory with all details welded in place.

All steel is ASTM A36 grade. All bolts are A325 high-strength bolts. All bolts used in the diaphragm connections and the type VI_{ca} details are 3/4 in. in diameter, while the bolts securing the removable top flange are 7/8 in. in diameter. All welding conforms to the applicable provisions of the American Welding Society Structural Welding Code.⁽¹⁷⁾ Manual and automatic welding performed by the fabricator is by the submerged-arc process. Nominal weld sizes of 3/16 in. and 5/16 in. are used throughout with 70 ksi electrodes.

Figures 5, 6, and 7 show the three box girders in various stages of fabrication. The bottom flanges and the interchangeable top flange were flame cut to the required curvature as shown in Figs. 5 and 6. The webs were flame cut to size, then rolled to the required curvature as shown in Fig. 6. The bottom flange, webs, and end diaphragms were fitted up in jigs as shown in Fig. 7, and welded. The interior diaphragms were then installed.

The fit of the interchangeable top flange was checked by shop assembly prior to transporting any of the girders. Girder 3, the first one tested, was shipped to Fritz Engineering Laboratory with the top flange in place. Temporary top lateral bracing members were provided for Girders 1 and 2 to ensure safe lifting and transportation. Figure 8 shows Girders 1 and 2 (top and bottom, respectively) during preparation for fatigue testing in Fritz Laboratory. The top lateral bracing members are still in place on Girder 1. The bracing on Girder 2 was temporarily removed to permit access for instrumentation.

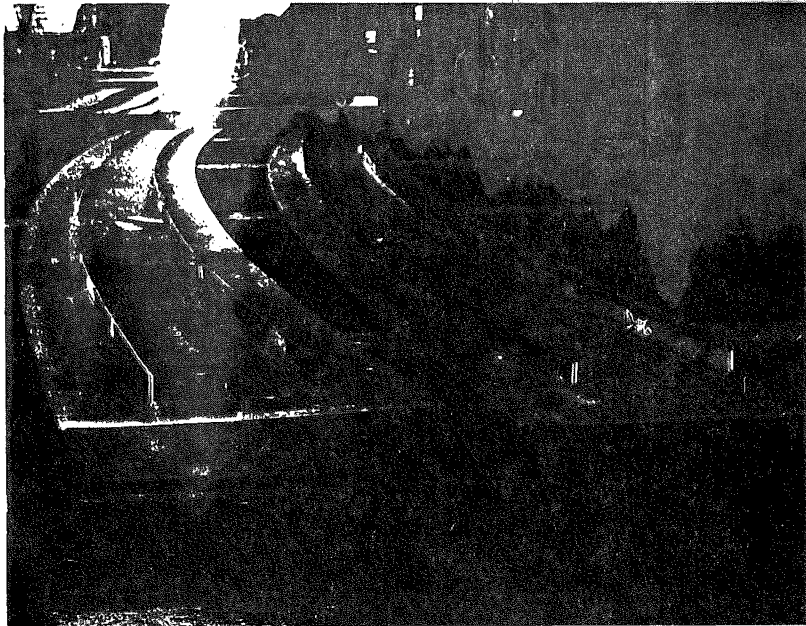


Fig. 5 Bottom Flanges after Flame Cutting to the Required Curvature and Welding Longitudinal Stiffeners

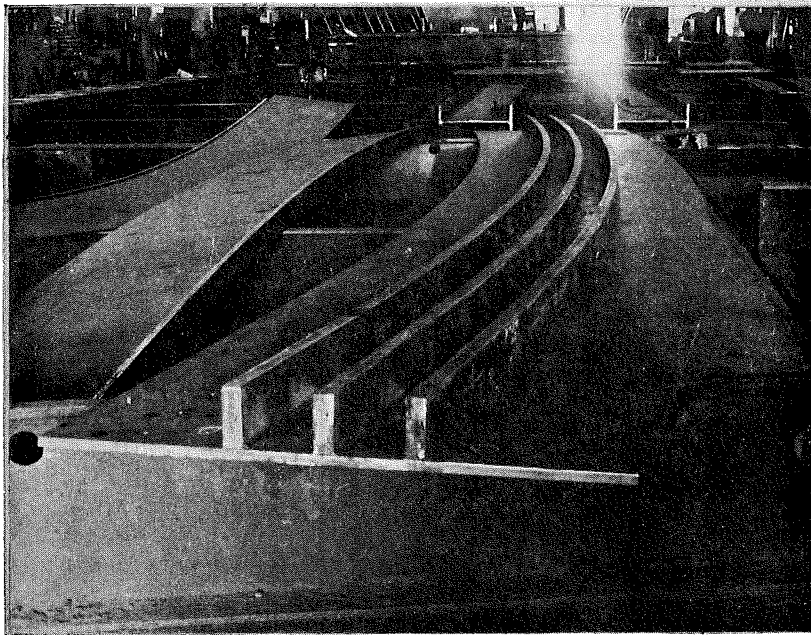


Fig. 6 Webs after Flame Cutting and Rolling to the Required Curvature and the Top Flange with Longitudinal Stiffeners in Place

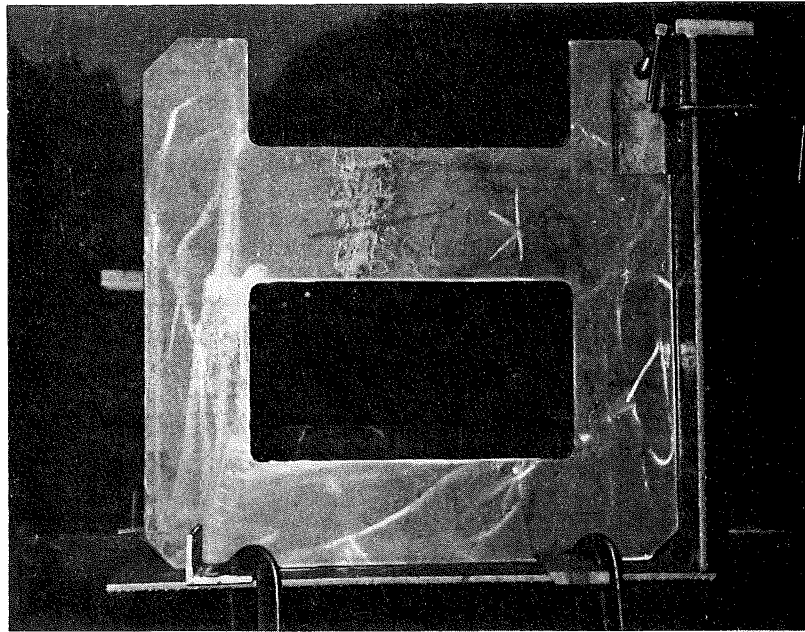


Fig. 7 Web, Bottom Flange and Plate-Type Diaphragm Fitted Up in Jig for Welding



Fig. 8 Girders 1 and 2 during Preparation for Testing Showing Temporary Top Lateral Bracing System

3. ERECTION AND INSTRUMENTATION OF BOX GIRDERS

3.1 Erection

Each of the curved box girders was tested in fatigue on the dynamic test bed in Fritz Engineering Laboratory, Lehigh University. Figures 9 and 10 show girder 3 in the dynamic test bed ready for testing. A detailed description of the dynamic test bed, its construction, and the associated testing equipment is available in Ref. 13.

Figures 11 and 12 show schematic plan and elevation views of a typical box girder in place for testing on the dynamic test bed. Load was applied to the girders by two 110 kip capacity (dynamic) Amsler hydraulic jacks placed over the inner web at the quarter points (Joints 3 and 7 in Fig. 1). Because of the anchorage bolt pattern on the dynamic test bed, a spreader beam was necessary to properly position the hydraulic jacks over the quarter points. The spreader beam was centered in the loading frames which transmitted the jack loads into the dynamic test bed. The loading frame was braced in the longitudinal direction by diagonals and all bolts anchoring the loading frame to columns to the floor were prestressed to minimize sway and uplifting of the frames. Two Amsler hydraulic jacks were used for both the static and cyclic load tests. The maximum jack strokes are 5 in. and 0.45 in. for static and cyclic loading, respectively. Deflections of the loading frame limit the usable available stroke to approximately 0.35 in. for cyclic loading. Two Amsler pulsators generate the hydraulic pressure required to drive the hydraulic jacks during the static and cyclic load tests. Synchronized mechanically, electrically, and hydraulically, these pulsators run at a constant speed of approximately 250 cycles per minute during the fatigue testing. The approximate load range is read off pressure gages connected directly to the hydraulic jacks.

Each girder is supported at the ends of the inner and outer webs (Joints 1, 2, 9, and 10 in Fig. 1) by a roller bearing assembly shown in Fig. 13. The roller bearing assembly simulates a spherical bearing except that rotation about a vertical axis is restrained. All other degrees of freedom corresponding to horizontal displacements and rotations about a

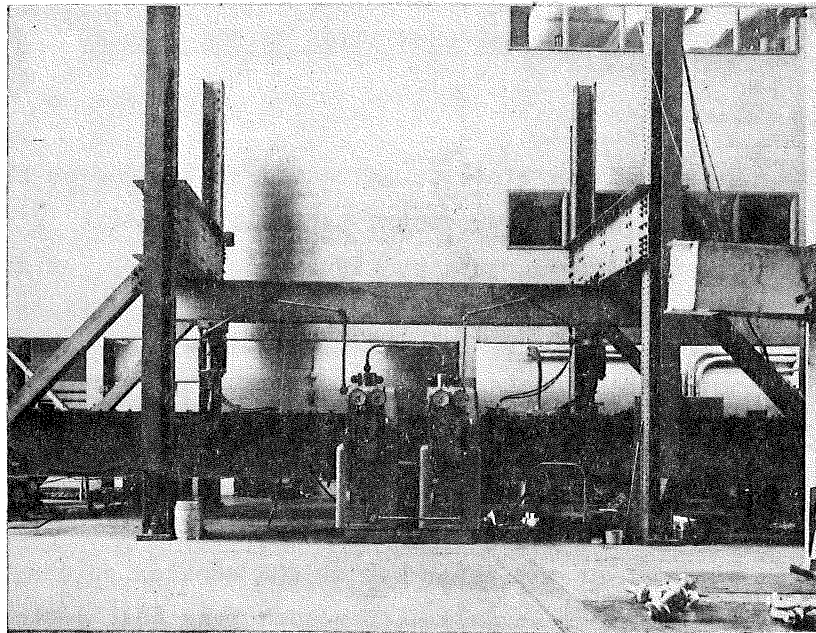


Fig. 9 Test Setup Viewed from South Showing Loading Frame, Amsler Pulsators and Hydraulic Jacks and Girder 3

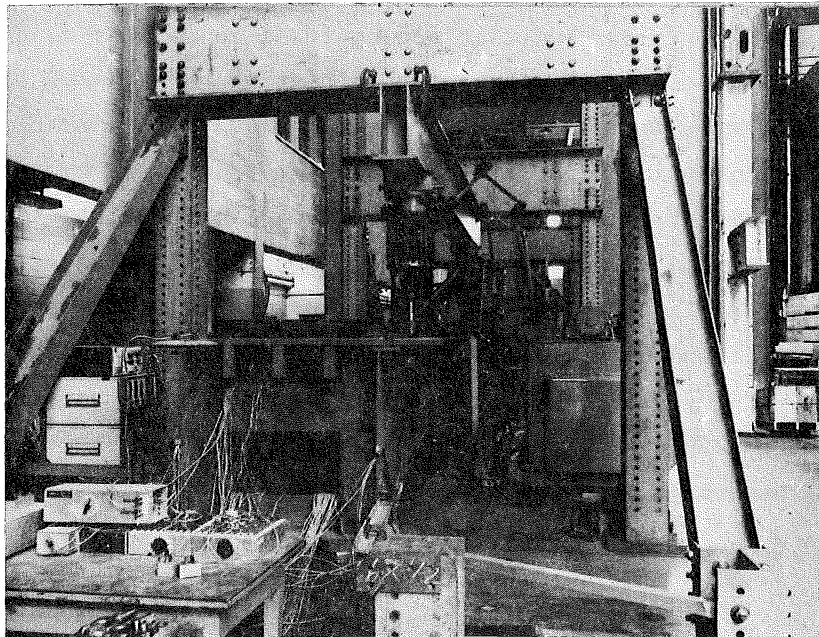


Fig. 10 Test Setup Viewed from West Showing Loading Frame, Girder 3 and Instrumentation

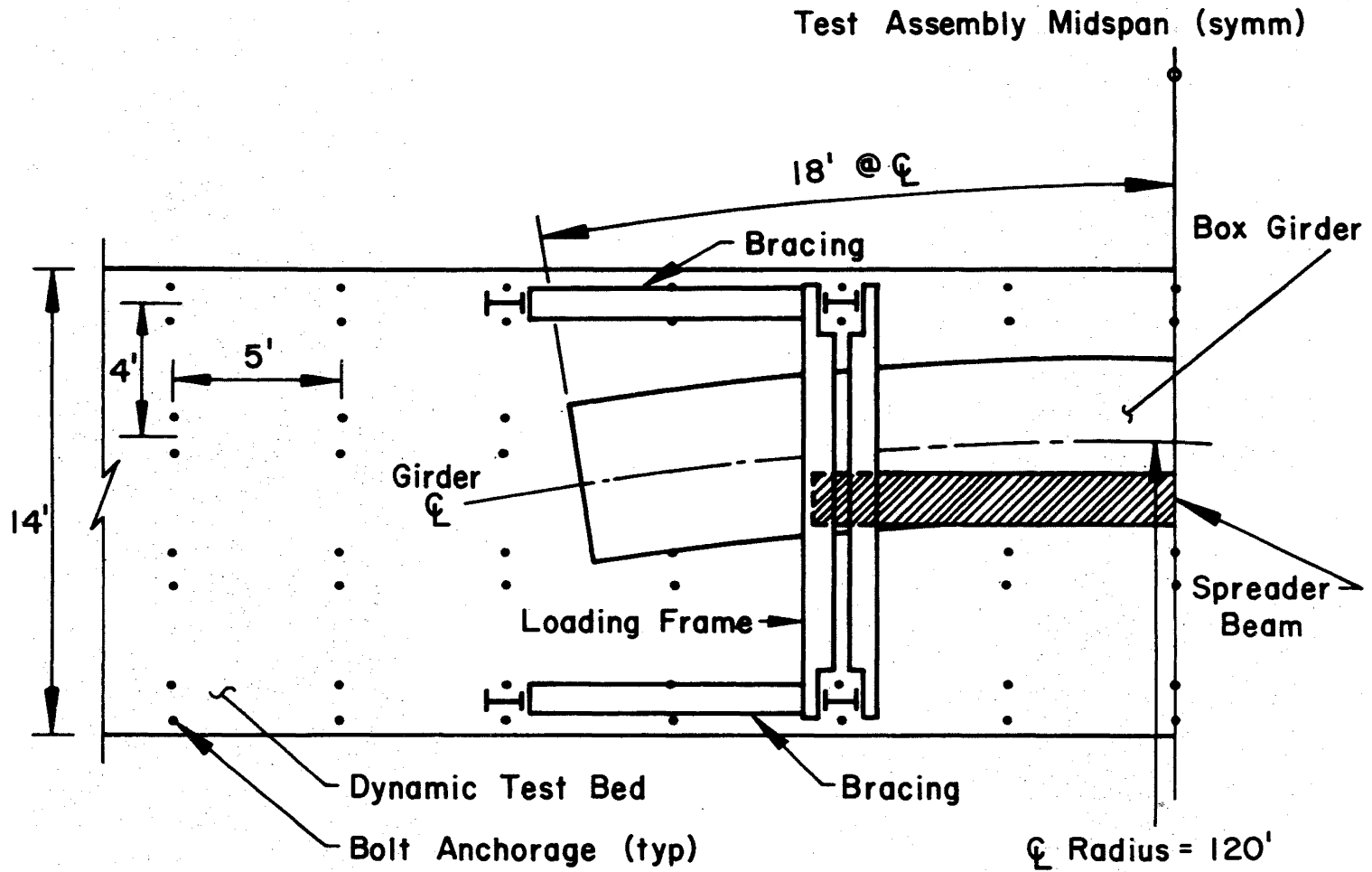


Fig. 11 Schematic Plan View of Dynamic Test Bed

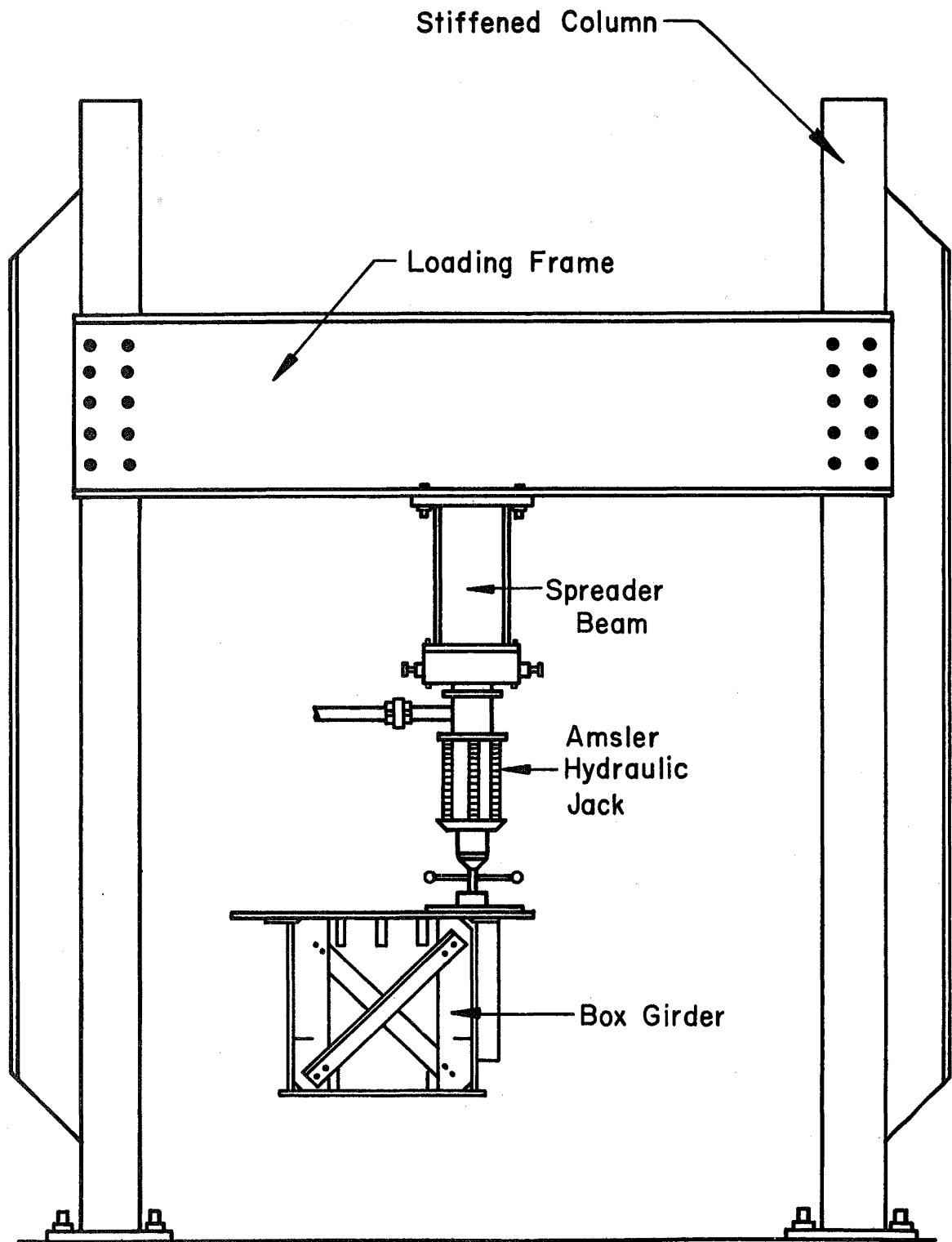


Fig. 12 Schematic Elevation View of Dynamic Test Bed at Loading Frames

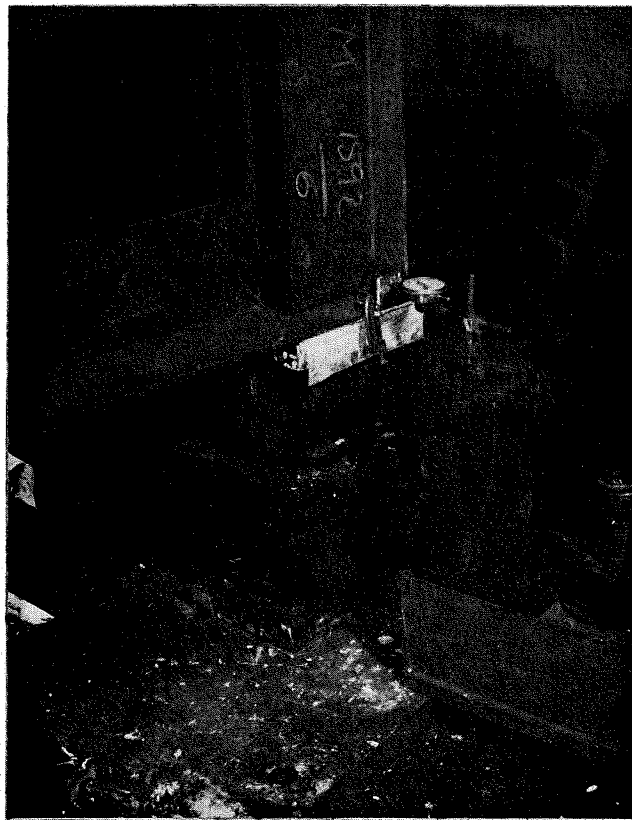


Fig. 13 Roller Bearing Assembly
at Joint 10 - All
Horizontal Degrees of
Freedom Permitted

horizontal axis are free except as required to provide overall stability of the girder during test.

The roller bearing assemblies consist of two 8 in. diameter steel rollers at right angles to each other, sandwiched between three 2 in. thick steel plates. The rollers are 9 in. in length and the top and bottom plates are 9 in. x 12 in. The middle plate is 12 in. square. The axis of the upper roller is in line with the girder radius. The bottom roller is at right angles to the upper roller. The proper alignment of the rollers and plates is maintained by two tapered alignment pins anchored in the steel plates and projecting into oversized holes at each interface of roller and plate. The alignment pins and plates are shown in Fig. 14. The orientation of the entire bearing assembly with respect to the box girder assembly is maintained by clamping the top plate of the roller bearing assembly to the bottom flange of the box girder and tack welding the bottom plate of the roller bearing assembly to the dynamic test bed. For safety reasons stop blocks are welded to all the plates to prevent excessive travel of the rollers in case of accident during erection or testing of the girders. Most of the stop blocks are an inch or two from the rollers as shown in Fig. 13 so that freedom of motion is assured. However certain stop blocks were fitted to the rollers at Joints 1 and 9 in order to maintain stability of the girders during testing.

As shown schematically in Fig. 15 three horizontal degrees of freedom are fixed to prevent rigid body motion of the girder. Radial displacements are prevented at Joints 1 and 9 tangential displacements are prevented at Joint 1. The above degrees of freedom are prevented by fitting the stop blocks tightly against the appropriate steel roller and welding it in place. Additional restraint to the horizontal rigid body motion of the assembly was provided by struts clamped at Joints 1 and 9 consistent with the horizontal boundary conditions shown in Fig. 15. Figure 16 shows the roller bearing assembly at Joint 9, as well as the placement of the stop blocks and strut to prevent radial displacements.

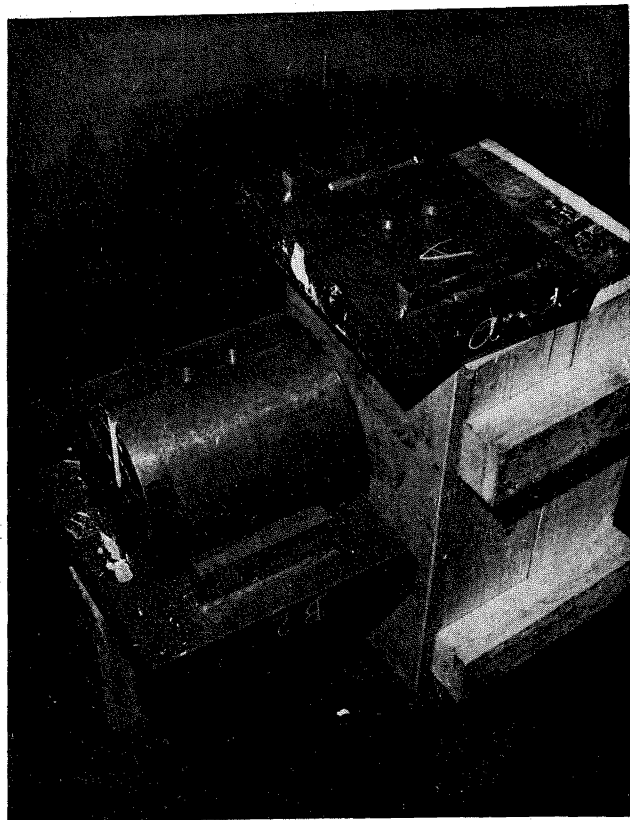
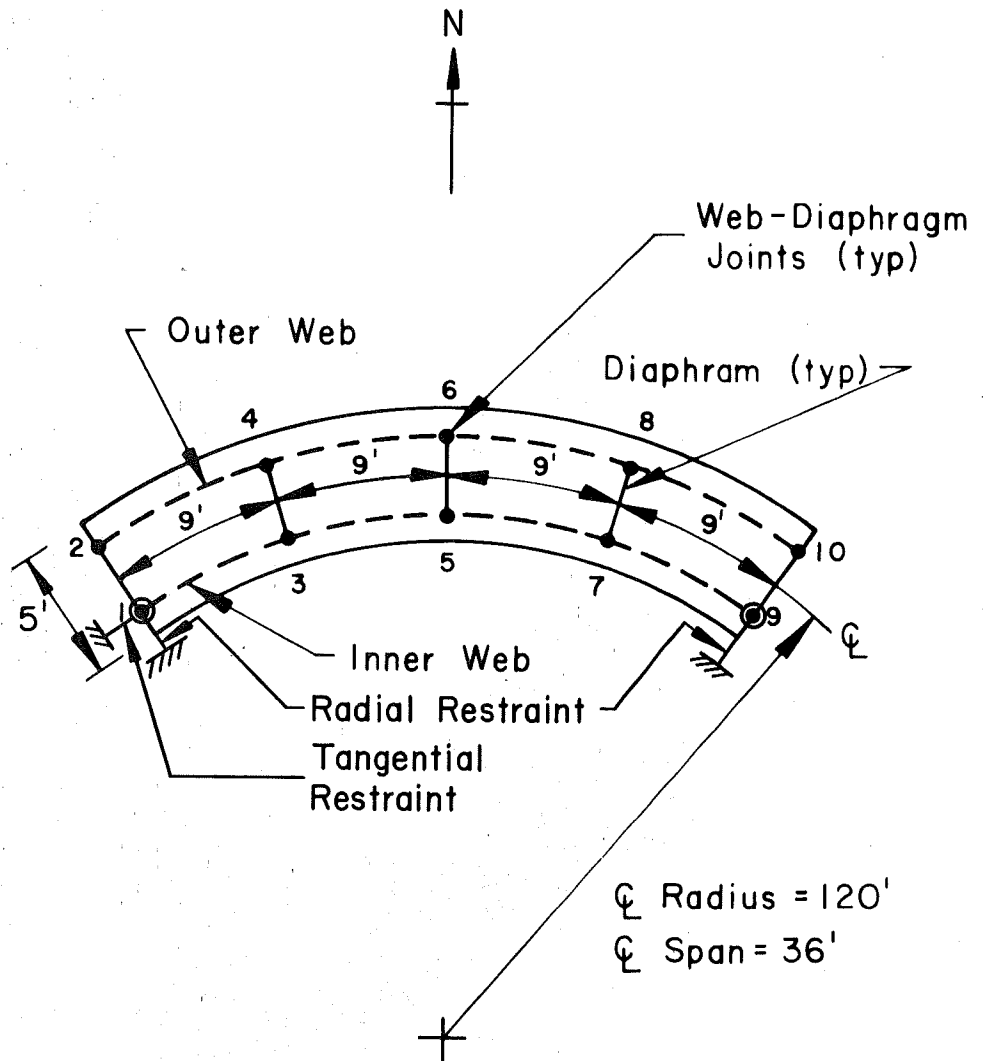


Fig. 14 Alignment Pins and Holes
at Interface of Rollers
and Plates



Load Positioned Over Joints 3 & 7

Fig. 15 Plan View of Typical Girder Showing the Loading Condition and the Horizontal Restraint Conditions

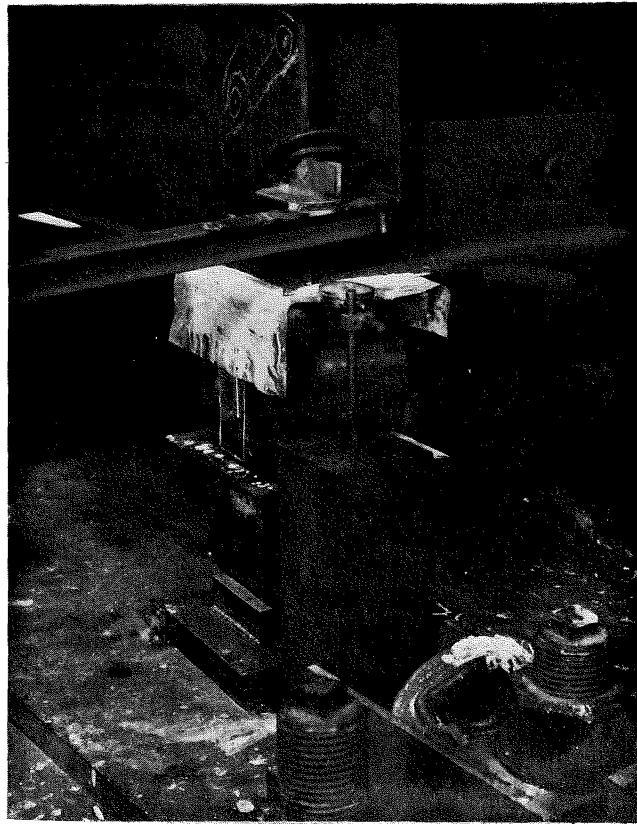
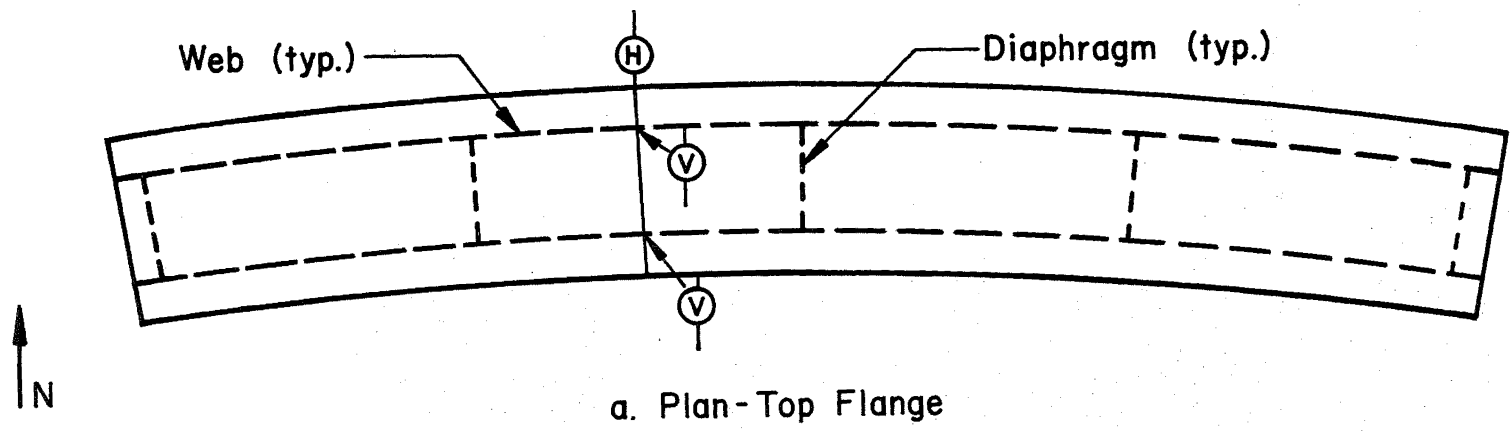


Fig. 16 Roller Bearing Assembly
at Joint 9 - Radial
Displacements Prevented



⊙H = Horizontal Deflection Dial Gage ⊙V = Vertical Deflection Dial Gage

30

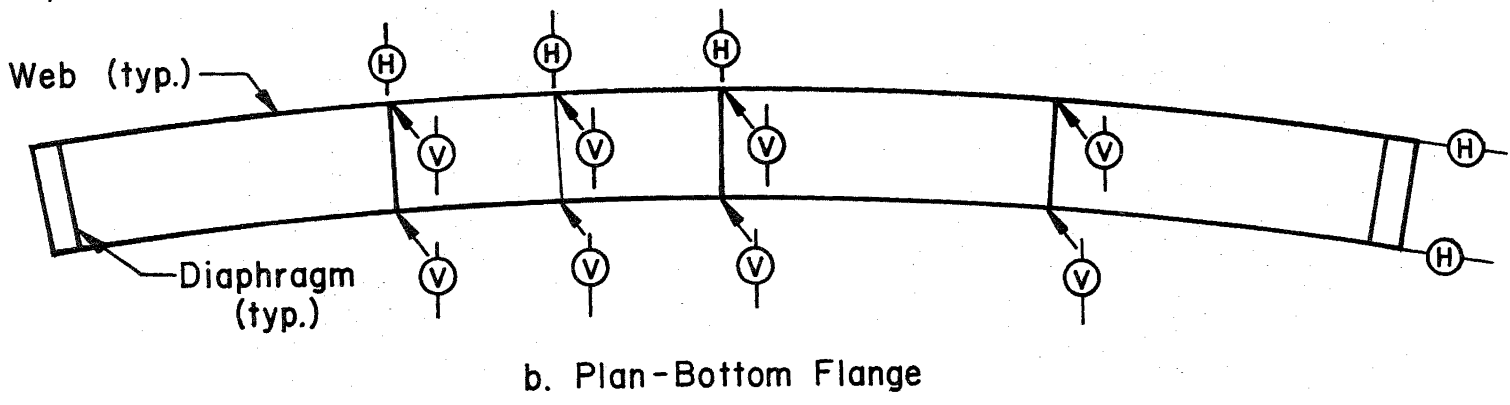


Fig. 17 Deflection Dial Gage Locations - Initial Static Load Tests

3.2 Instrumentation

Several sets of instrumentation were used to monitor the behavior of each girder during the static and cyclic load tests. The instrumentation for each test was tailored to the differing purposes of the tests.

The static load tests were carried out to check the alignment of each girder and the correlation between the actual and predicted stresses.⁽⁸⁾ These objectives were best met by monitoring the overall behavior of each girder as characterized by the deflections and strains at a number of points.

Vertical and horizontal deflections under static loads were measured by Ames dial gages placed at the locations shown in Fig. 17. Figures 13 and 16 show the horizontal dial gages placed at Joints 9 and 10 during the static load test of Girder 2. The dial gages had a least scale division of 0.001 in. and a stroke of 1 in.

Strains in the girders during the static load tests were recorded by electrical resistance strain gages used in conjunction with a 120-channel B&F data acquisition system. The strain gages were located on the webs and flanges of each girder at several gage sections shown in Figs. 18 through 20. Each cross section that is gaged is numbered. The instrumentation at a particular cross section is given a type number. The locations of the strain gages for each type are shown in Figs. 21 through 23. All strain gages have a nominal gage length of $\frac{1}{2}$ in. and are oriented to record the longitudinal normal strains. In addition to the strain gages shown in Figs. 18 through 23 strain gages were also placed in the vicinity of the welded details under study as shown, for example, in Fig. 24. Although these strain gages were provided primarily for use in the cyclic load tests (periodic tests involving a very few cycles for the purpose of measuring maximum and minimum strains), the strains near the welded details were also recorded in the static load tests for comparison to the cyclic strains.

The cyclic load tests were periodically carried out to determine the stress ranges near the various details under study. As described later in Art. 4.2 the cyclic load range (maximum load minus minimum load) used throughout the fatigue testing of each assembly is based on the strain

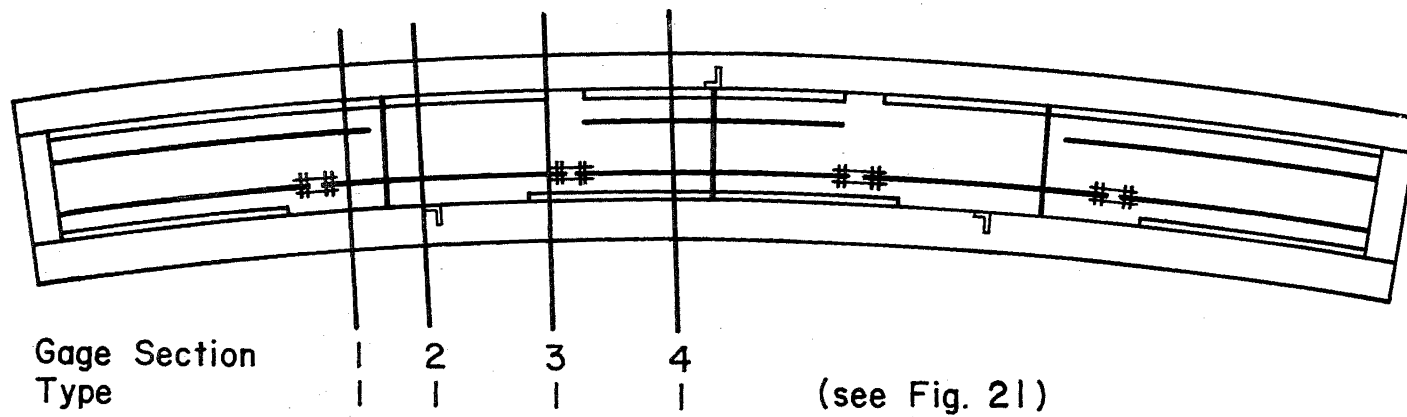


Fig. 18 Plan of Box Girder Instrumentation - Girder 1

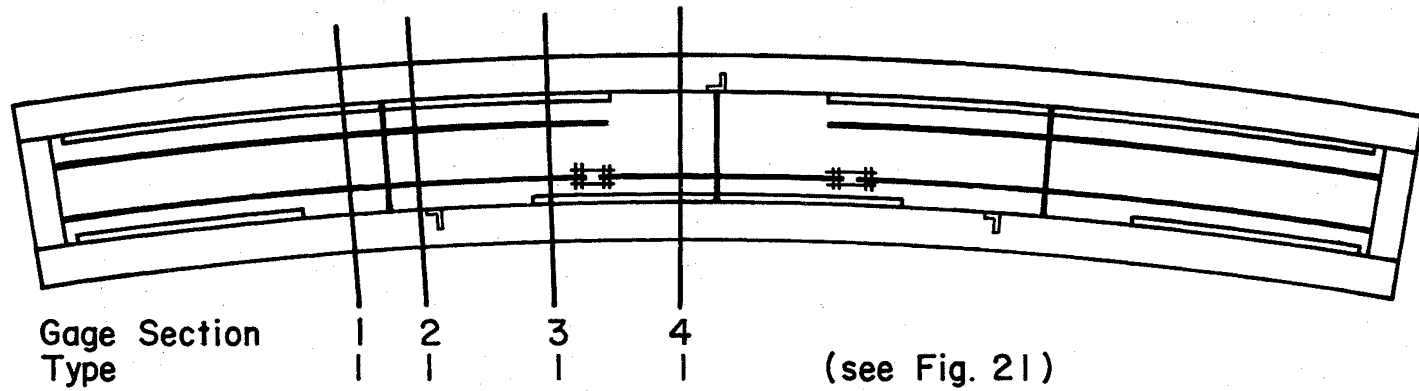


Fig. 19 Plan of Box Girder Instrumentation - Girder 2

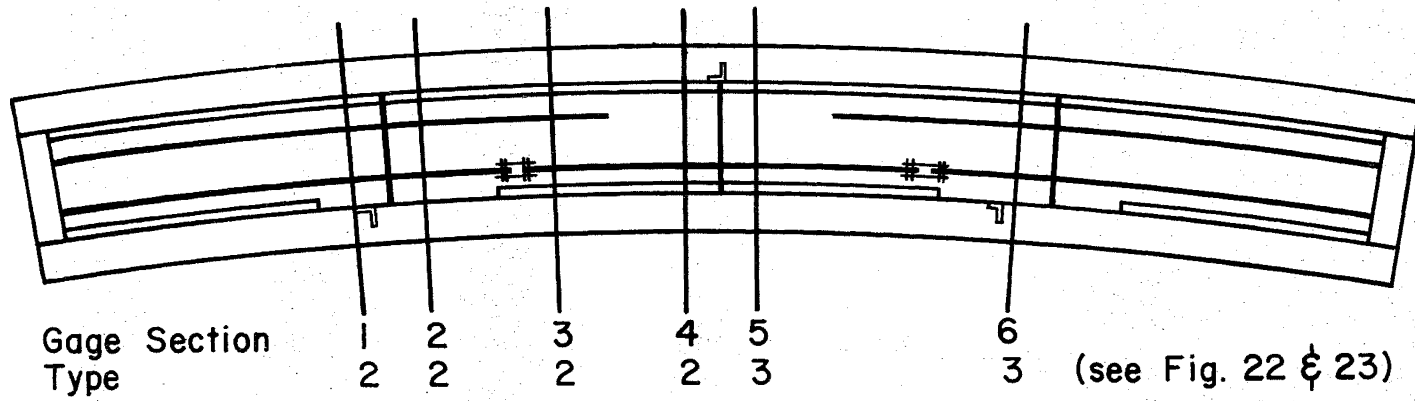


Fig. 20 Plan of Box Girder Instrumentation - Girder 3

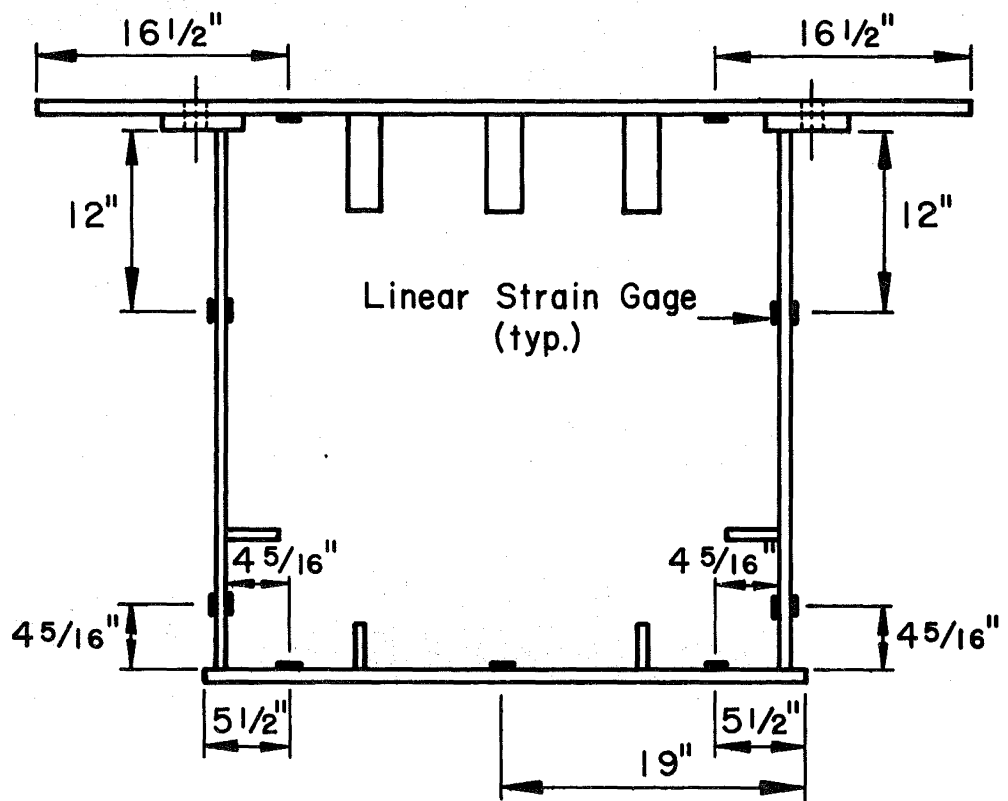


Fig. 21 Typical Gage Section - Type 1

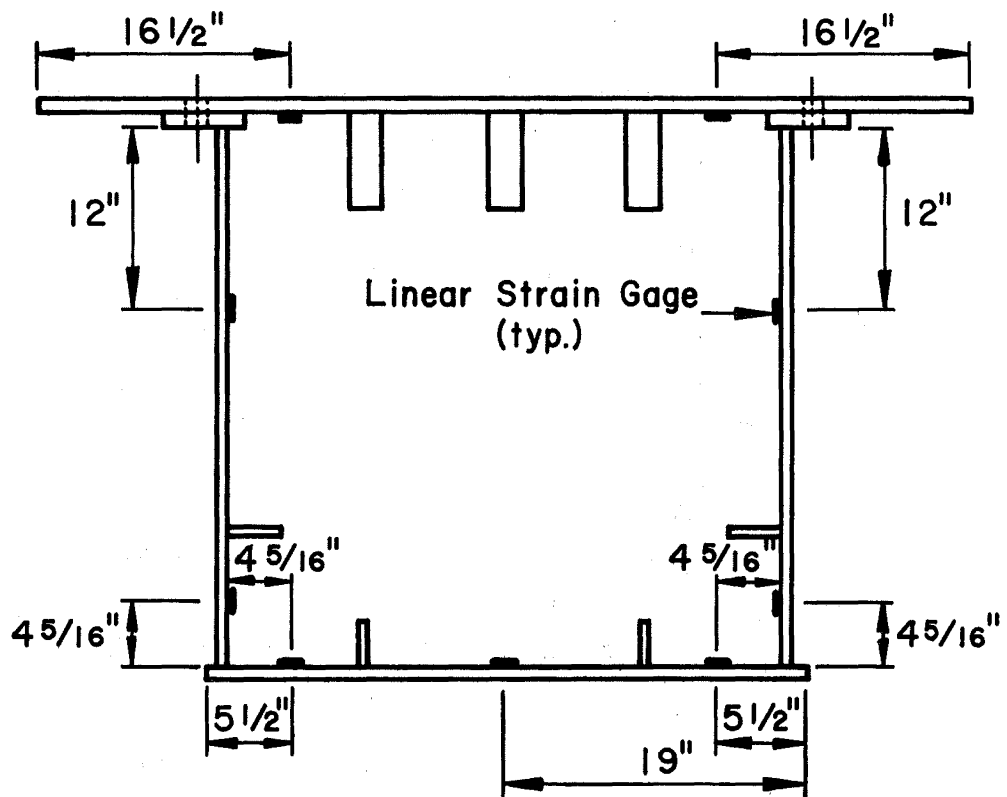


Fig. 22 Typical Gage Section - Type 2

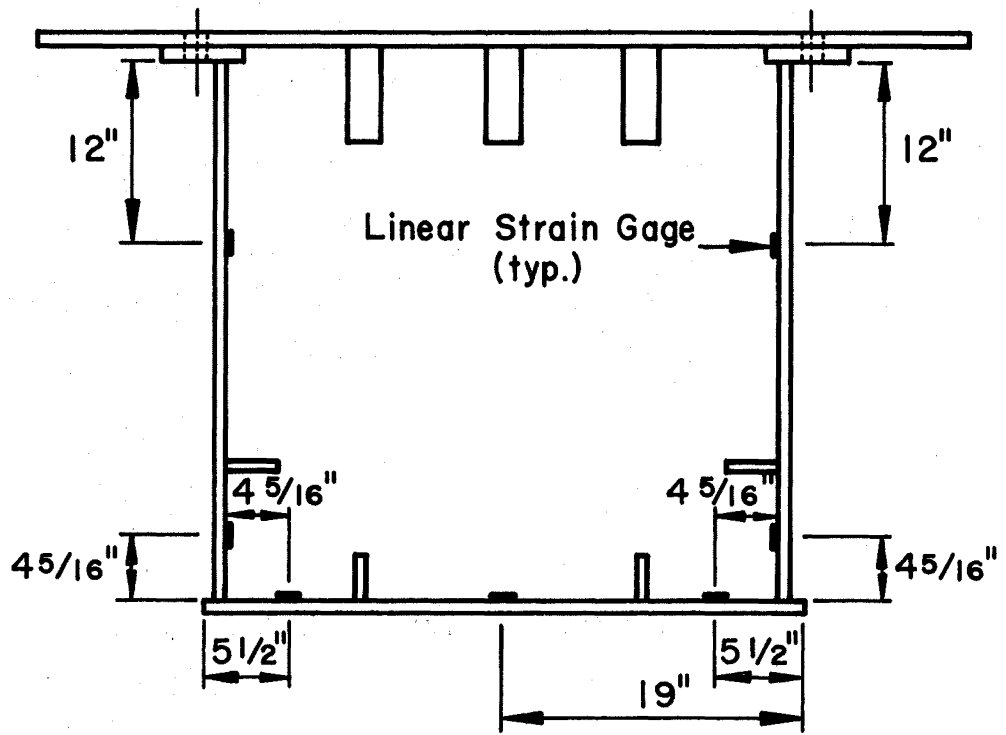


Fig. 23 Typical Gage Section - Type 3



Fig. 24 Linear Strain Gages at Detail Types
 V_c and VI_{ca}

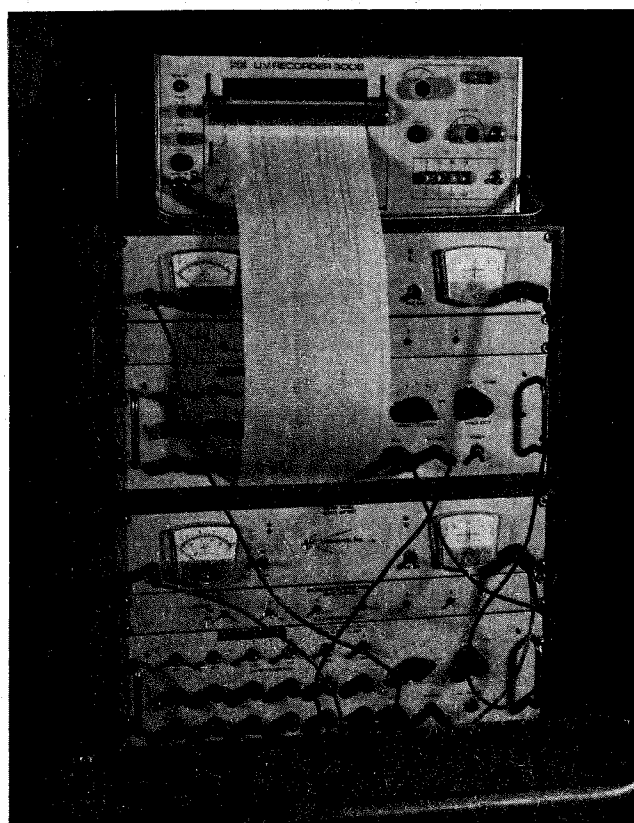


Fig. 25 12-Channel Ultraviolet
Oscillograph Recorder

ranges measured at the details under study in the initial cyclic load test. Additional cyclic load tests were periodically performed at approximately 250,000 cycle intervals throughout the fatigue testing to monitor the stress ranges near the welded details.

The strain gages at the gage sections (Figs. 18 to 23) were also read during the cyclic load tests, and serve as a check on the strain gages placed near the Group 2, 3, and 4 details. The typical locations and orientation of the linear strain gages near the welded details are shown in Table 1. The indicated separation distances are provided to ensure that the gage indicates the nominal stress range at the detail without the influence of the stress concentration caused by the welded detail. Figure 24 shows two details (Types V_c and VI_{ca}) and the strain gages associated with them. Strain gages were not placed at Group 1 details or at detail Type VII_{cb} . The nominal stress ranges at these details are readily available from stress ranges measured at adjacent gage sections (Figs. 18 through 23).

During the cyclic load tests the strain range at the several details and at the gage sections are recorded on light-sensitive paper by the 12-channel ultraviolet oscillograph recorder shown in Fig. 25. From calibration curves and the oscillograph output, the strain range for each gage under cyclic loading is determined and converted into a nominal stress range at the detail.

During the periodic cyclic load tests the midspan vertical deflection at the inner web is measured by the double dial gage rig mounted as shown in Fig. 26. The dial gage rig is also used throughout the fatigue tests to monitor the midspan deflection, thereby indicating whether the overall stiffness of the assembly is deteriorated by fatigue crack growth. The lower dial gage also triggers a switch to shut down the Amsler pulsators if the vertical deflection becomes too great. Thus safe, operation of the machinery is assured without the continuous presence of research personnel.

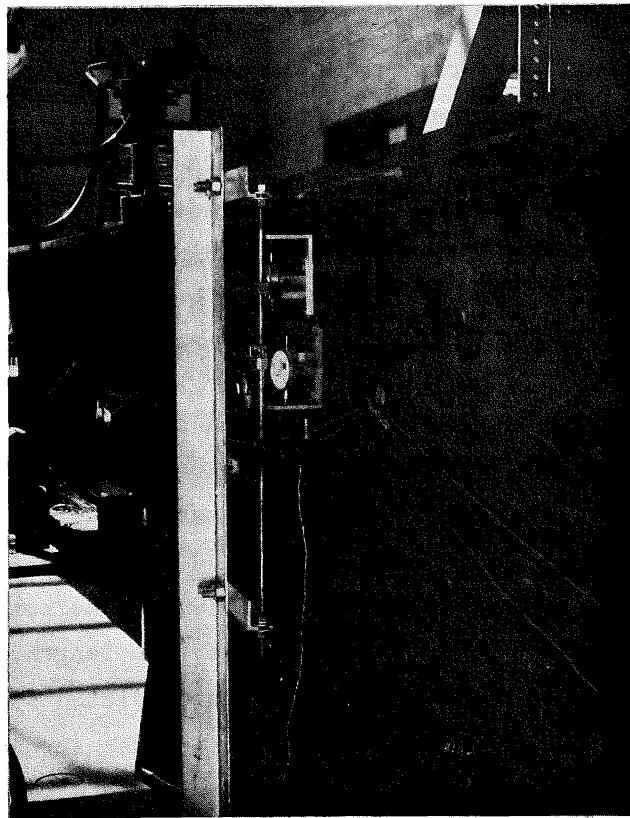


Fig. 26 Double Dial Gage Rig
which Monitors Midspan
Deflection under Cyclic
Load and Performs
Emergency Shutdown

4. INITIAL STATIC AND CYCLIC LOAD TESTS

4.1 Initial Static Load Test

Following the erection of each girder on the dynamic test bed, an initial static load test is performed to check the alignment of the assembly and to provide measured stresses and deflections for comparison to the static analysis of each girder (Art. 2.1). The results of the initial static load tests also provides estimates of the stress ranges and deflections to be expected during the cyclic loading.

The initial static load test consists of loading the girder from zero to 100 kips in 20 kip increments. All strain gages are read at each load increment by a 120-channel B&F data acquisition system. Horizontal and vertical deflections are also measured by reading the Ames dial gages (Fig. 17) at each load increment. Complete readings of strains and deflections are also made as each girder is unloaded in 20 kip increments, thereby providing a check of the readings taken while loading.

The predicted stress range profiles based on the SAP IV static analyses (Art. 2.1) and the measured stresses from the initial static load test are shown in Figs. 27 through 33. In each figure the stress range, S_r (ordinate), at a given point is plotted as a function of the parameter, X/L (abscissa), where X is the position of the point along the centerline of the girder and L is the centerline span length. Only the half span of a girder (west span) is shown. The predicted stress range profile is shown as a continuous curve representing the stress range, S_r , corresponding to a static load range of 100 kips. Due to the symmetry of girder geometry, loading and detail placement about midspan the predicted stress range profiles are only shown for the western half of each girder (Fig. 1). The predicted stress range profiles for the eastern half are the mirror images of the profiles shown. The stress ranges measured during the initial static load tests are shown as circles and squares in the figures. In order to demonstrate the validity of the assumption of symmetry about midspan, the measured stress ranges corresponding to a static load range of 100 kips are plotted for both halves of each girder. The solid and open symbols shown in the figures represent stress ranges measured on the eastern and western halves of the assemblies, respectively.

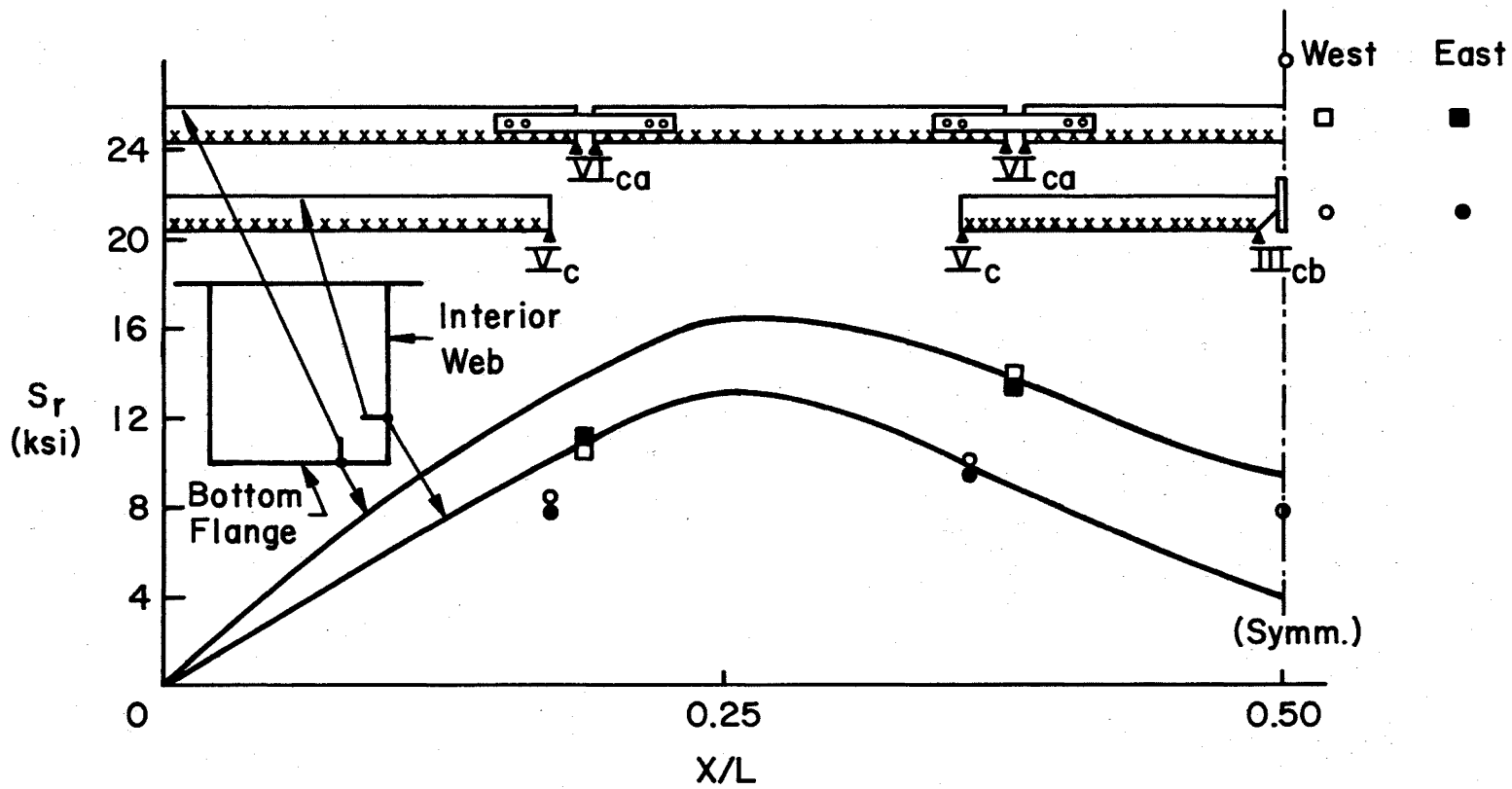


Fig. 27 Stress Range Profiles and Measured Stresses from Initial Static Load Test - Girder 1

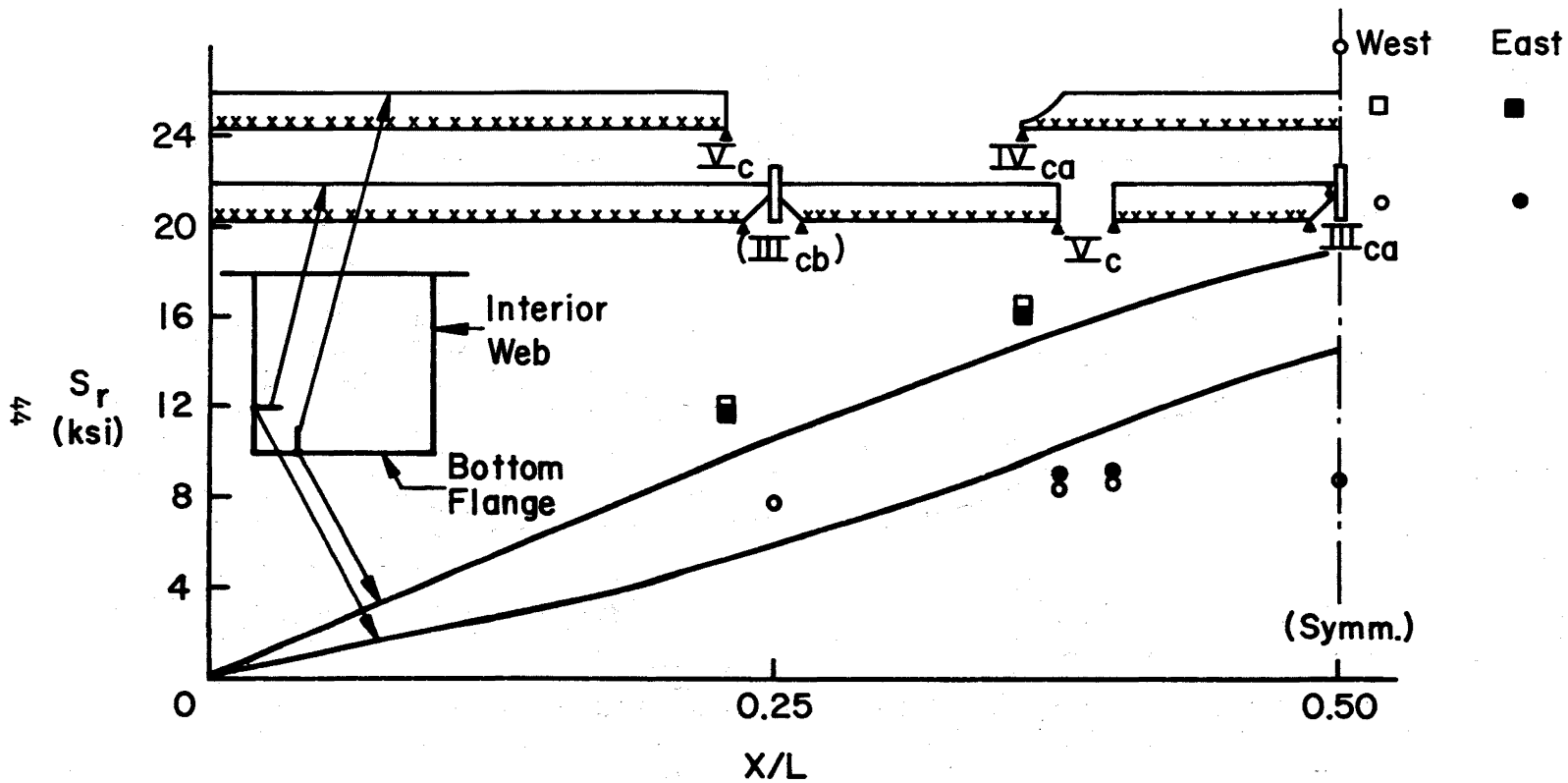


Fig. 28 Stress Range Profiles and Measured Stresses from Initial Static Load Test - Girder 1

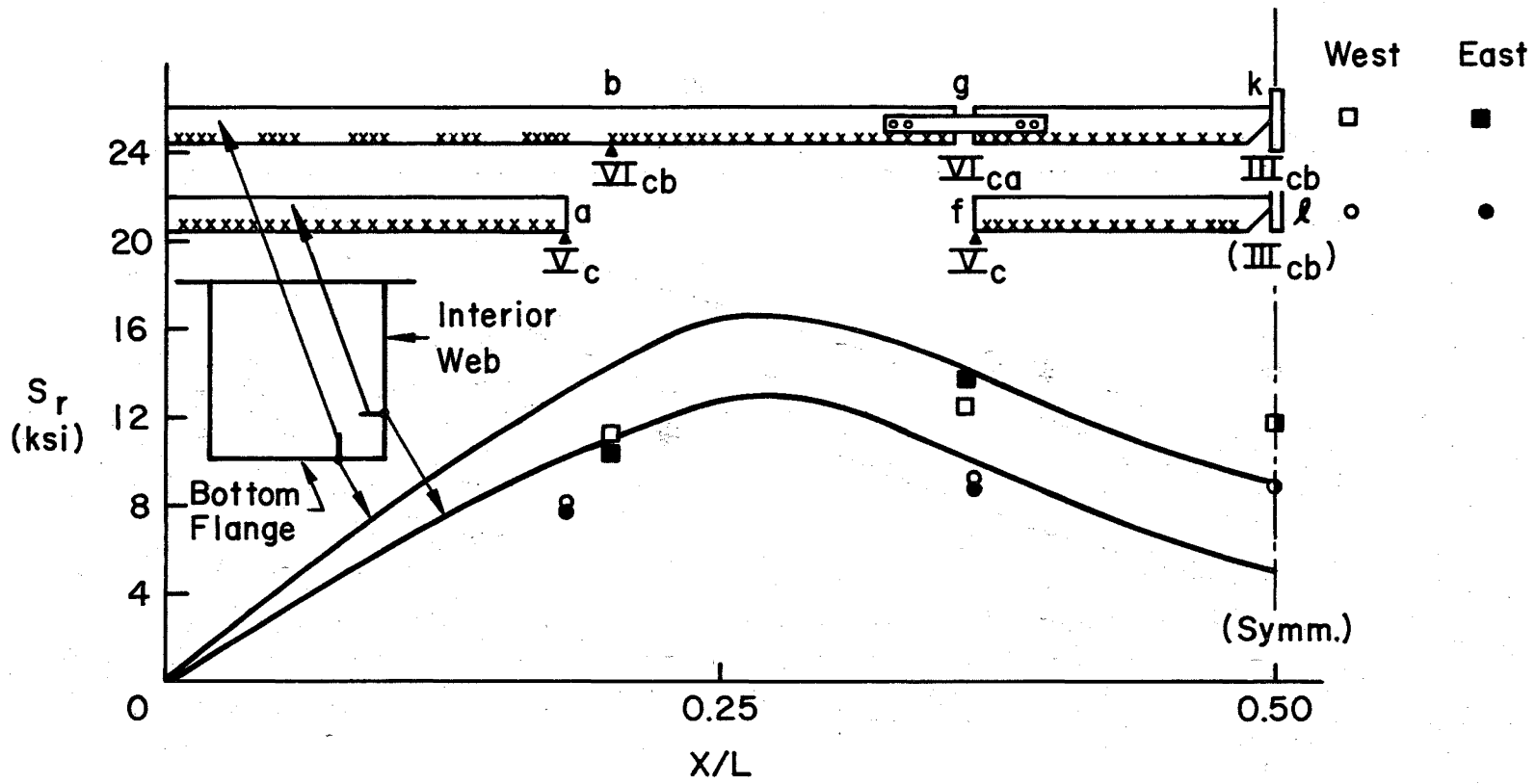


Fig. 29 Stress Range Profiles and Measured Stresses from Initial Static Load Test - Girder 2

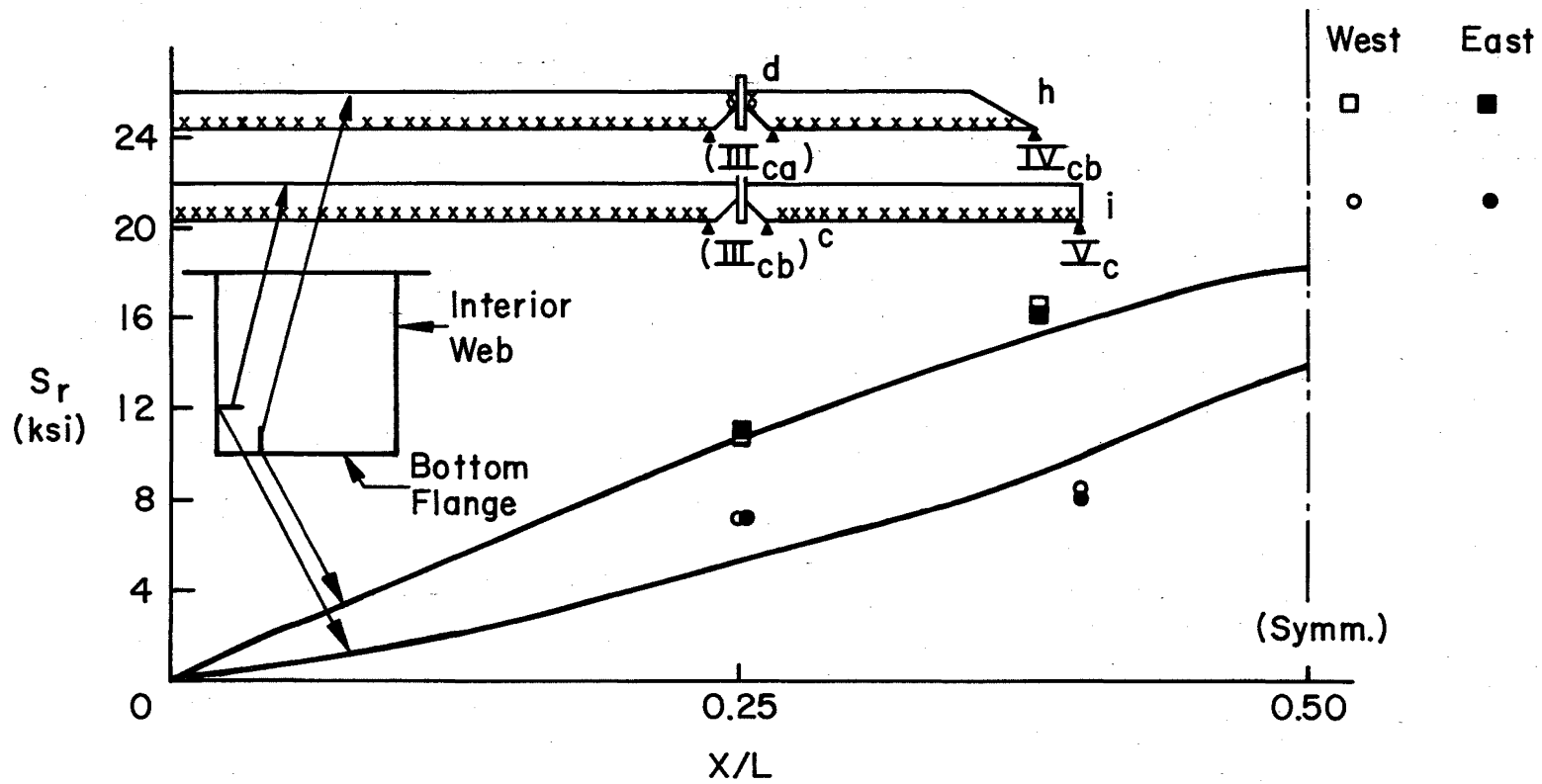


Fig. 30 Stress Range Profiles and Measured Stresses from Initial Static Load Test - Girder 2

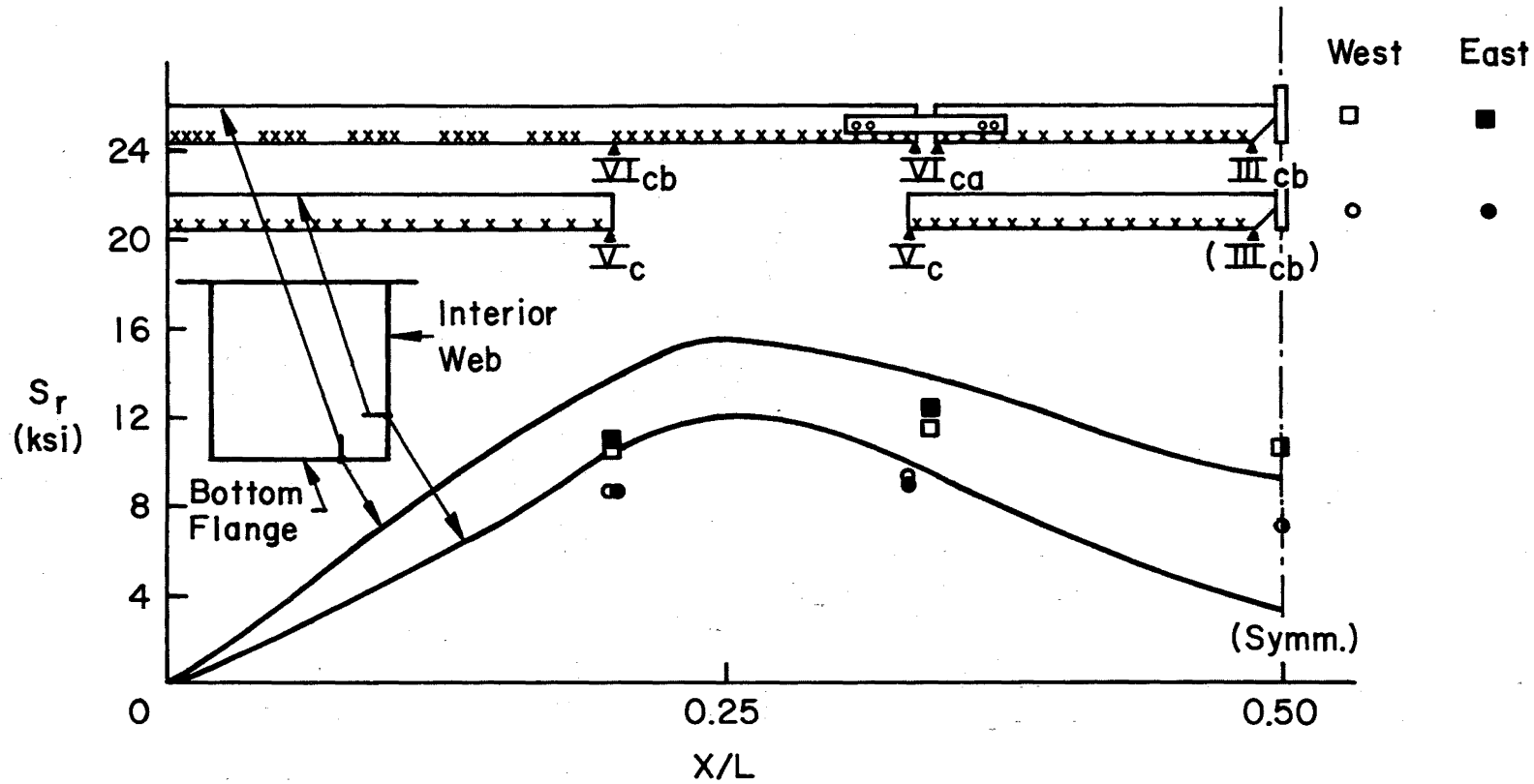


Fig. 31 Stress Range Profiles and Measured Stresses from Initial Static Load Test - Girder 3

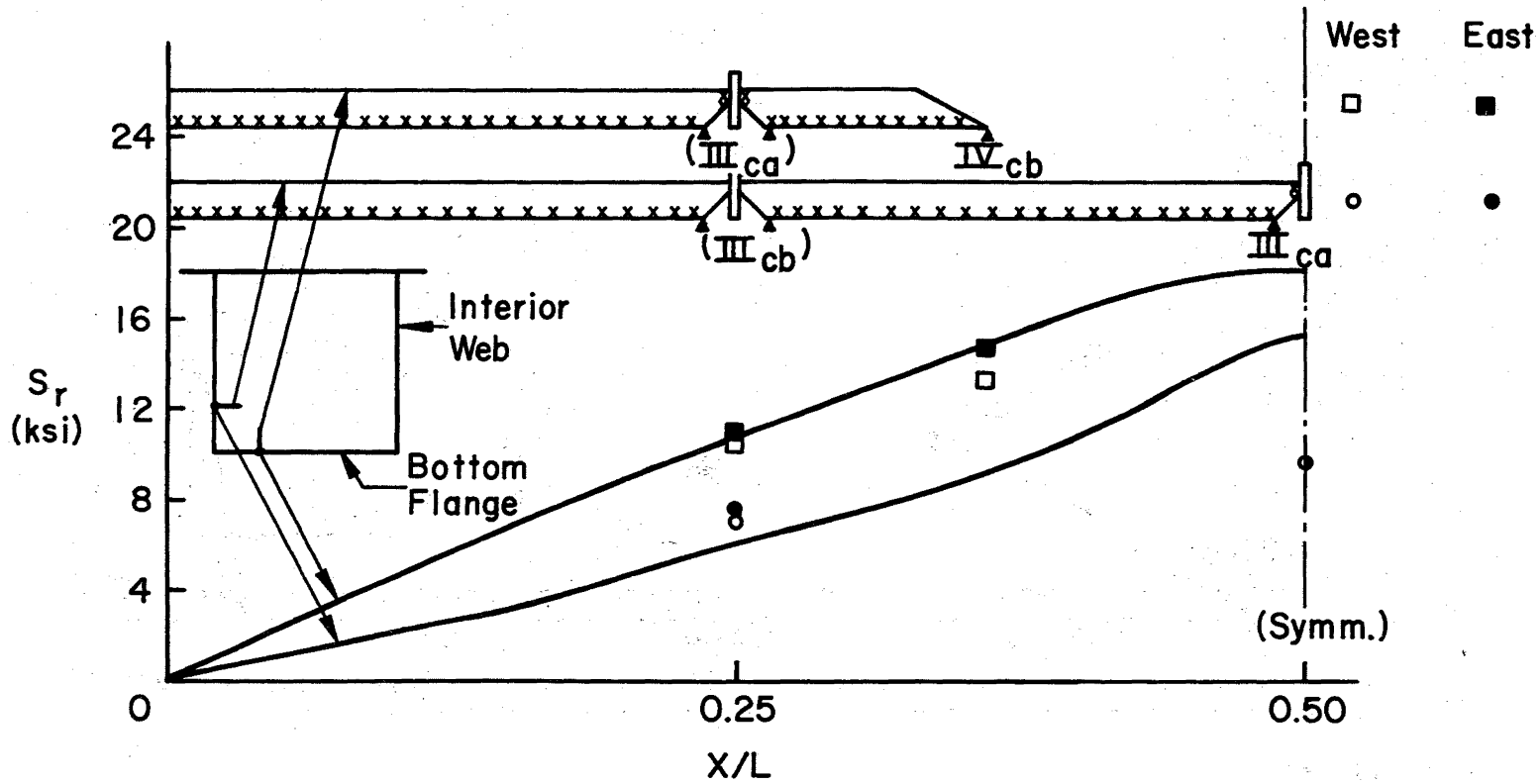


Fig. 32 Stress Range Profiles and Measured Stresses from Initial Static Load Test - Girder 3

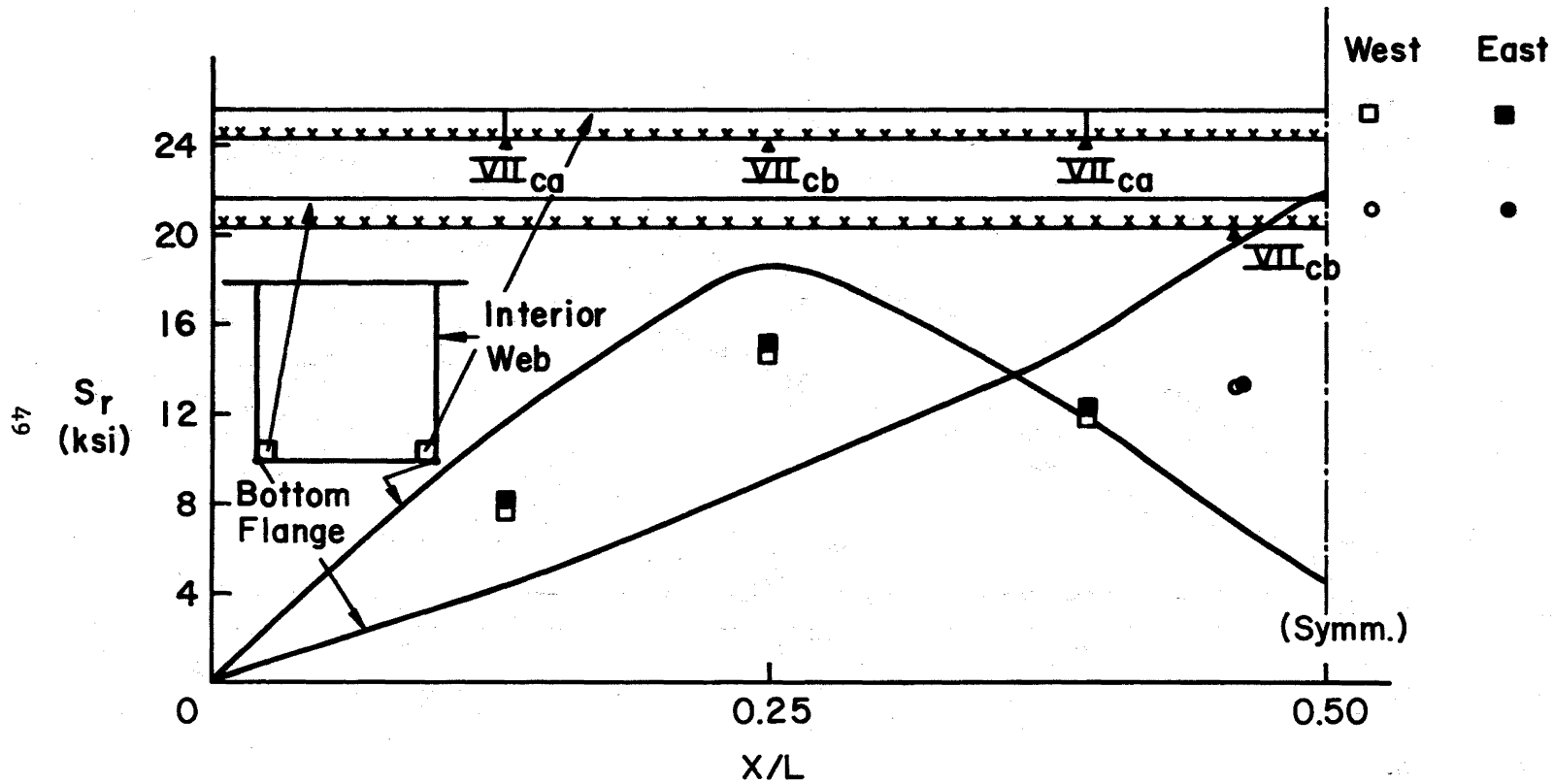


Fig. 33 Stress Range Profiles and Measured Stresses from Initial Static Load Test - Girder 3

The proper alignment of the girders in the dynamic test bed is indicated by the symmetry of the static load test results about midspan. Also, considering the complexity of the box girders, the predicted and measured stress range profiles show reasonable agreement.

Table 3 summarizes the predicted and measured vertical deflections at the interior diaphragm locations for a static load of 100 kips. The horizontal displacements are generally too small to be measured reliably.

4.2 Initial Cyclic Load Test

After checking the alignment of the girder by means of the initial static load test, the initial cyclic load test is then performed. The purpose of the initial cyclic load test is to determine the jack load range to be maintained throughout the fatigue testing and to obtain an initial record of the stress ranges near all details due to cyclic load.

The jack load range for a girder is selected by trying to match the stress range profiles measured in the initial cyclic load test to those provided by the finite element analysis of the given girder (Art. 2.1).⁽⁸⁾ In the analysis and design of each box girder the predicted stress range profiles were used to locate each welded detail so that all details would develop through cracks at approximately the same cycle life (as close to 2,000,000 as possible). Premature failure of one or more details would necessitate time-consuming and expensive fatigue crack repair to maintain the integrity of the girder for the duration of the test. By closely matching the measured and predicted stress range profiles, fatigue data can be obtained for all details with a minimum of fatigue crack repairs.

Preliminary cyclic load tests of the first girder tested, girder 3, were carried out with a load range of 50 kips per jack. Based on the results of these tests the required load range for the fatigue tests was estimated to be 95 to 100 kips with a minimum load of 8 to 10 kips to prevent uplift at the supports due to dynamic behavior. These values were used for the initial cyclic load tests of all girders.

During the initial cyclic load tests the stress range near all details and at each gage section was measured using the linear strain gages

Table 3 Predicted and Measured Vertical Deflections
at Interior Diaphragms

Girder	Joint Number (Fig. 1)	Predicted Vertical Deflection (in)	Measured Vertical Deflection (in)
1	3	0.351	0.360
	4	0.284	0.230
	5	0.422	0.477
	6	0.420	0.333
	7	0.351	0.373
	8	0.284	0.241
2	3	0.347	0.333
	4	0.282	0.247
	5	0.420	0.416
	6	0.414	0.342
	7	0.347	0.342
	8	0.282	0.247
3	3	0.339	0.316
	4	0.308	0.240
	5	0.410	0.394
	6	0.445	0.335
	7	0.339	0.322
	8	0.308	0.247

and ultraviolet oscillograph recorder (Art. 3.2). The midspan deflection was measured using the dial gage rig (Fig. 26).

The result of the initial cyclic load test was compared to the stress ranges predicted by the finite element analysis to determine if adjustments to the load range were required. The predicted stress range profiles and the measured stress ranges under cyclic loading shown in Figs. 34 through 40 were the basis for this determination. The continuous curves in Figs. 34 through 40 are the same stress range profiles presented in Figs. 27 through 33 and are symmetric about midspan. The measured stress ranges are plotted for both halves of the girder in order to illustrate the symmetry of the results about midspan. The circles and squares denote the measured stress ranges at the Group 2 and Group 3 details shown at the top of each figure. The solid and open symbols represent details on the east and west halves of the girder, respectively.

The measured stress range profiles show a slight change in shape from the predicted stress range profiles for all three girders. In general, the measured stress ranges are higher than predicted along the outer web and lower than predicted along the inner web. This shift makes the failure of different details at different times inevitable. The approach adopted was to use a jack load range near the dynamic capacity of the Amsler equipment and make the necessary repairs of the details that fail prematurely due to unintentionally high stress ranges.

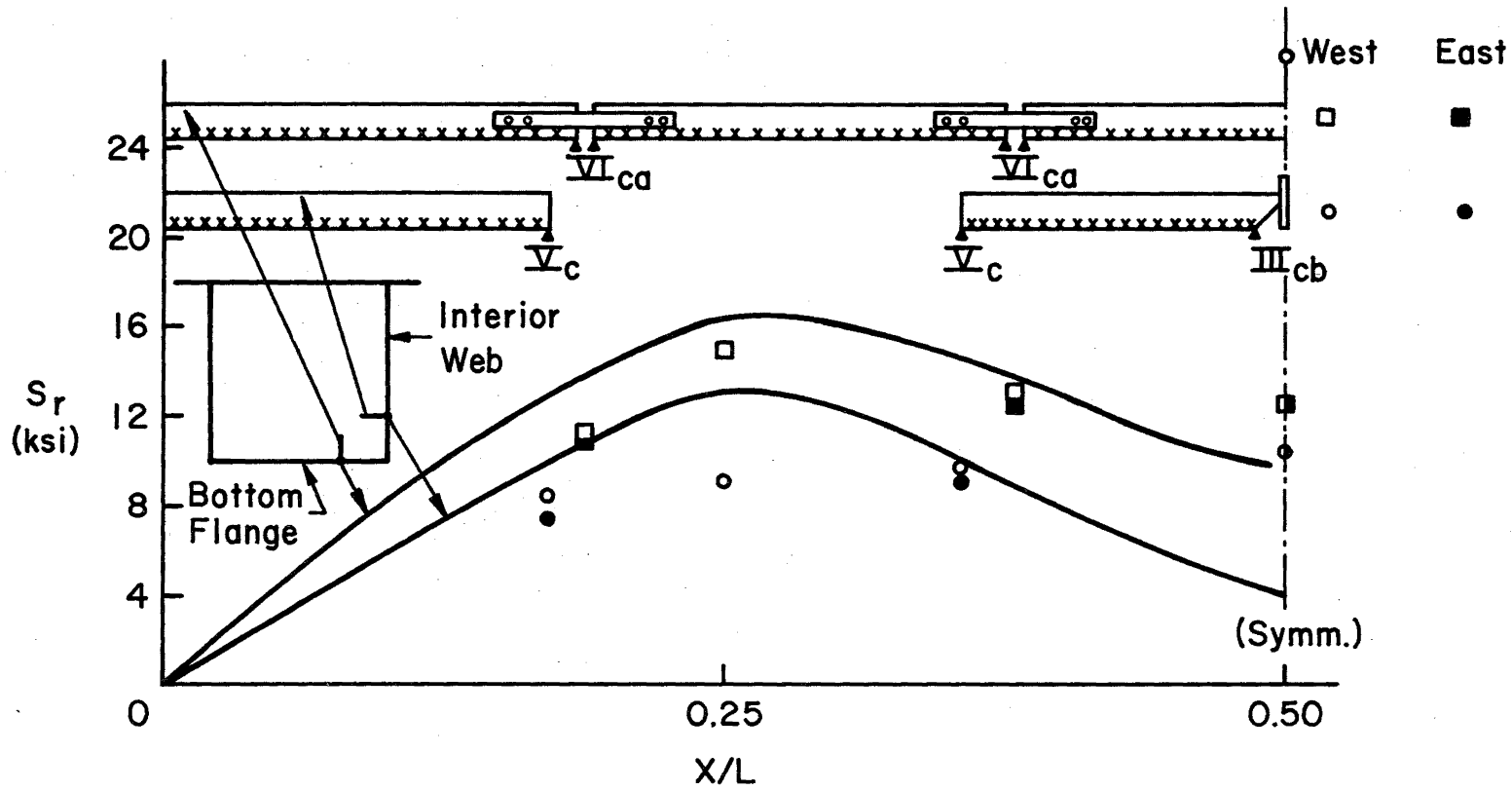


Fig. 34 Stress Range Profiles and Measured Stress Ranges under Cyclic Loading - Girder 1
(Jack Load Range - 10 to 107 kips)

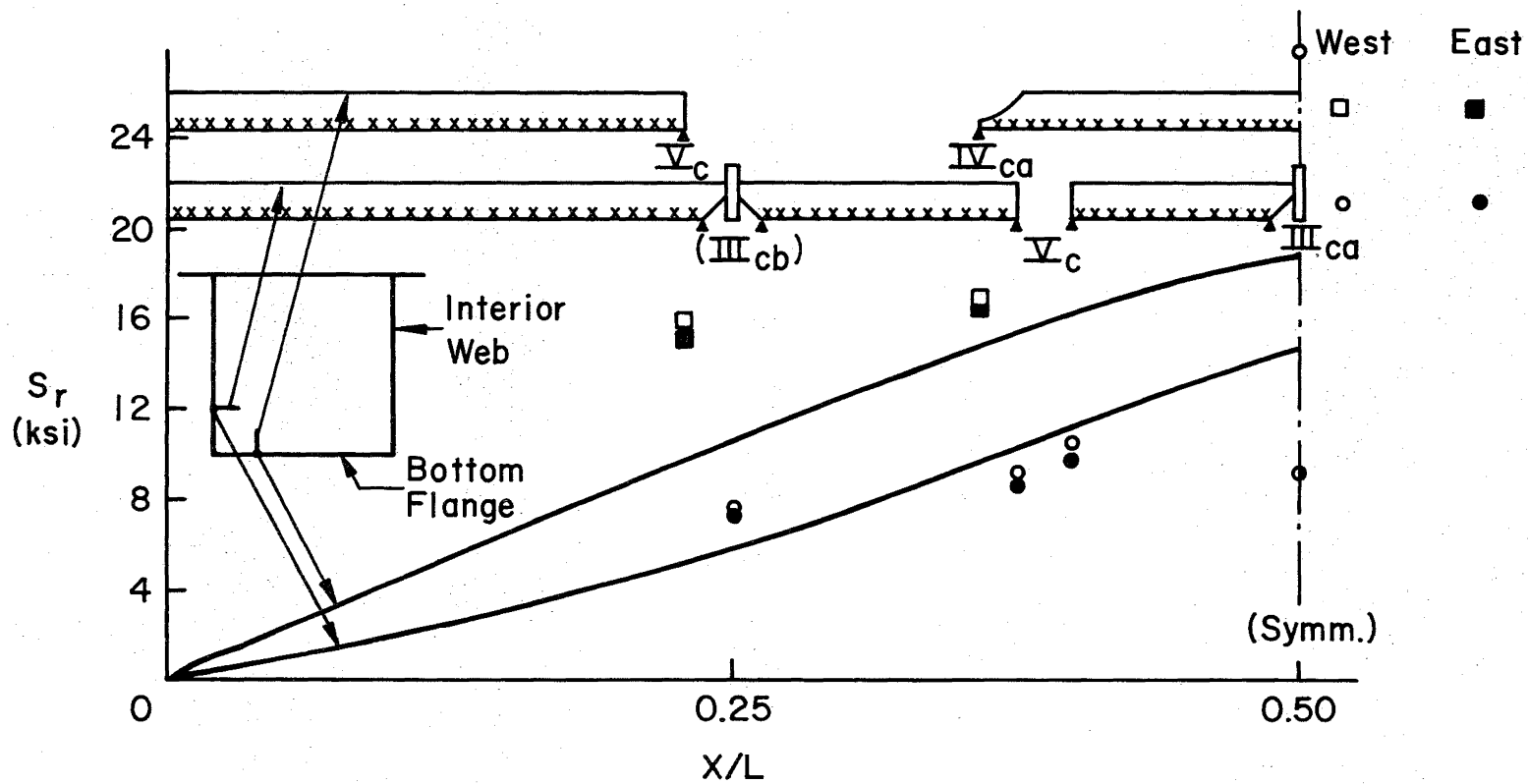


Fig. 35 Stress Range Profiles and Measured Stress Ranges under Cyclic Loading - Girder 1 (Jack Load Range - 10 to 107 kips)

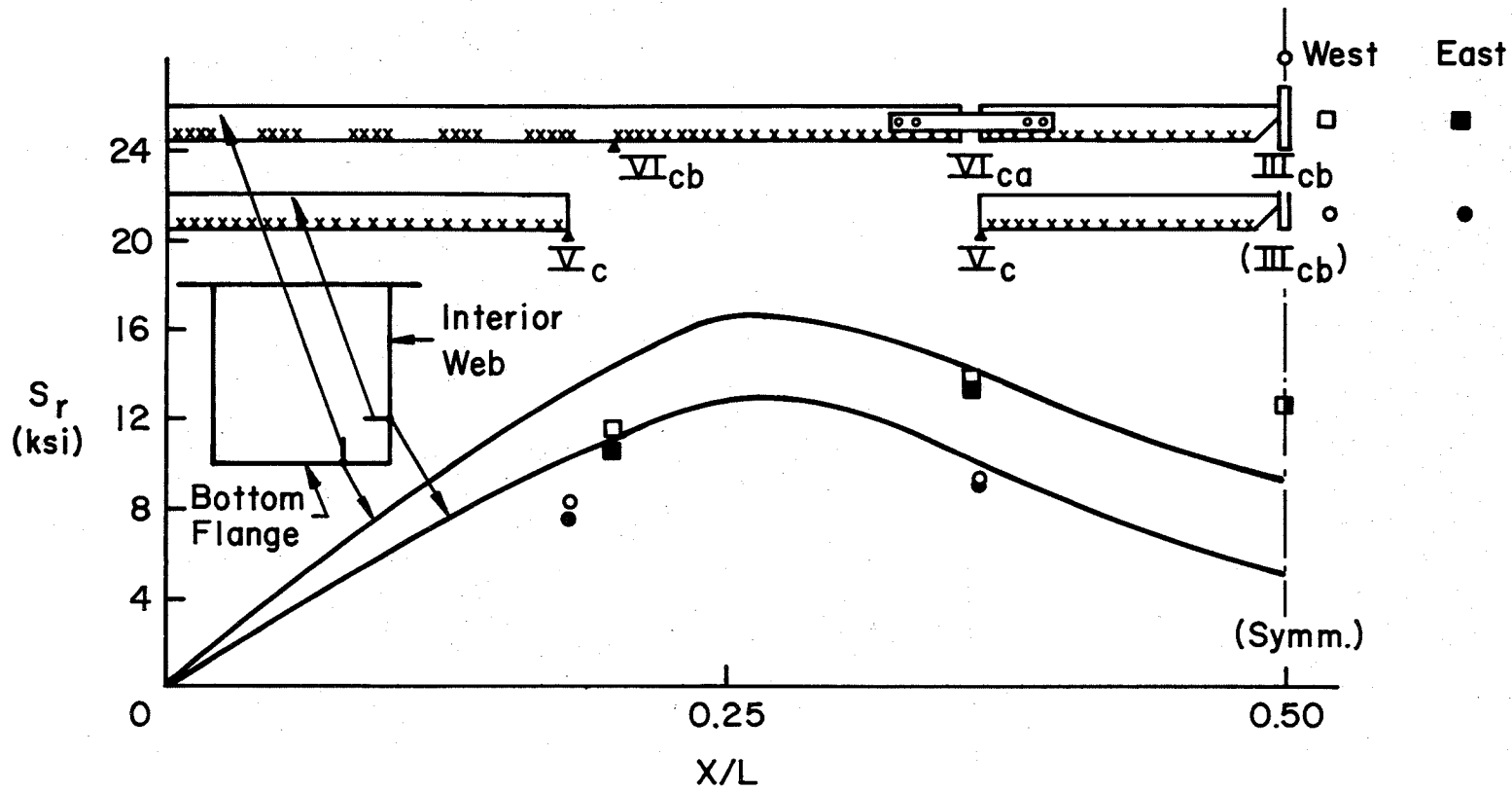


Fig. 36 Stress Range Profiles and Measured Stress Ranges under Cyclic Loading - Girder 2 (Jack Load Range - 11 to 109 kips)

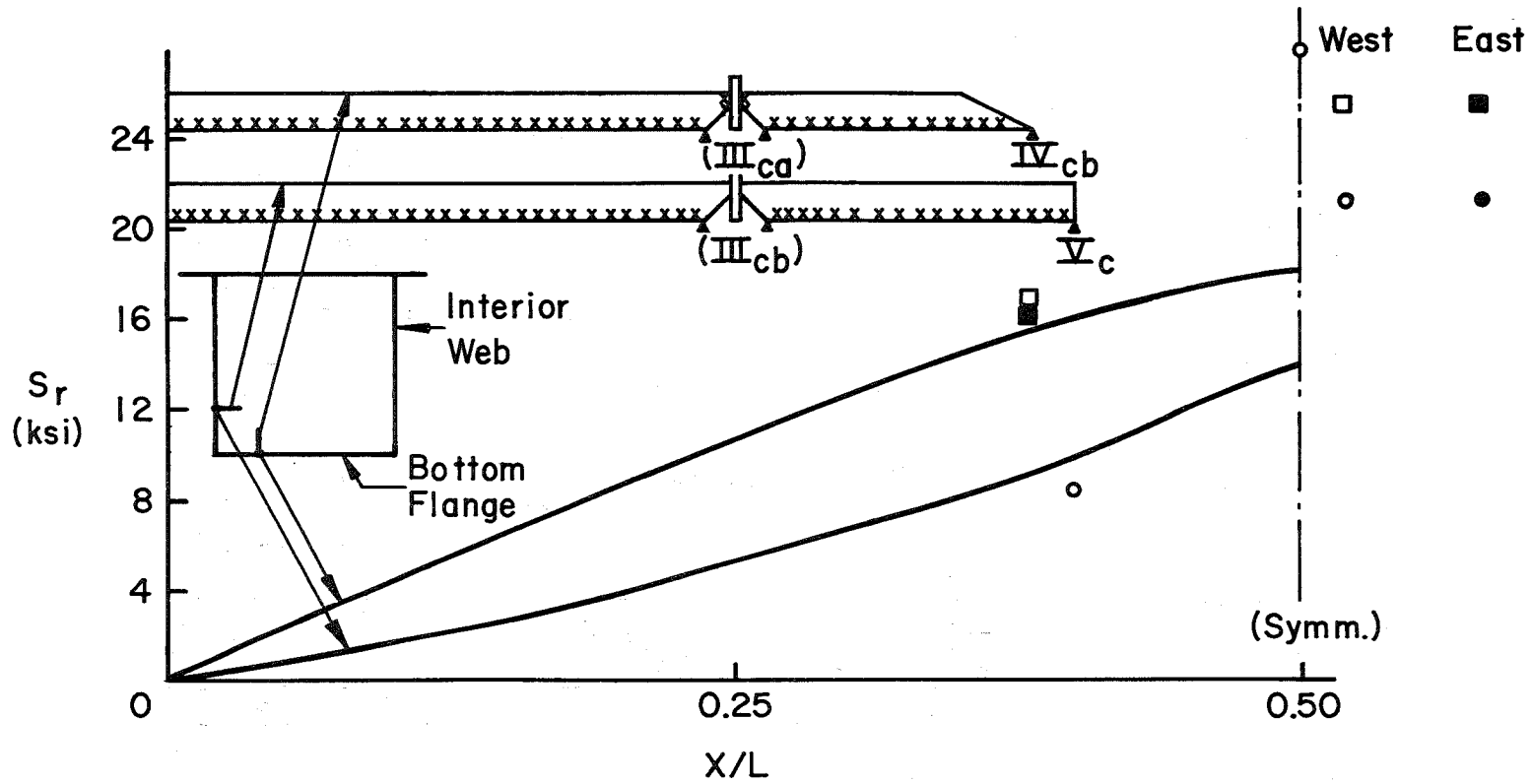


Fig. 37 Stress Range Profiles and Measured Stress Ranges under Cyclic Loading - Girder 2 (Jack Load Range - 11 to 109 kips)

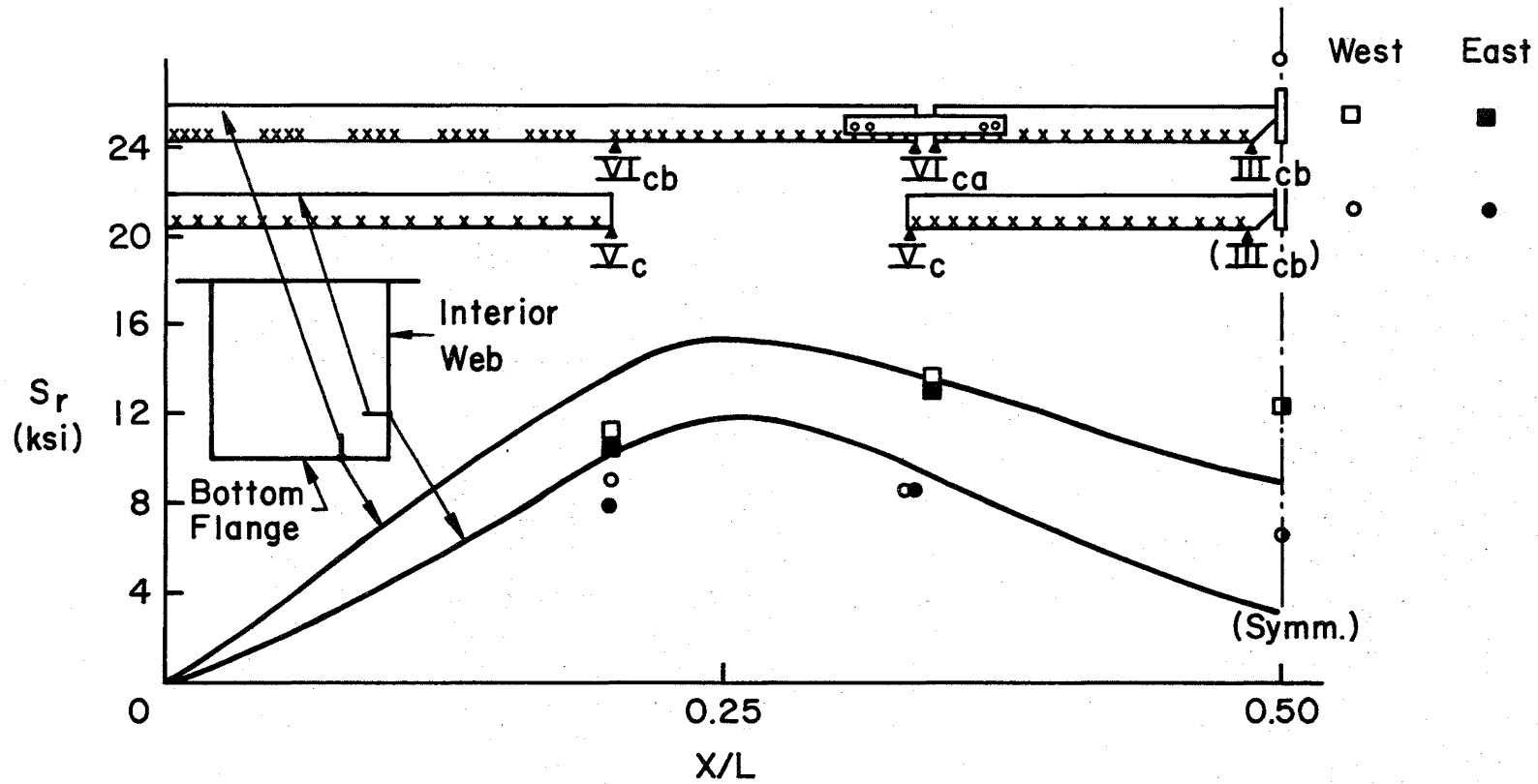


Fig. 38 Stress Range Profiles and Measured Stress Ranges under Cyclic Loading - Girder 3 (Jack Load Range - 9 to 109 kips)

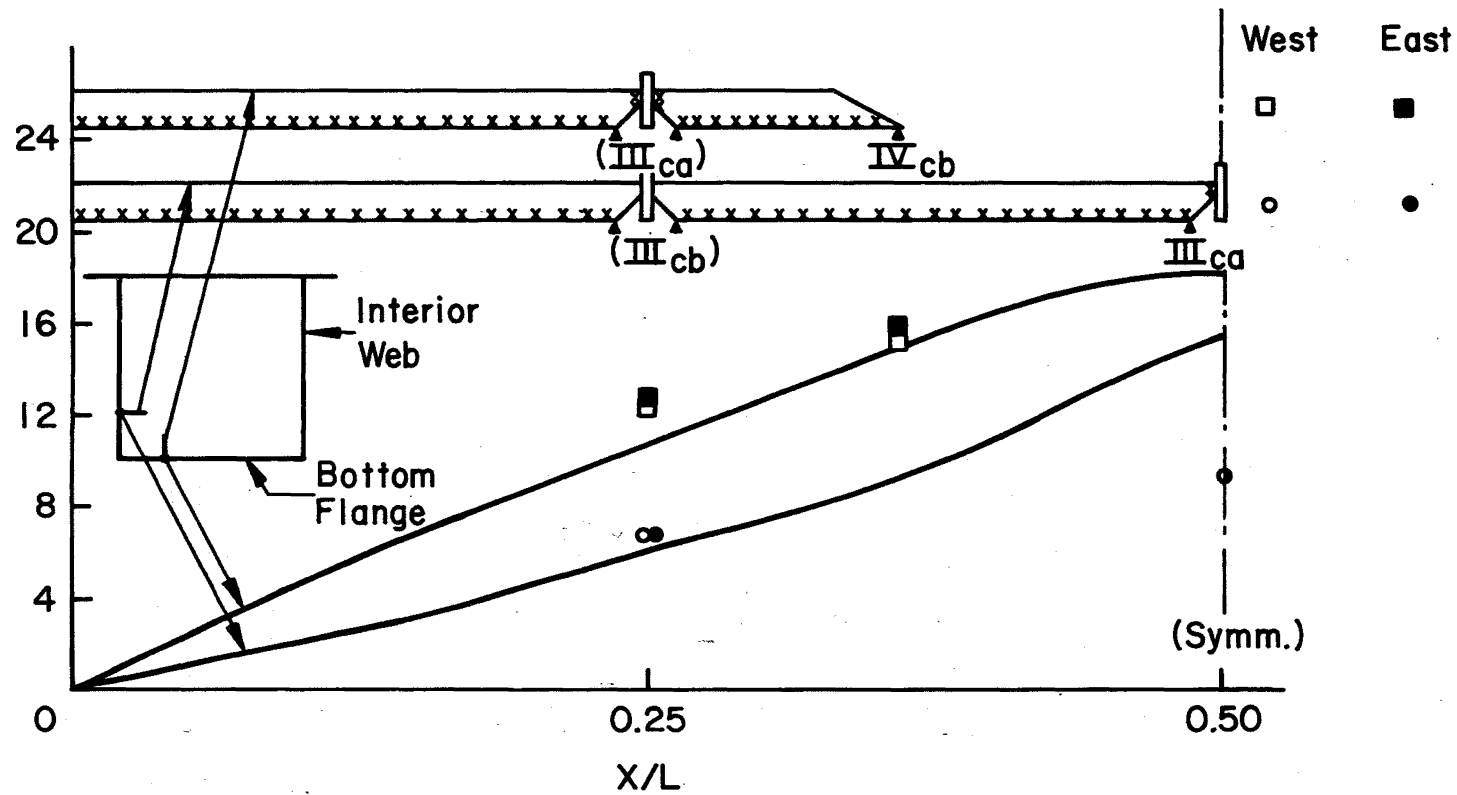


Fig. 39 Stress Range Profiles and Measured Stress Ranges under Cyclic Loading - Girder 3 (Jack Load Range - 9 to 109 kips)

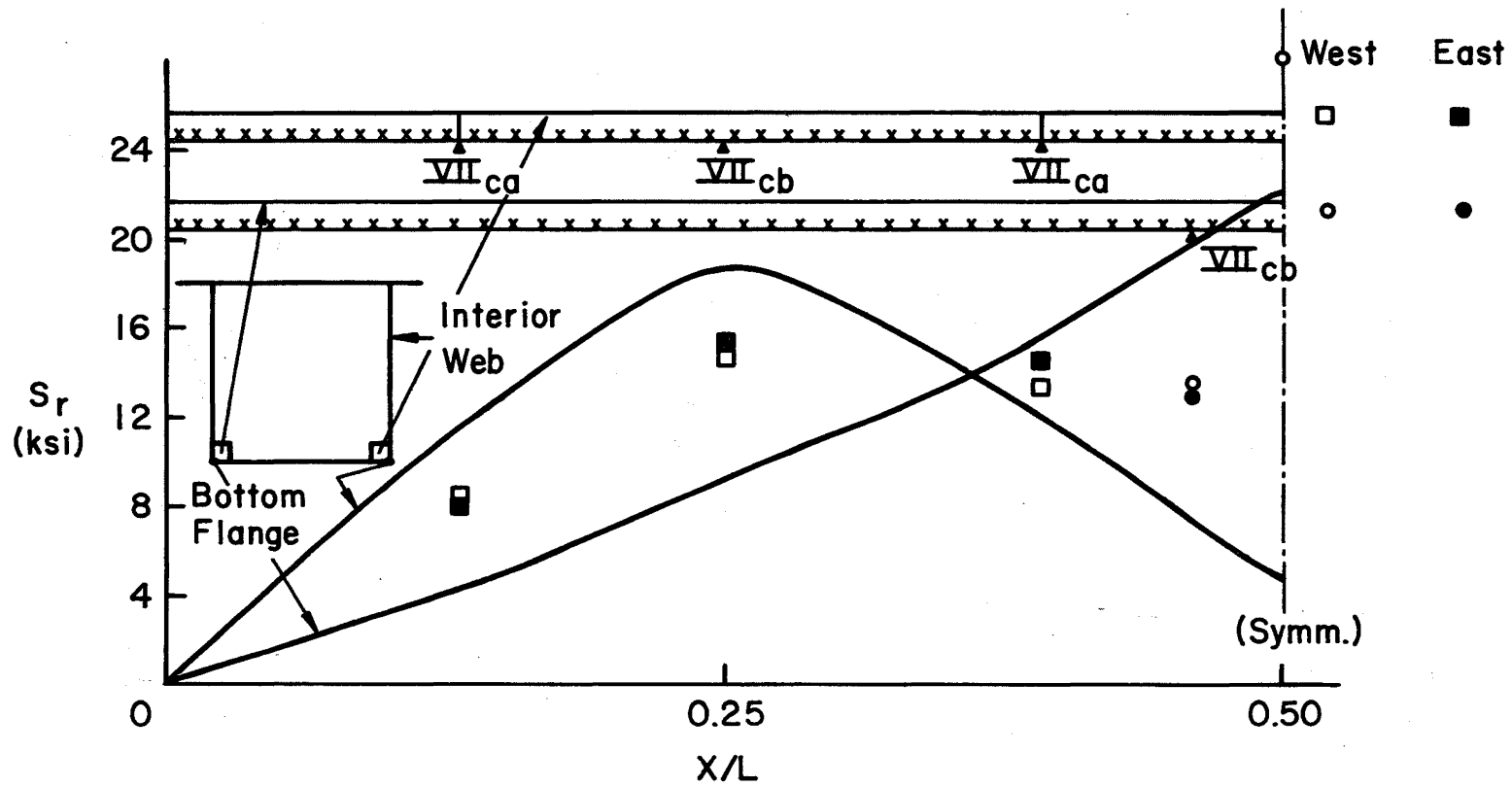


Fig. 40 Stress Range Profiles and Measured Stress Ranges under Cyclic Loading - Girder 3 (Jack Load Range - 9 to 109 kips)

5. FATIGUE TESTING

5.1 General Procedure

After performing the initial static and cyclic load tests, a girder is ready for fatigue testing. Each girder is subjected to a constant cyclic load range selected on the basis of the cyclic load test results. The constant amplitude load cycles are applied at a rate of approximately 250 cycles per minute. Frequent inspection of the girders monitors fatigue crack growth at the welded details under study. Additional cyclic load tests are performed at approximately 250,000 cycle intervals to record the stress ranges at the details throughout the fatigue tests.

The girders were tested in the following order: Girder 3, Girder 1, and Girder 2. The order of testing was arbitrary.

The fatigue testing of Girder 3 required 7 weeks due to initial problems with excessive noise and support motion as well as extensive repairs of the interior diaphragms which were required early in the tests. Girder 3 was subjected to a cyclic load range of 100 kips with a 9 kip minimum load. The average midspan deflection was 0.405 in. as measured by the double dial gage rig. Girder 3 was subjected to 2.25 million constant amplitude load cycles.

The fatigue tests of Girder 1 went smoothly. The time required to complete the fatigue testing was four weeks. The girder was subjected to a cyclic load range of 97 kips with a minimum load of 10 kips. The average measured midspan deflection was 0.430 in. The fatigue test of Girder 1 ended at 2.02 million cycles.

The fatigue testing of Girder 2 also required 4 weeks. A cyclic load range of 98 kips and minimum load of 11 kips were applied. The average measured midspan deflection was 0.421 in. The fatigue test of Girder 2 was suspended at 1.47 million cycles when repair of the fatigue cracks which developed in the bottom flange near the west quarter-point could not be continued and still maintain the integrity of the girder. This condition was anticipated because of the high stress range which existed at this point.

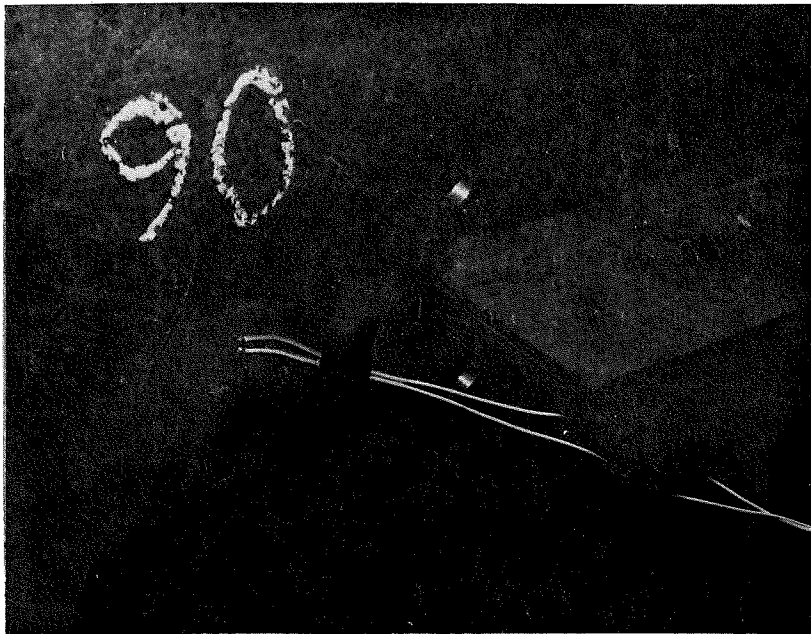


Fig. 41 Holes Drilled through the Web to
Blunt Tip of a Through Crack at
a Type V_c Detail



Fig. 42 High-Strength Bolted Splice across
a Through Crack Originating at a
Type VII_{ca} Detail
(Viewed from Beneath Girder 3)

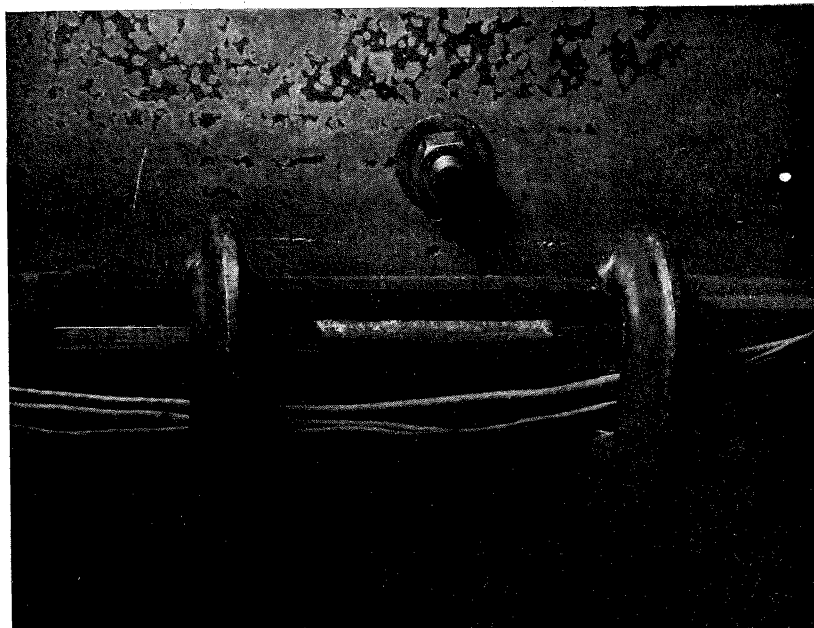


Fig. 43 High-Strength Bolt Installed in a Hole Drilled at the Tip of a Through Crack

5.2 Crack Detection and Repair

During the fatigue testing, each girder was frequently inspected for visible fatigue cracks. The inspections were made at approximately 75,000 cycle intervals and normally under a static load of about 50 kips per jack. Most visual inspections were made with a 10X magnifying glass and a cleaner fluid. The cleaner fluid is sprayed on the metal surface and seeps into a crack if one is present. As the fluid on the flat surface rapidly evaporates the distinct line of a crack becomes visible due to the liquid in the crack. This inspection method proved very efficient and productive in inspecting the large number of potential crack locations on each girder.

The frequent visual inspections concentrated on monitoring primary fatigue crack growth at the Group 2, 3, and 4 details. Careful inspection of the Group 1 details associated with the interior diaphragms was also performed to monitor both primary and secondary fatigue crack growth. In addition to the above inspections the entire girder was checked approximately every 200,000 cycles to ensure the safety and integrity of the girder throughout the fatigue tests.

When a visible crack is discovered its location is recorded along with the present number of load cycles on the girder. If the crack is not through the thickness of a web or flange no repairs are made immediately, but the growth of the crack is monitored. When a crack has grown through the web or flange thickness, or is initially discovered as a through crack, then repairs are made to prevent premature failure of the girder. The crack repair could consist of drilling a hole to blunt the crack tip as shown in Fig. 41, or bolting splice plates over the cracked section as in Fig. 42 or both. The extent of the repairs and the sizes of drilled holes and/or splice plates depends upon the location and size of the fatigue crack. Examples of two other types of crack repair used extensively on the box girders are shown in Fig. 43. The one repair consists of a 1-1/16" diameter hole drilled near the leading tip of a fatigue crack. A 1" diameter A325 high-strength bolt is then installed in the hole and tightened $\frac{1}{2}$ turn beyond the snug position. This simple repair proved very effective in arresting fatigue crack growth. The second repair used splice plates clamped to the projecting edge of the bottom flange when an

edge crack was present. This type of repair was most effective in the plate girder tests reported in Ref. 15. It is not so effective for box girders however because of the difficulty of clamping to the girder. Further comments on the effectiveness of the methods of fatigue crack repair used are provided in Appendix C. The purpose of the fatigue crack repair was to allow each girder to reach 2 million cycles, if possible, without impairing the integrity of the girder. This goal was achieved on Girders 1 and 3. The fatigue testing of Girder 2 was cut off at 1.47 million cycles because the repairs required to continue testing were not feasible. Since most of the required data had already been obtained by 1.47 million cycles the necessary repair to allow 2.0 million cycles to be reached could not be economically justified.

6. RESULTS OF FATIGUE TESTS

In the following articles the terms primary and secondary fatigue crack growth are used to differentiate between two types of fatigue crack growth. Primary fatigue crack growth is caused by the longitudinal normal stress ranges produced primarily by bending and warping torsion. Secondary fatigue crack growth is caused by transverse forces at the diaphragms and the introduction of out-of-plane forces and displacements to the webs and flanges.

6.1 Primary Fatigue Crack Growth

Primary fatigue crack growth occurred at nearly all the welded details placed on the three girders as expected (Tables 1 and 2). Figures 44 through 46 are schematic diagrams showing the locations of the welded details on each girder. Elevations of the north and south webs (as viewed from the south) are shown above and below the plan view. All details are symmetric about midspan.

Each detail location is identified by an alphanumeric designation. The locations of the Group 1 details (Art. 2.2) are assigned numbers corresponding to the web-diaphragm joints (Fig. 1) at which the details are placed. The locations of the Group 2, 3, and 4 details (Art. 2.2) are identified by a letter or letters as shown in Figs. 44 through 46. Details to the west of midspan are identified by a single letter such as a, b, c, etc. The corresponding symmetric details to the east of midspan are identified by double letters such as aa, bb, cc, etc. For example, on Girder 1, the Type V_c details located at potential crack locations a and aa are symmetric with respect to midspan. These details should experience nearly identical nominal stress ranges and fail at approximately the same number of cycles.

The measured nominal stress ranges for all potential crack locations are presented in Tables 4 through 6. The number of cycles at which visible and through-thickness cracks were discovered is also presented in the right-hand columns of these tables. Potential crack locations which did not develop visible cracks by the end of the testing of each assembly have no entries in these columns.

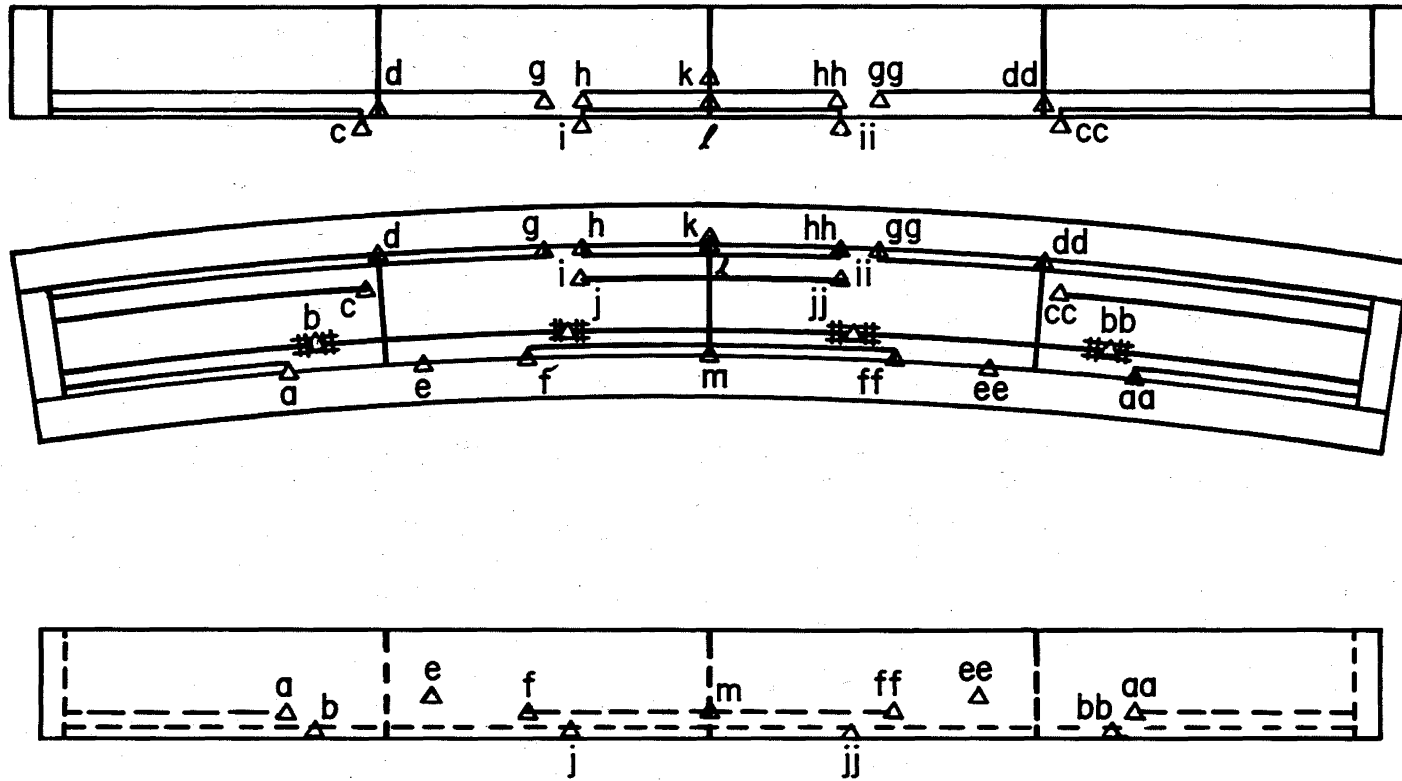


Fig. 44 Potential Crack Locations - Girder 1

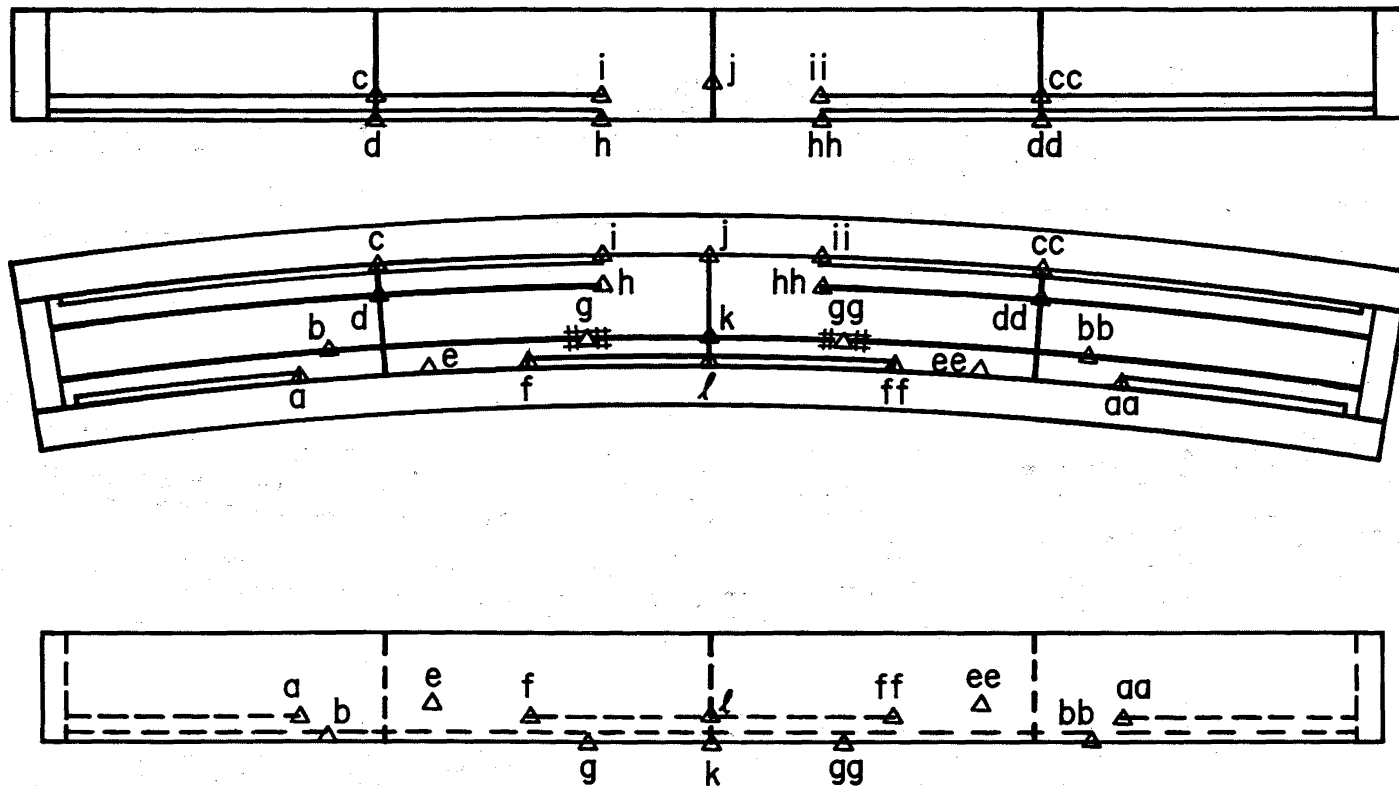


Fig. 45 Potential Crack Locations - Girder 2

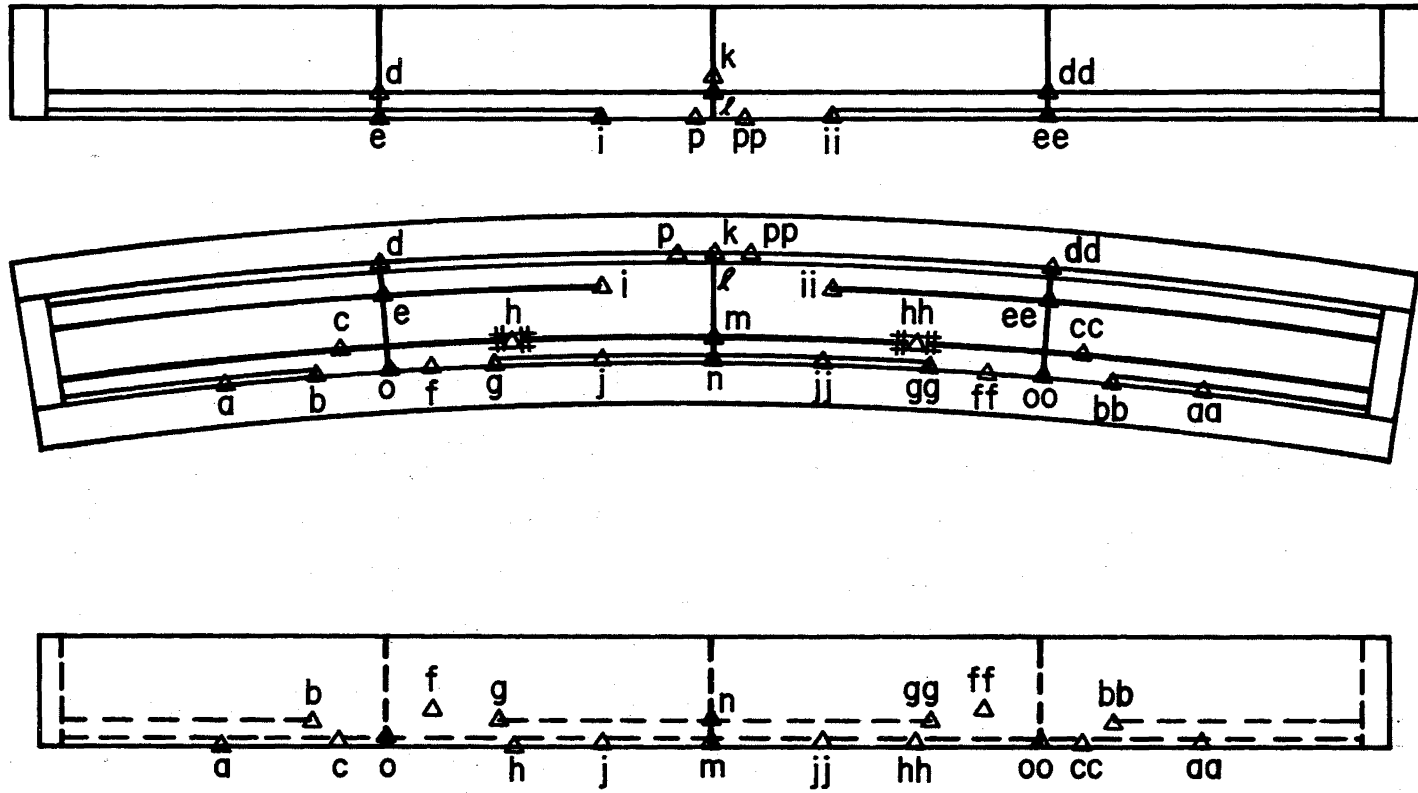


Fig. 46 Potential Crack Locations - Girder 3

The nominal stress ranges shown in Tables 4 through 6 are based on the cyclic load tests which were performed at regular intervals throughout the fatigue tests as described in Arts. 4.2 and 5.1. The nominal stress ranges were computed from strains measured by the strain gages located near the gage sections (Figs. 18 through 23) and at the welded details (Table 1). The computations made use of the predicted and measured stress range profiles (Figs. 34 through 40) to adjust the strains to account for the small distance between the strain gages and the potential crack locations.

In Tables 4 through 6 the number of cycles required to develop visible and through-thickness cracks are shown in millions of cycles. This data was obtained from records of the regular inspections of each assembly at approximately 75,000 cycle intervals. A detail is assumed to have failed when a through-thickness crack develops since the remaining useful life of the detail is generally negligible.

The fatigue test results presented in Tables 4 through 6 are also shown in the form of S_r vs. N diagrams in Figs. 47 through 59. These diagrams relate the number of cycles, N , required to develop a visible or through-thickness crack to the nominal stress range, S_r , at the detail. A set of S_r - N diagrams is shown for each girder. All details on a given girder belonging to a particular AASHTO detail category are shown on a single S_r - N diagram. The corresponding AASHTO detail category design curve is also shown.

In Figs. 47 through 59 the open symbols with a horizontal arrow extending to the right signify that the given detail did not develop a visible crack in the course of the fatigue tests. An open symbol denotes the number of cycles at which a visible crack was discovered. A solid symbol indicates the number of cycles at which a through-thickness crack was discovered. An open symbol connected to a solid symbol by a horizontal line indicates a crack, initially discovered as a visible crack, which later developed into a through crack at the corresponding number of cycles.

6.2 Secondary Fatigue Crack Growth

Due to the very local nature of the stresses involved, it is not possible to consider secondary fatigue crack growth in terms of the

Table 4 Measured Nominal Stress Ranges at Potential Crack Locations and Cycles to Visible and Through Cracks - Girder 1

Detail Type	AASHTO Fatigue Category	Potential Crack Location	Measured S_r (ksi)	Cycles (10^6)	
				Visible Crack	Through Crack
I _{ca}	C	3	16.3		1.460
		(4)	13.5		
		(5)	12.4		
		6	13.9	0.912*	1.460
		7	16.3	0.912*	1.460
		(8)	13.5		
III _{ca}	C-D	l	9.2		
III _{cb}	E	(d)	8.3		
		(dd)	8.3		1.564
		m	10.4	0.829	0.860
IV _{ca}	C	i	16.9	0.460	0.701
		ii	16.3	0.829	1.077
V _c	E	a	8.4		
		aa	7.5		
		c	14.6		0.460
		cc	15.1	0.460	0.770
		f	9.5	0.829	1.077
		ff	9.1	1.214	1.460
		g	9.2	1.214	1.460
		gg	9.0		1.671
		h	10.6		
		hh	9.5	1.214	1.460
VI _{ca}	C-D	b	11.2		
		bb	10.8		
		j	13.1		
		jj	12.7		
VIII _c	D	e	9.1		
		ee	8.7		
		k	4.7		

No entries in the last two columns implies no visible or through cracks were found at the detail by 2.02 million cycles.

*Crack initiated by secondary fatigue crack growth at diaphragm (see Arts. 6.2 and 7.2).

Table 5 Measured Nominal Stress Ranges at Potential Crack Locations and Cycles to Visible and Through Cracks - Girder 2

Detail Type	AASHTO Fatigue Category	Potential Crack Location	Measured S_r (ksi)	Cycles (10^6)	
				Visible Crack	Through Crack
I _{cb}	C	3	16.1	1.392	1.467
		(4)	13.0		1.101
		(5)	11.6		
		6	14.1		1.272
		7	16.1		
		(8)	13.0		
III _{ca}	C-D	(d)	11.6	0.661	1.021*
		(dd)	11.4	0.853	
III _{cb}	E	(c)	7.2	0.740	1.021*
		(cc)	7.2		
		k	12.5	0.584	
		(l)	8.0		
IV _{cb}	C	h	16.9	0.383	0.853
		hh	16.2	0.661	1.021
V _c	E	a	8.2	0.853	1.392
		aa	7.4		
		f	9.2		
		ff	9.1		
		i	8.5		
		ii	8.4		
VI _{ca}	C-D	g	13.7	1.101	
		gg	13.2		
VI _{cb}	C-D	b	11.4		
		bb	10.5		
VIII _c	D	e	7.9		
		ee	7.5		
		j	4.30		

*Fatigue cracks repaired at 1.021 million cycles prior to becoming through-thickness cracks.

Table 6 Measured Nominal Stress Ranges at Potential Crack Locations and Cycles to Visible and Through Cracks - Girder 3

Detail Type	AASHTO Fatigue Category	Potential Crack Location	Measured S_r (ksi)	Cycles (10^6)	
				Visible Crack	Through Crack
I _{cb}	C	(5)	13.0		
		6	13.7		
II _c	C	3	14.6	0.463*	
		(4)	11.4		
		7	14.4	0.463*	1.135
		(8)	11.0		
III _{ca}	C-D	(e)	12.2	0.084*	
		(ee)	12.6		
		l	9.2		
III _{cb}	E	(d)	6.6		
		(dd)	6.6		
		m	12.6		
		(n)	6.8		
IV _{cb}	C	i	15.2	0.971	1.369
		ii	15.7	0.971	1.369
V _c	E	b	9.2		
		bb	8.1		
		g	8.7		1.556
		gg	8.7		1.761
VI _{ca}	C-D	h	13.9		
		hh	13.2		
VI _{cb}	C-D	c	11.4		
		cc	10.6		
VII _{ca}	E	a	8.2	0.084	1.500
		aa	8.0	0.084	1.761
		j	13.3	0.084	0.541
		jj	14.5	0.084	0.463
VII _{cb}	B	o	14.6		
		oo	15.5		
		p	13.5		
		pp	12.9		
VIII _c	D	f	9.7		
		ff	9.0		
		k	6.0		

*Crack initiated by displacement-induced secondary fatigue crack growth at diaphragm (see Arts. 6.2 and 7.2).

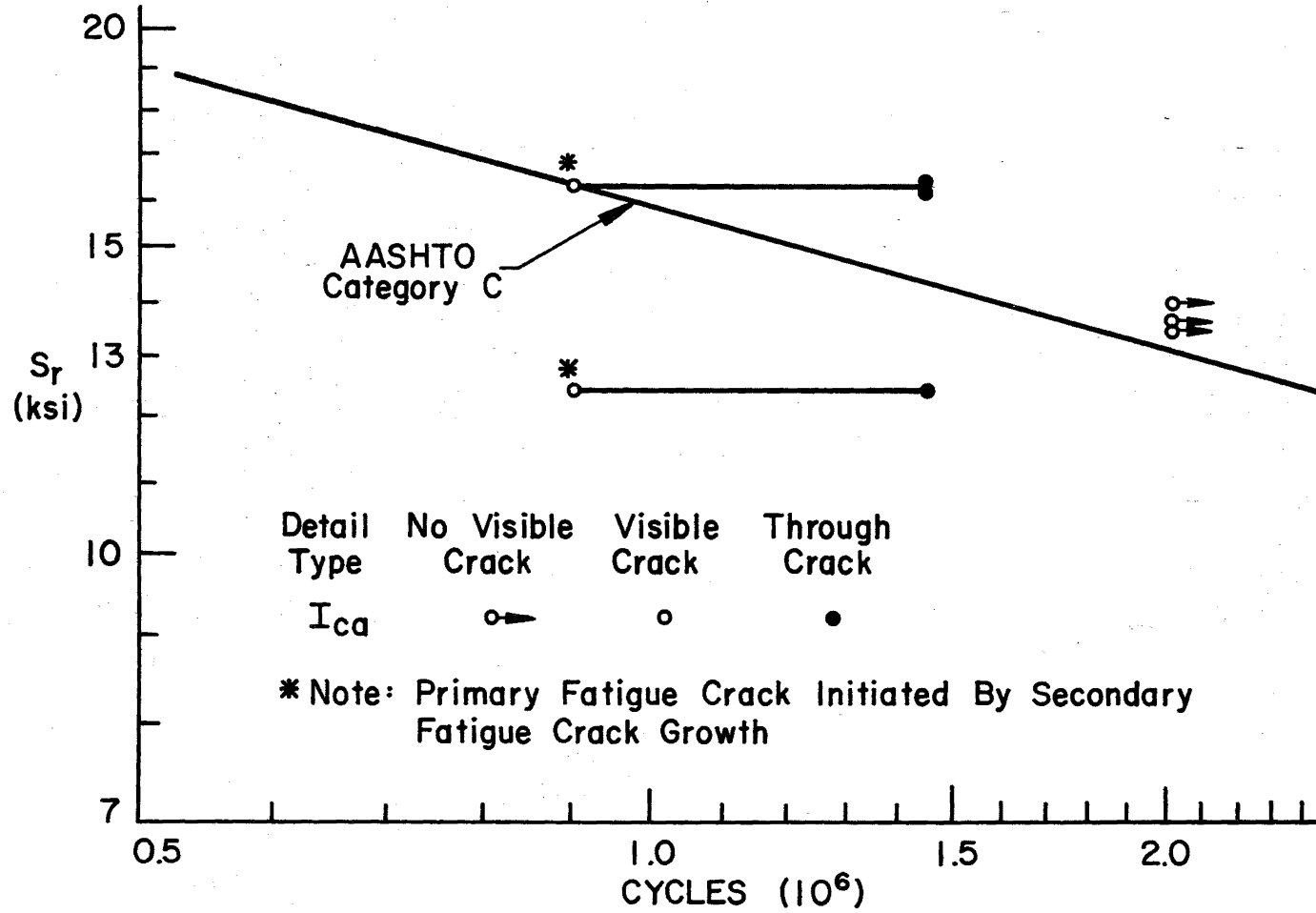


Fig. 47 Fatigue Results - Girder 1 - Category C Group 1 Details

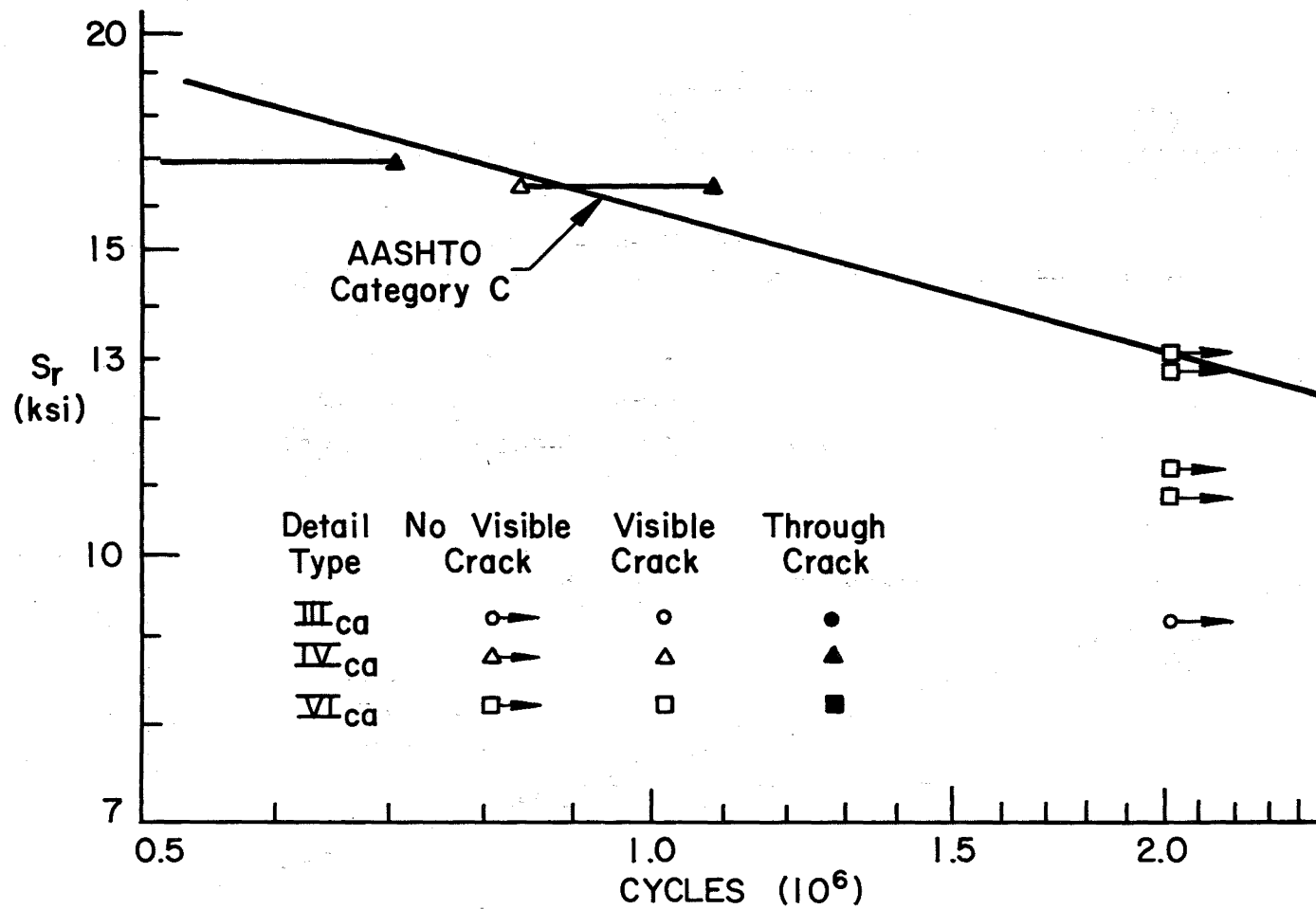


Fig. 48 Fatigue Results - Girder 1 - Category C
Group 2, 3, and 4 Details

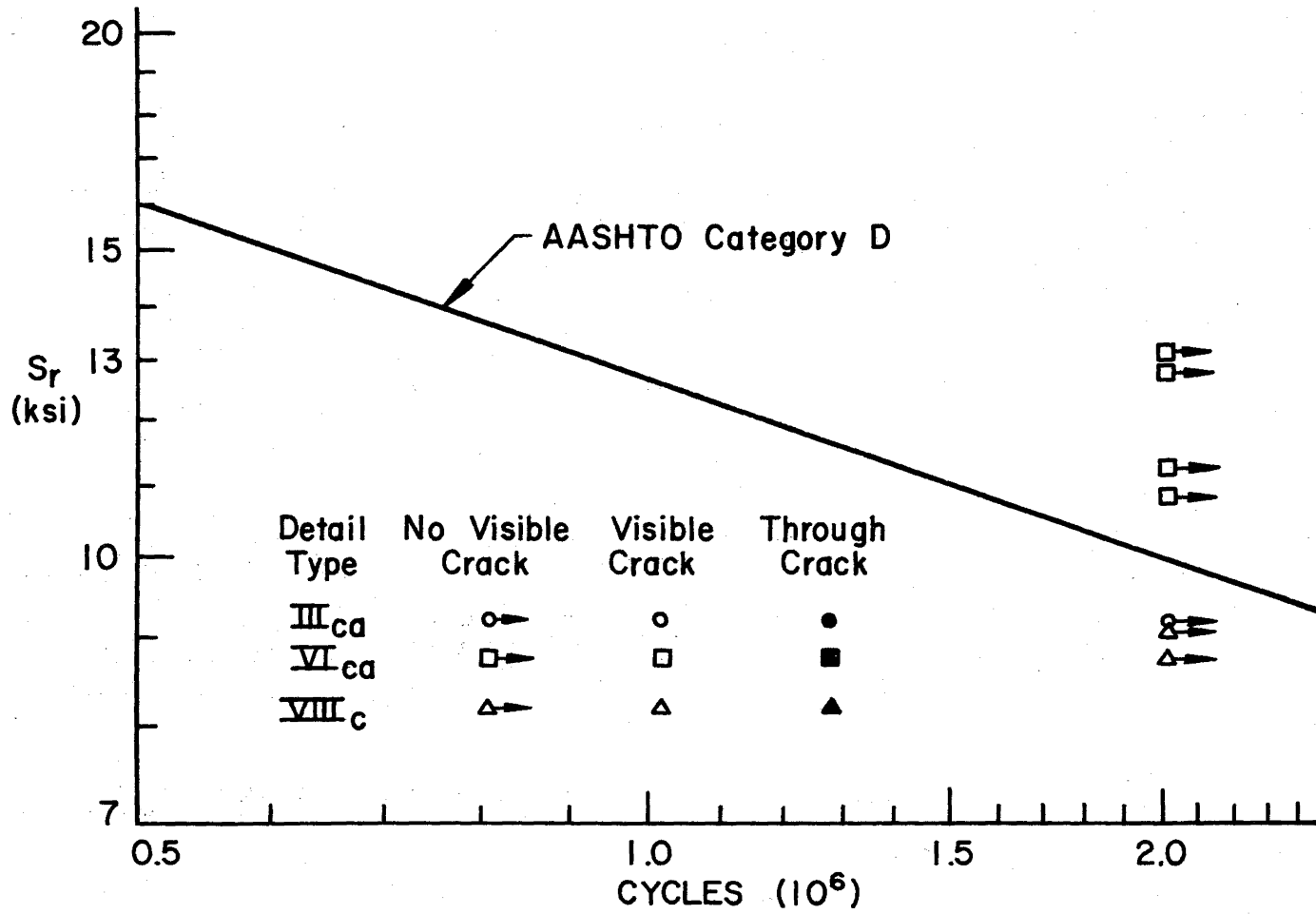


Fig. 49 Fatigue Results - Girder 1 - Category D
Group 2, 3 and 4 Details

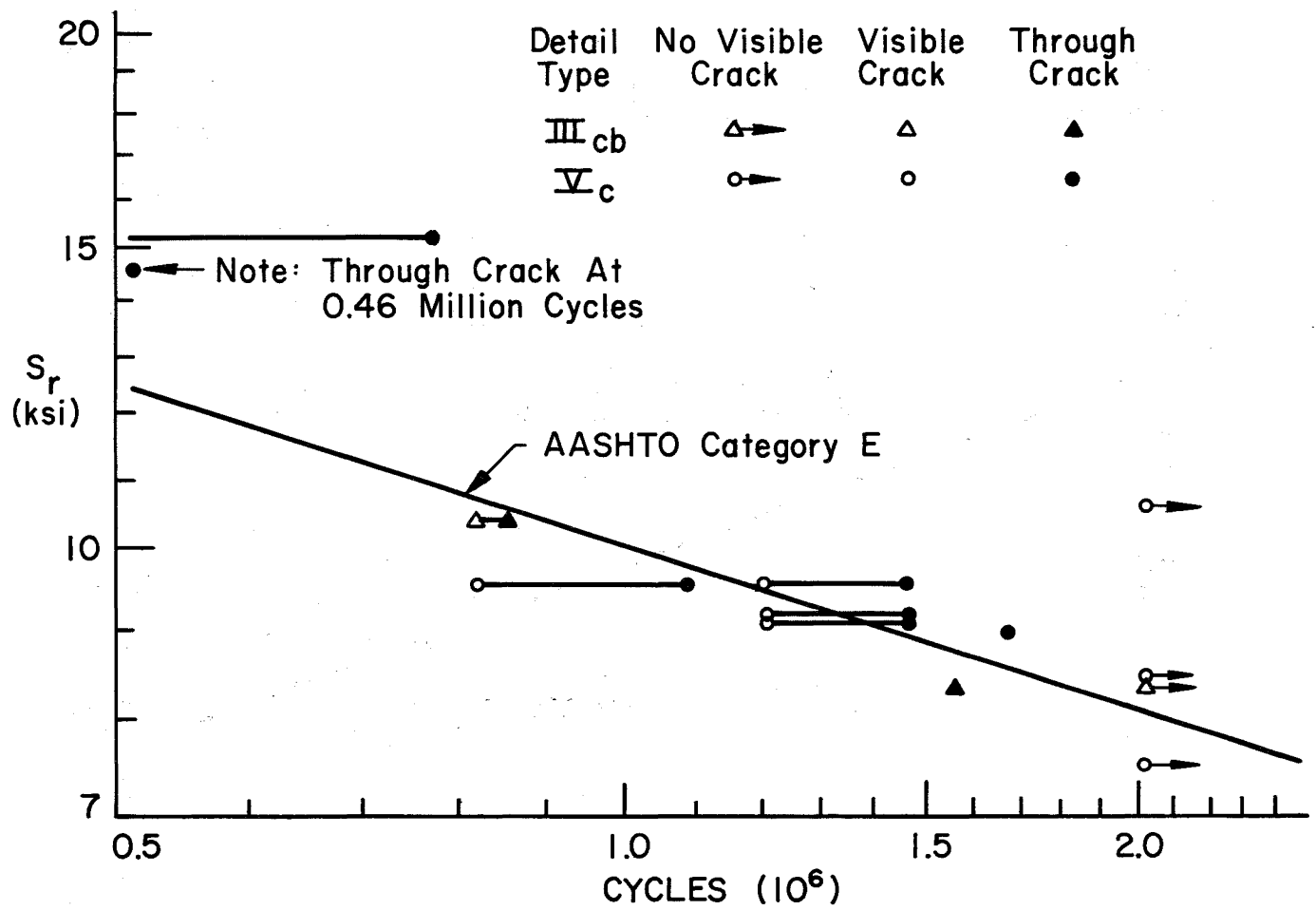


Fig. 50 Fatigue Results - Girder 1 - Category E
Group 2, 3, and 4 Details

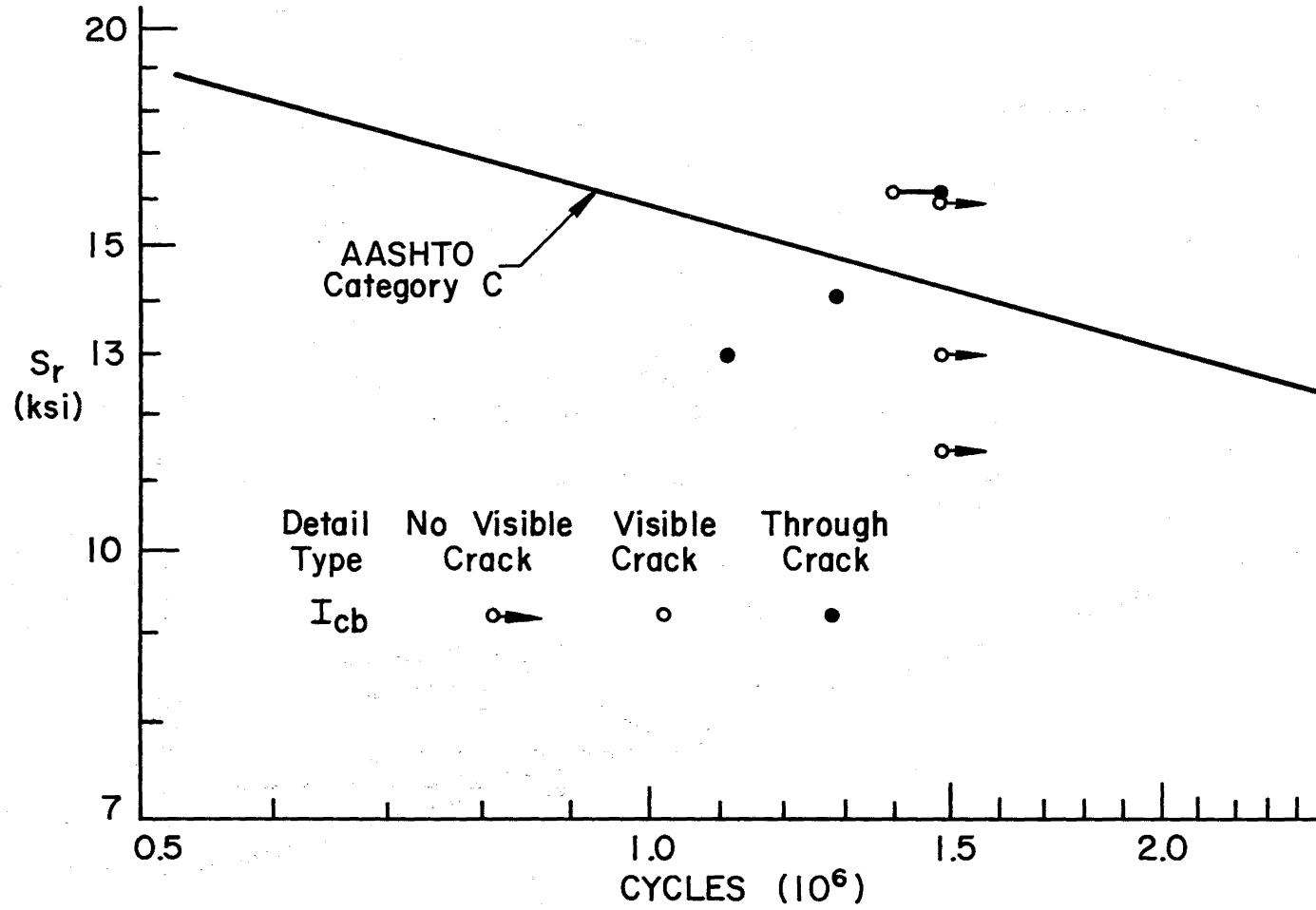


Fig. 51 Fatigue Results - Girder 2 - Category C
Group 1 Details

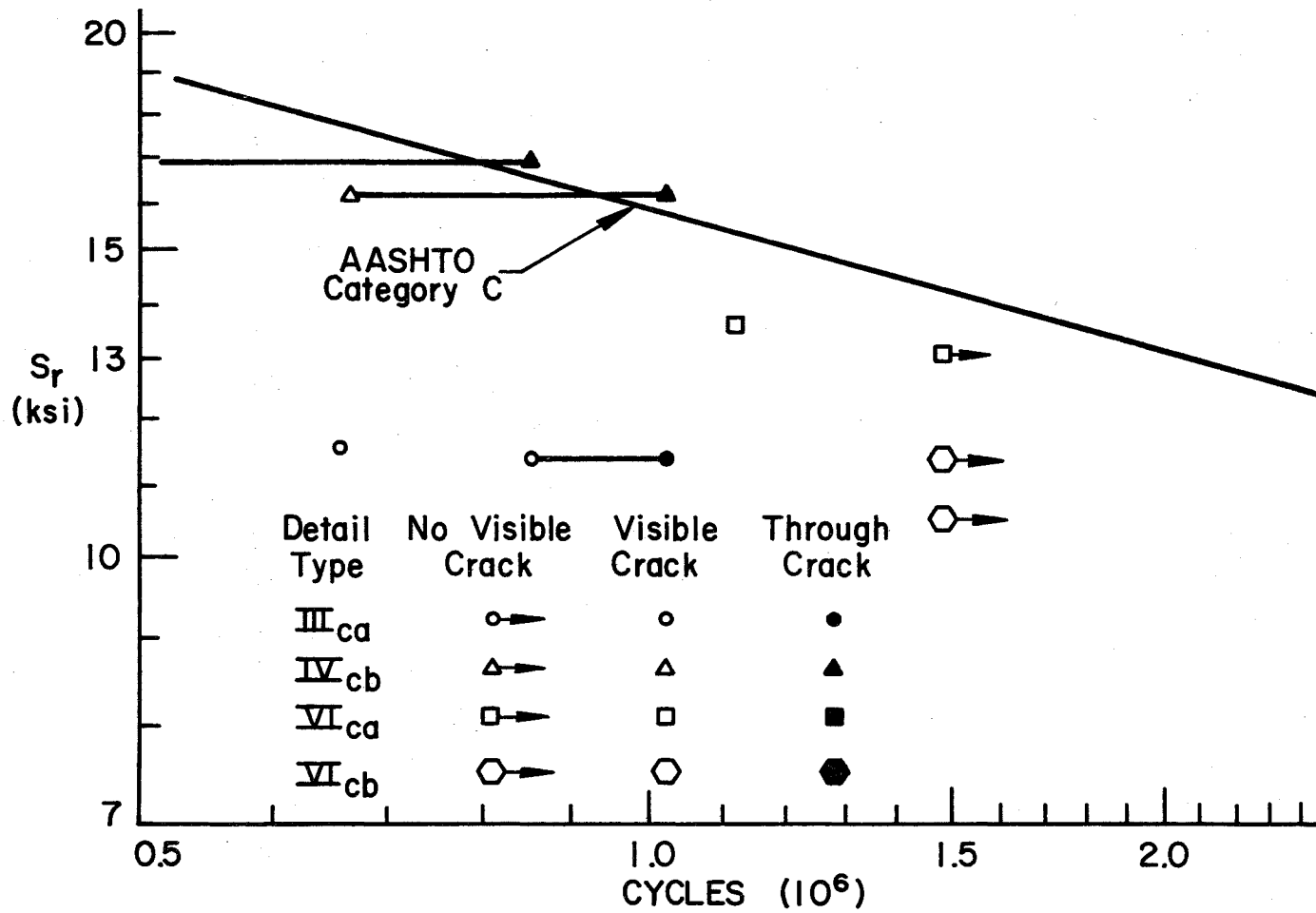


Fig. 52 Fatigue Results - Girder 2 - Category C
Group 2, 3 and 4 Details

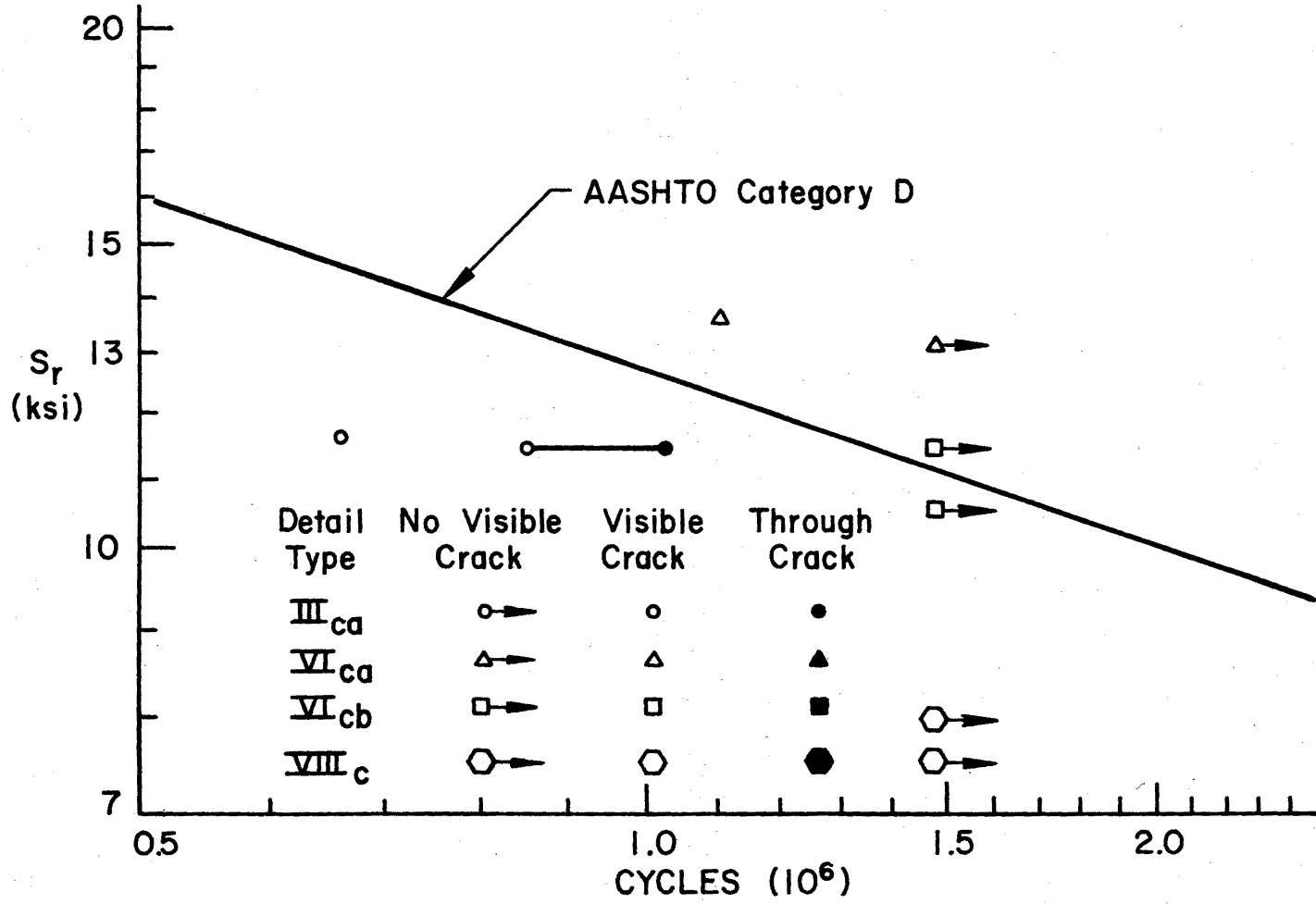


Fig. 53 Fatigue Results - Girder 2 - Category D
Group 2, 3 and 4 Details

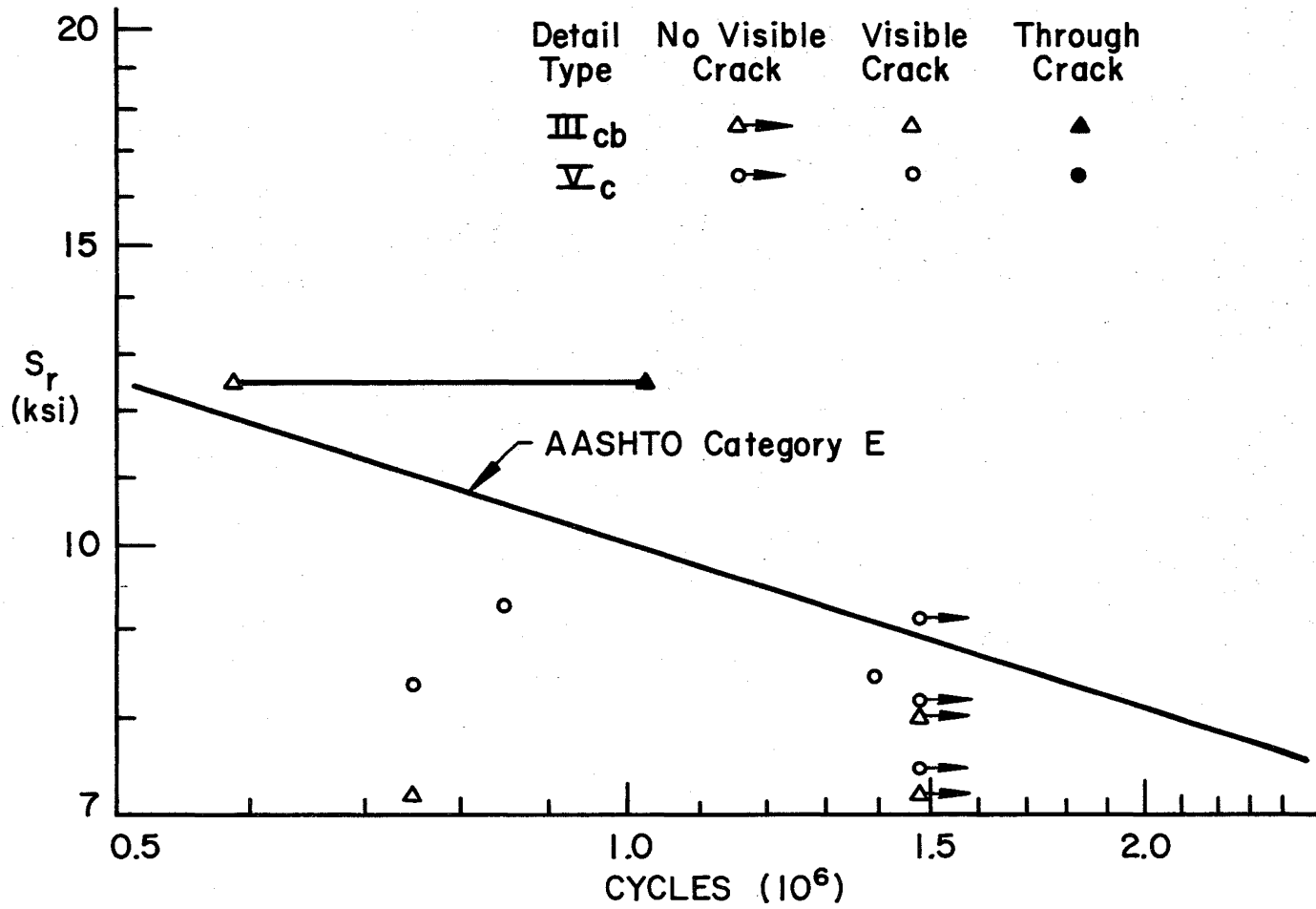


Fig. 54 Fatigue Results - Girder 2 - Category E
Group 2, 3 and 4 Details

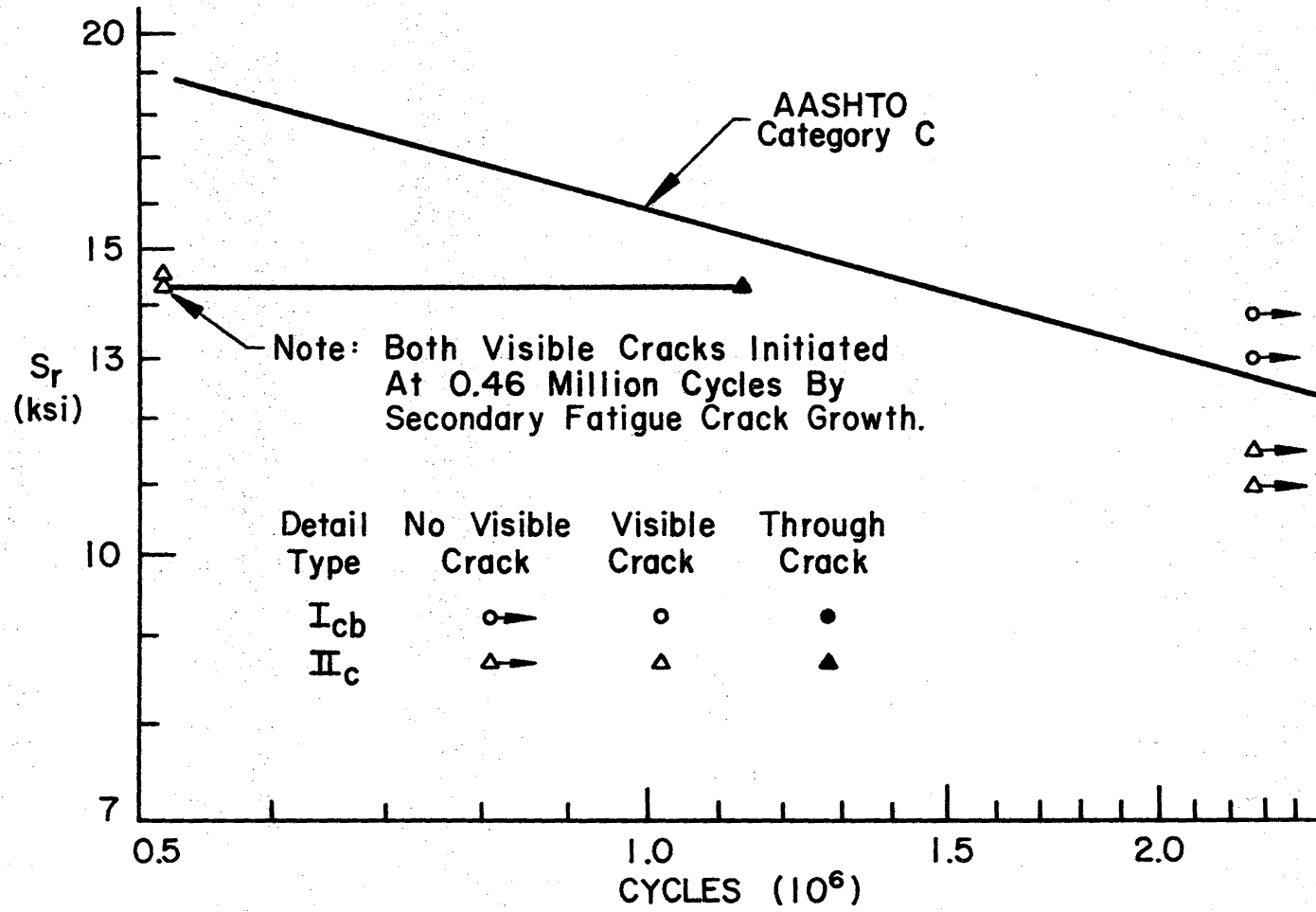


Fig. 55 Fatigue Results - Girder 3 - Category C
Group 1 Details

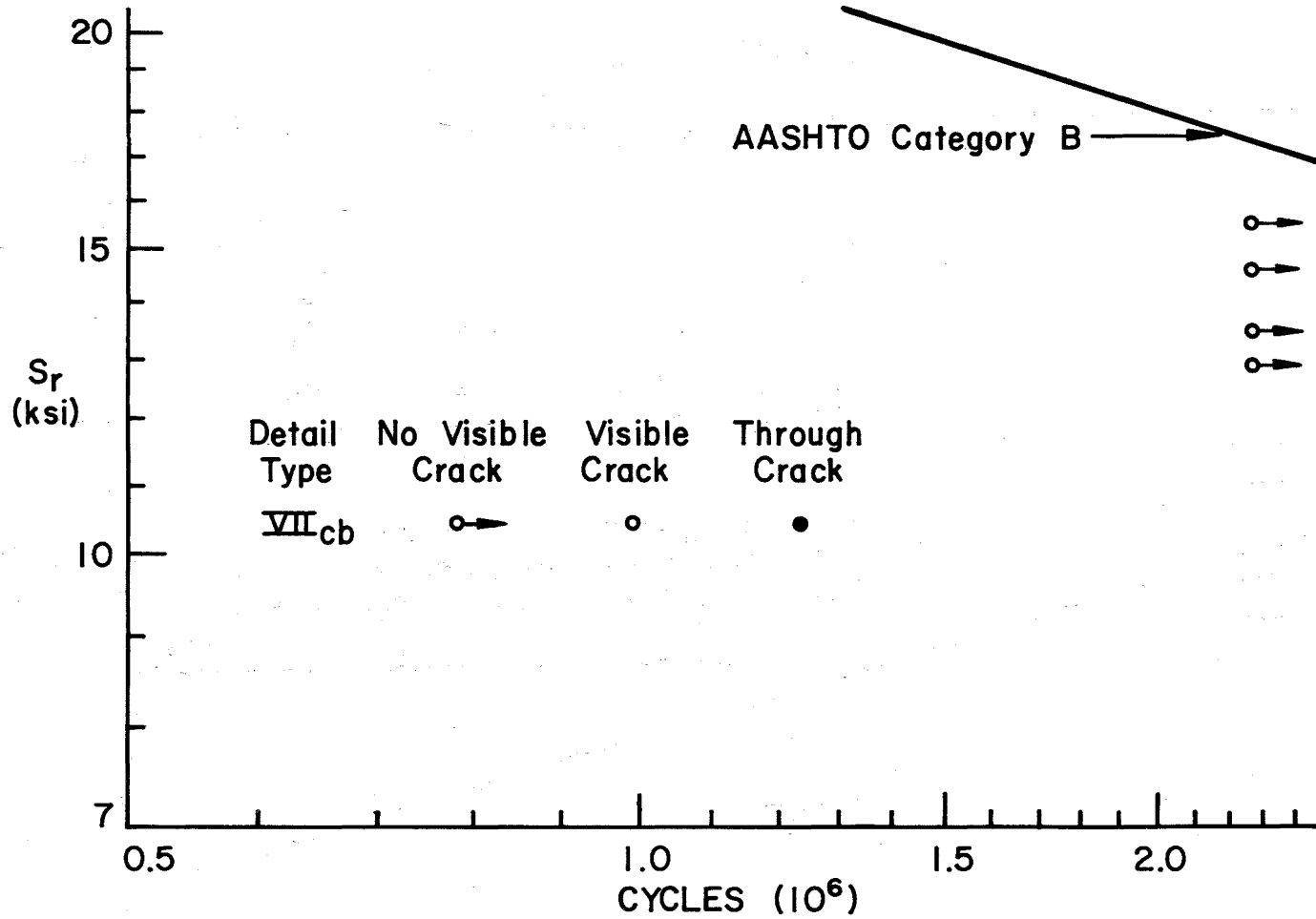


Fig. 56 Fatigue Results - Girder 3 - Category B
Group 2, 3, and 4 Details

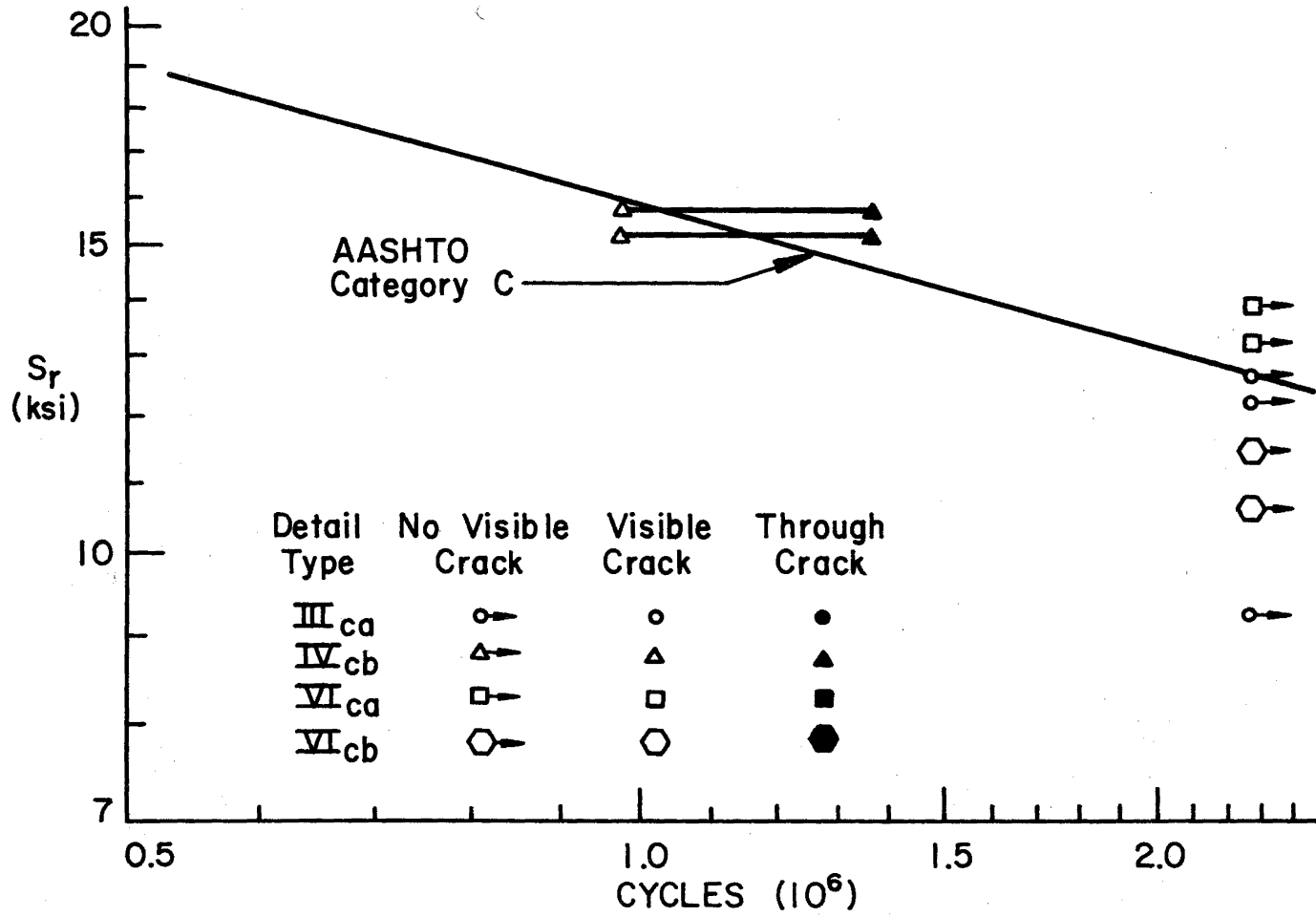


Fig. 57 Fatigue Results - Girder 3 Category C
Group 2, 3 and 4 Details

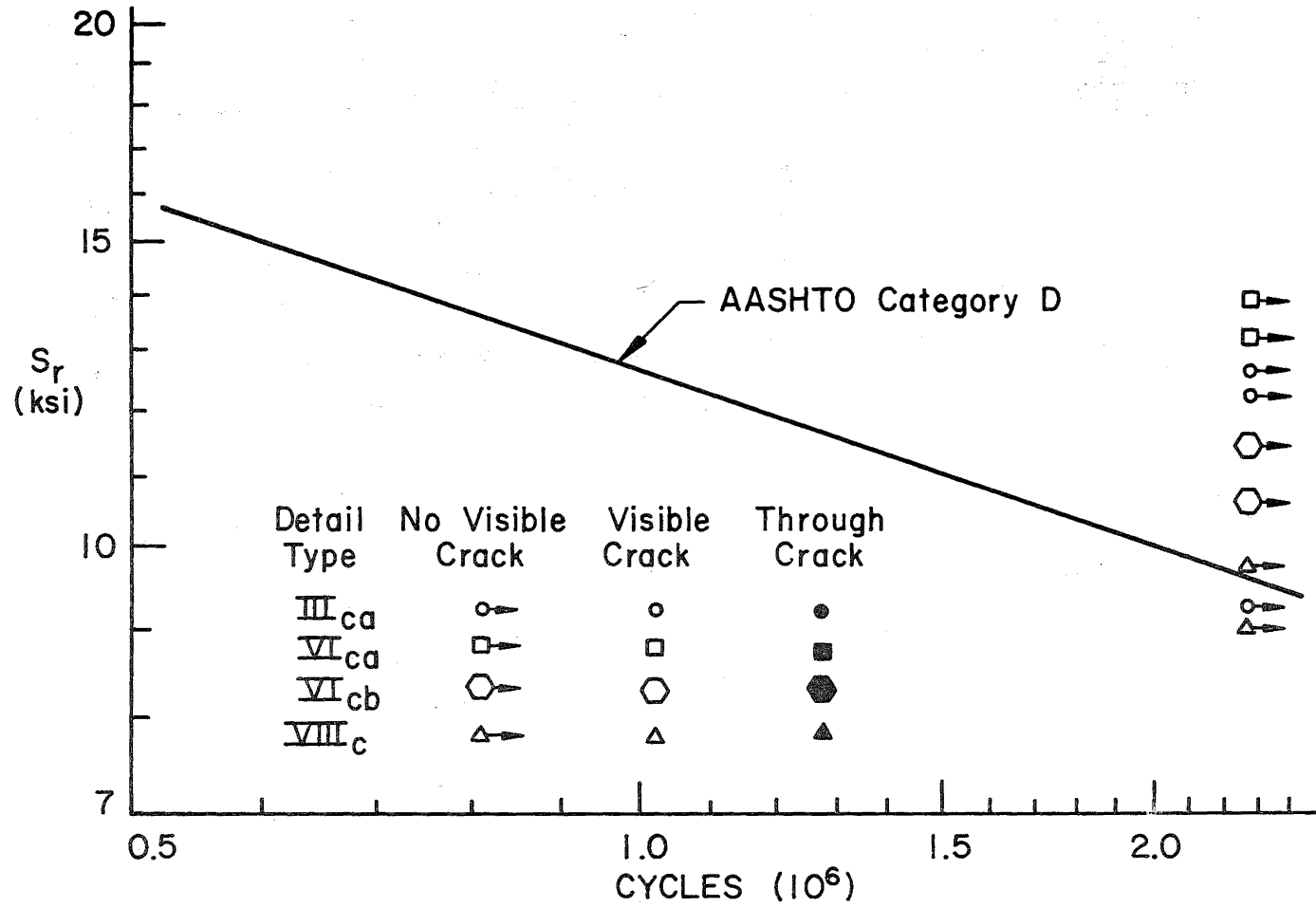


Fig. 58 Fatigue Results - Girder 3 - Category D
Group 2, 3, and 4 Details

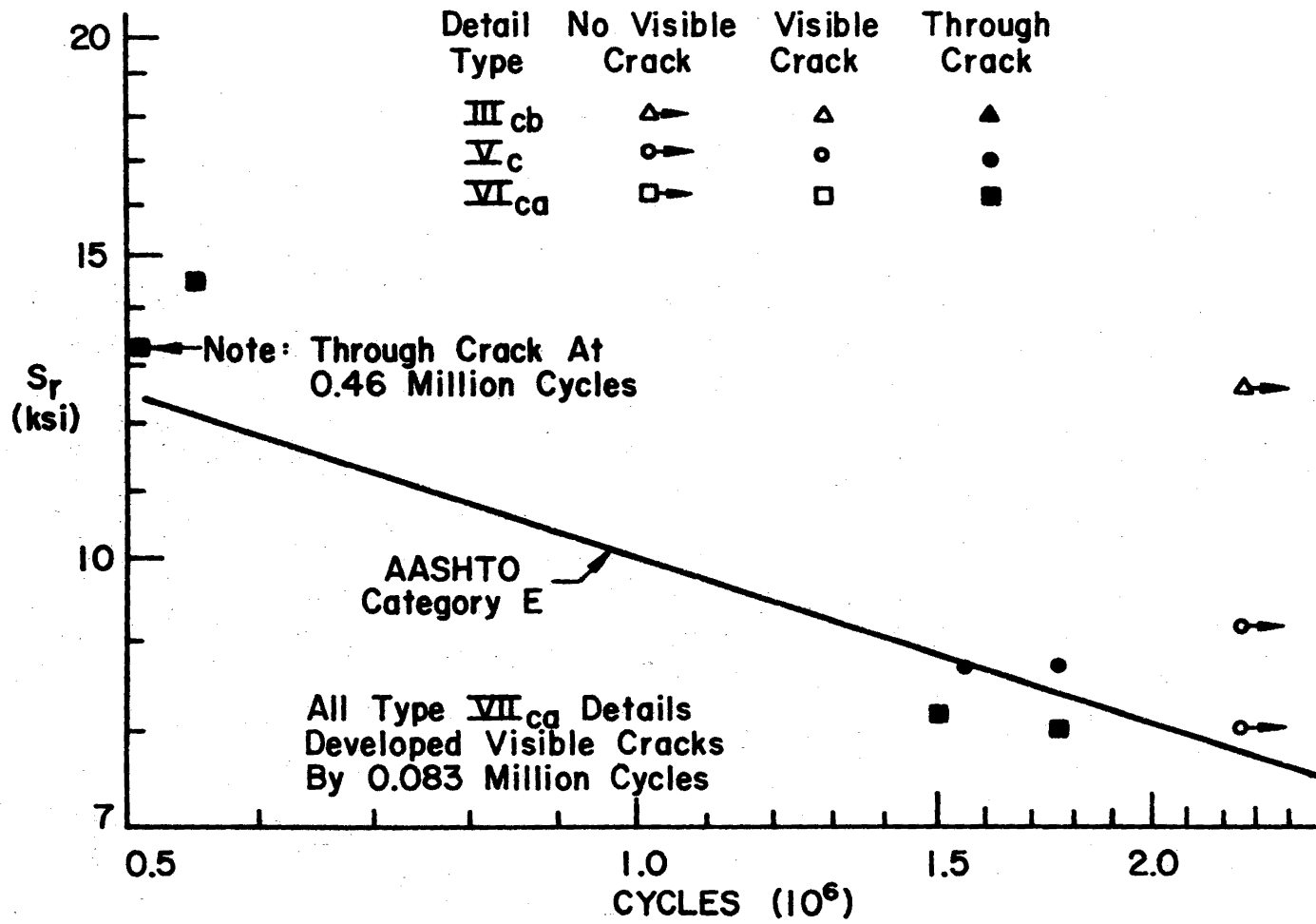


Fig. 59 Fatigue Results - Girder 3 - Category E Group 2, 3, and 4 Details

nominal stress range S_r versus the cycles N to a specified crack condition. The discussion of secondary fatigue crack growth is therefore limited to more qualitative observations of the performance of the box girders.

The first girder tested, Girder 3, experienced considerable secondary fatigue crack growth early in the test. The first sign that crack growth was occurring came at 83,400 cycles when a slight increase in the midspan deflection triggered the emergency shutdown switch (Art. 3.2 and Fig. 26). A complete inspection revealed secondary fatigue crack growth at a number of different locations. Close inspection of the interior diaphragms revealed cracks as shown in Fig. 60. A through crack in this diaphragm developed at the cutout which allows the longitudinal bottom flange stiffener to pass through the diaphragm as shown in Fig. 61. A similar crack was discovered at the diaphragm connecting Joints 3 and 4. Inspection of the midspan diaphragm (Joints 5 and 6) showed no damage to the diaphragm itself but damage was evident at the connection of the diaphragm to the webs. At the top of the web at Joint 5, the diaphragm had punched through the web as shown in Fig. 62. A similar punching effect, though not so severe, was observed at the bottom of the web at Joints 4 and 8. At the top of the web at Joint 6 the diaphragm had torn away from the web as shown in Fig. 63. Similar tearing of the web-diaphragm weld was found at the top of the web at Joint 8. Also, as shown in Fig. 64 the Type III_{ca} detail at detail location e cracked at the cope due to motion of the diaphragm relative to the bottom flange.

As discussed in Art. 2.1, one of the objectives of this investigation is to determine the influence of diaphragm rigidity on overall fatigue behavior. Secondary crack growth was therefore anticipated to occur in the diaphragms and at the diaphragm to web and/or flange connections. The plate type diaphragms in girder 3 were purposely not welded to the bottom flange at the load points so that the extent of secondary crack growth due to displacement induced stress could be examined. However the severity of the damage so early in the test program was not anticipated. It was therefore felt prudent to immediately ensure that no further secondary cracking would develop which may interfere with the development of the expected primary fatigue cracks.

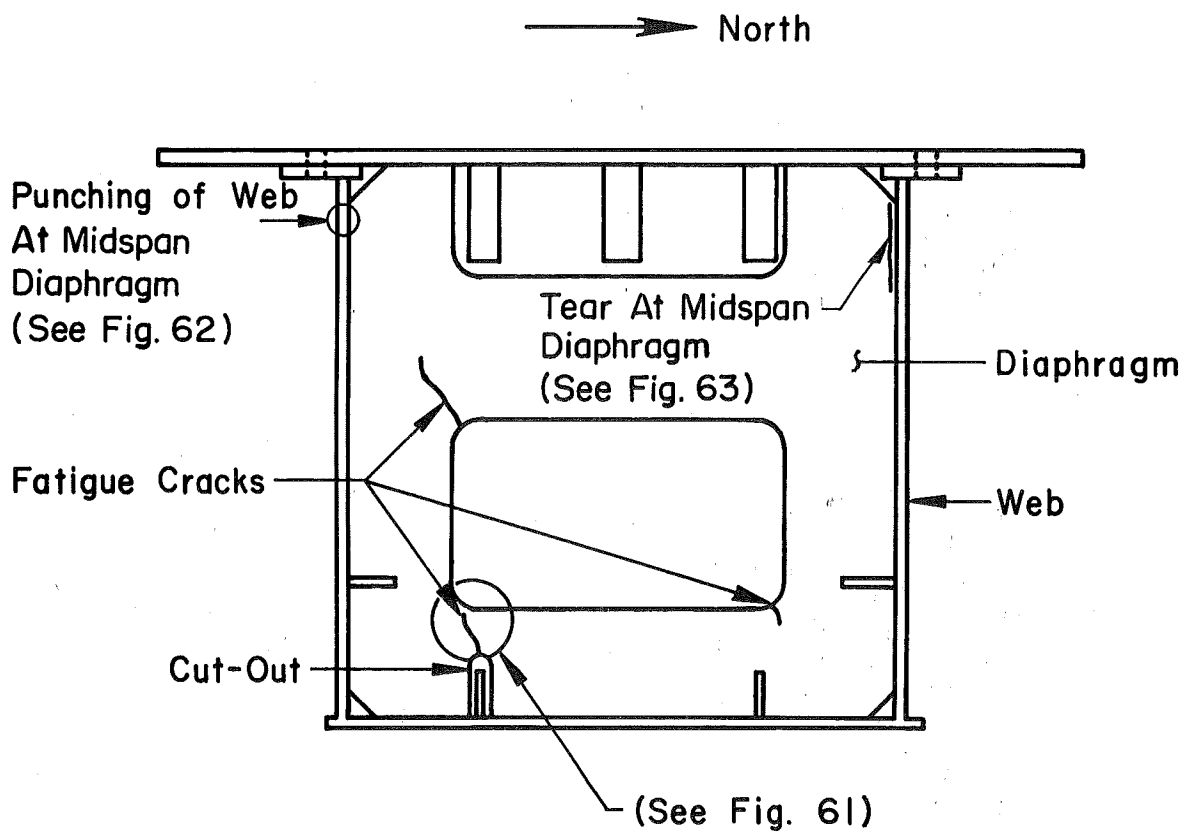


Fig. 60 Girder 3 - Interior Diaphragms from the East at 0.084 Million Cycles

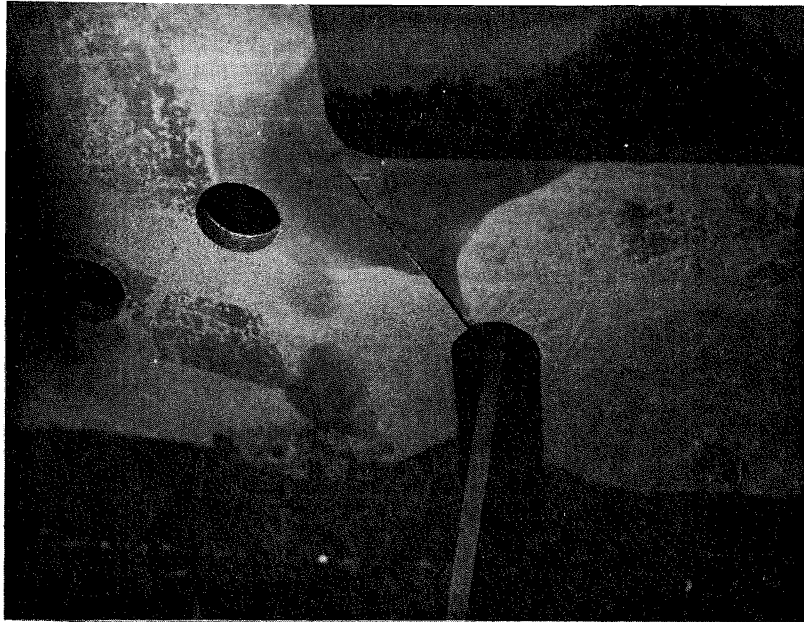


Fig. 61 Girder 3 - Diaphragm at Joints 7 and 8 Viewed from East after 0.084 Million Cycles Showing Crack at Top of Cutout

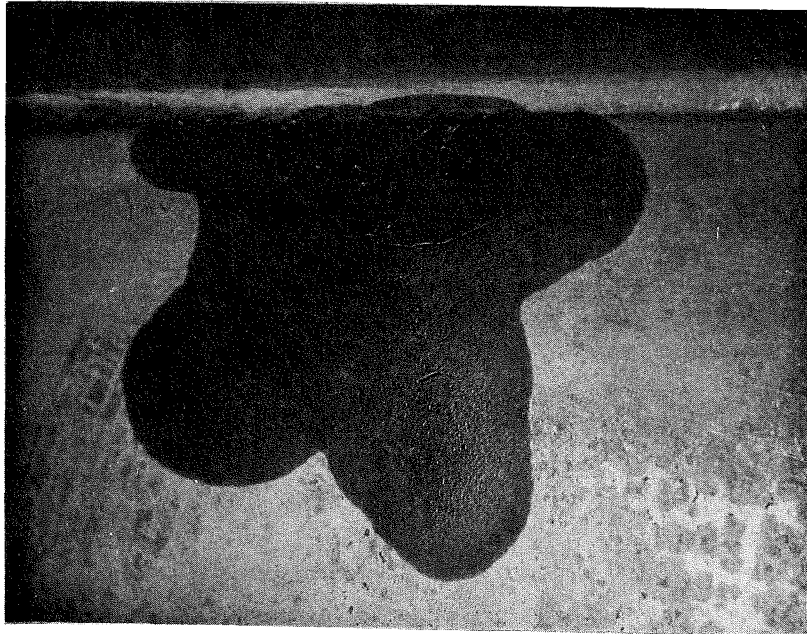


Fig. 62 Girder 3 - Punching in Web at Joint 5 at Top of Diaphragm as Viewed from the South after 0.084 Million Cycles

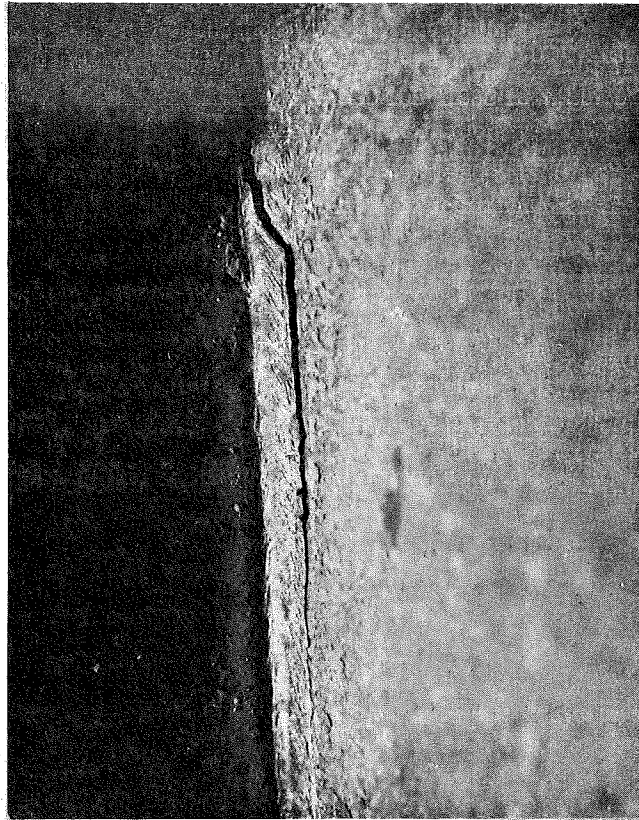


Fig. 63 Girder 3 - Diaphragm Torn
away from Web at Joint 6
as Viewed from the East
after 0.084 Million Cycles

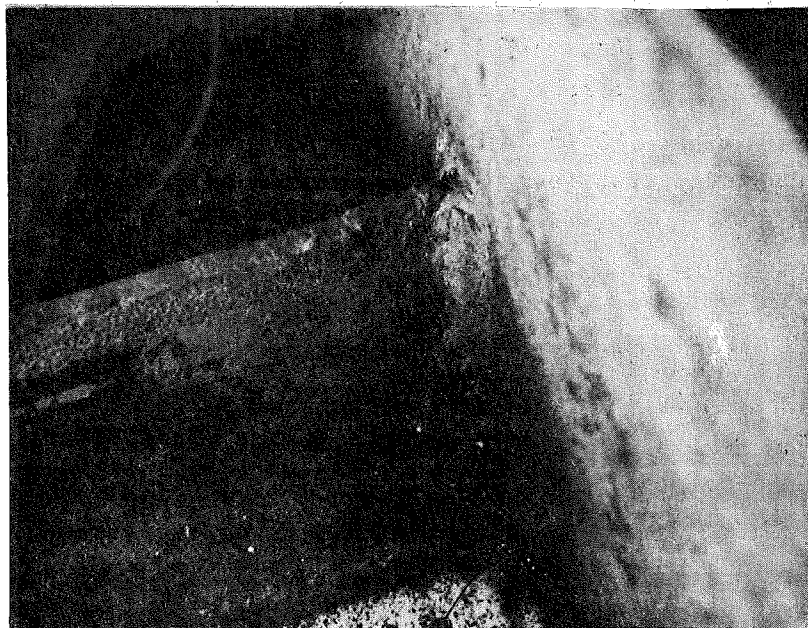


Fig. 64 Girder 3 - Type III at Location e
after 0.084 Million^{ca} Cycles

Secondary fatigue crack growth was arrested by (1) bolting heavy angles across the plate diaphragms as shown in Fig. 65 to reduce the stress in the diaphragms, (2) welding the top of the diaphragms directly to the flanges at the top of each web by means of gusset plates as shown in Fig. 66 and, (3) welding the plate diaphragms at the quarter points (Joints 3 and 4 and Joints 7 and 8) to the bottom flange. The latter two ensured that the diaphragm forces would not be carried by the web by web bending. Of course, the analyses of Girder 3 were examined closely to determine if the calculated stress ranges in the bottom flange and the small flanges at the top of each web were compatible with the weld details to be introduced, so that the fatigue strength of the girder would not be substantially reduced below 2 million cycles.

Relatively little secondary fatigue crack growth occurred in the remainder of the fatigue testing of Girder 3. At 0.46 million cycles visible cracks were discovered in the bottom flange. These cracks occurred at the cutouts which allow the longitudinal stiffener to pass through the diaphragms at Joints 3 and 4, and 7 and 8. The cracks were perpendicular to the diaphragm at the termination of the repair weld mentioned above which connects the diaphragms to the bottom flange. The secondary fatigue crack nearest Joint 7 later "turned" in response to the maximum principal stress. Although initiated by secondary fatigue crack growth, the crack began to behave like a primary fatigue crack, growing perpendicular to the longitudinal bending stress. By 1.13 million cycles a through crack had developed in the bottom flange. No other secondary fatigue crack growth was observed before the fatigue testing of Girder 3 ended at 2.27 million cycles.

Based on the experience with severe secondary fatigue crack growth in Girder 3, Girders 1 and 2 were modified prior to fatigue testing. Gusset plates were welded to the tops of all interior diaphragms to transfer out-of-plane forces directly into the flanges at the tops of the webs (Fig. 66). In addition, any interior diaphragms that were intentionally not welded to the bottom flange during fabrication were welded to transfer diaphragm forces directly to the bottom flange instead of to the webs. With these modifications, the fatigue testing of Girder 1 began.

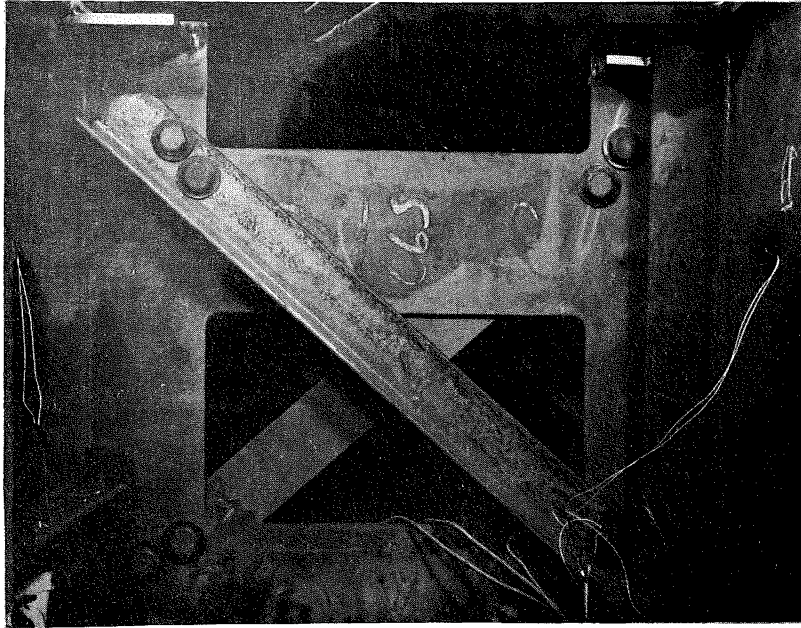


Fig. 65 Girder 3 - Cross Bracing Used to Reinforce Interior Diaphragms

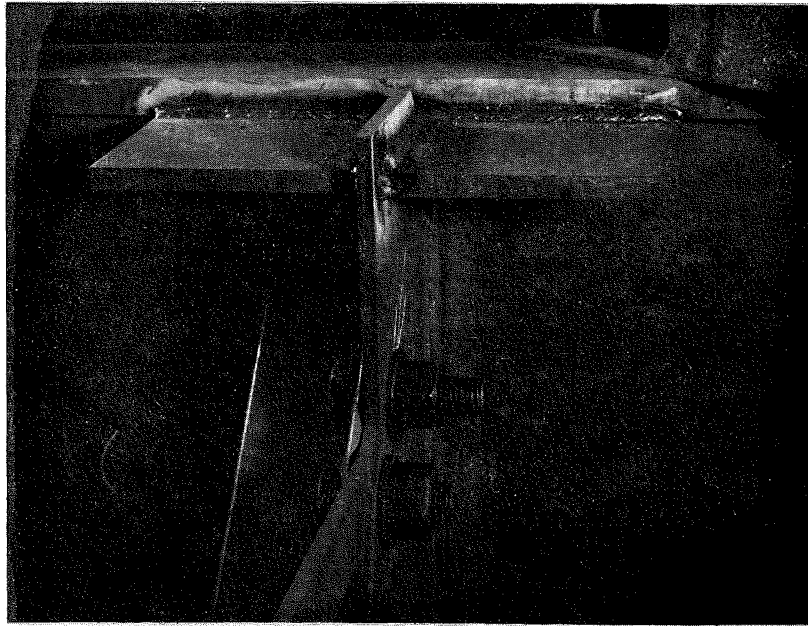
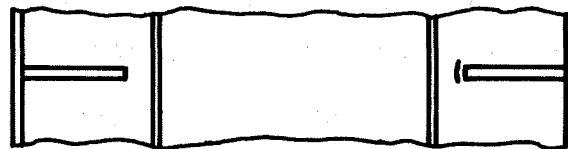
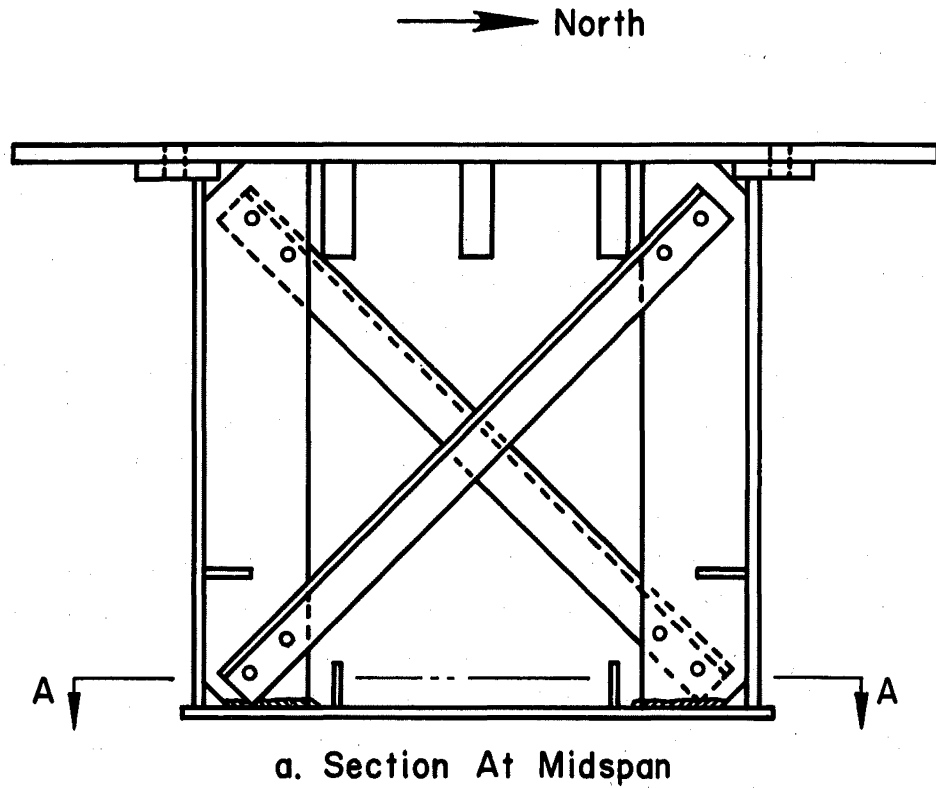


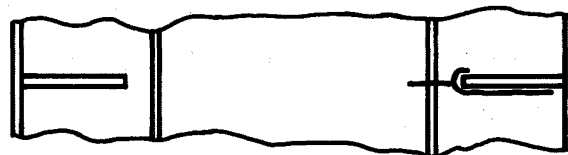
Fig. 66 Girder 3 - Plates Used to Connect Interior Diaphragms to Top Flange (Plates can also be seen in Fig. 65)

Secondary fatigue crack growth did not seriously damage Girder 1. No punching or tearing of the web was observed and no fatigue crack growth was observed in the diaphragms. Secondary fatigue cracks were observed at the juncture of the transverse web stiffeners and the bottom flange. These cracks occurred at Joints 3, 6, and 7. The cracks at Joints 6 and 7 were visible at 0.91 million cycles, while the crack at Joint 3 was not visible until 1.46 million cycles. Figure 67(a) shows the diaphragm at Joints 5 and 6 as viewed from the east. The partial plan view indicated in Fig. 67(b) shows the first stage of secondary fatigue crack growth at Joint 6. The secondary fatigue crack begins to grow perpendicular to the web stiffener due to transverse forces introduced into the bottom flange by the diaphragm. As the crack grows away from the web stiffener the longitudinal normal stress due to bending and warping torsion begins to dominate the stress field at the crack tip. The crack then turns as shown in Fig. 67(c) and begins to behave as a primary fatigue crack, growing across the bottom flange. The fatigue cracks at Joints 6 and 7 exhibited this behavior, becoming through-thickness cracks at 1.46 million cycles. The secondary fatigue crack at Joint 3 did not become a through-thickness crack. Fatigue testing of Girder 1 ended at 2.02 million cycles.

No secondary fatigue crack growth was observed in Girder 2. The fatigue testing was suspended at 1.47 million cycles. Due to extensive primary fatigue crack growth in the bottom flange, the repair of which was not deemed necessary to meet the objectives of the program.



b. Section A-A At 0.91 Million Cycles



c. Section A-A At 1.46 Million Cycles

Fig. 67 Girder 1 - Primary Fatigue Crack Growth Initiated by Secondary Fatigue Crack Growth at Junction of Web Stiffener and Bottom Flange

7. DISCUSSION OF TEST RESULTS

7.1 Primary Fatigue Crack Growth

7.1.1 Type I_{ca} and I_{cb} Details

The fatigue test results for all Type I_{ca} and I_{cb} details are shown in Fig. 68.

The six Type I_{ca} details tested were subjected to nominal stress ranges of 12.4 to 16.5 ksi. Five of the Type I_{ca} details demonstrated fatigue strengths exceeding the AASHTO Category C design curve. The sixth detail developed a through crack after 1.46 million cycles at a nominal stress range of 13.9 ksi. Although this falls far below the AASHTO Category C design curve it is important to note that this crack, as well as a crack at the other Type I_{ca} detail that fell above the design curve, was initiated by secondary fatigue crack growth. The detail whose fatigue strength falls below the AASHTO Category C design curve is the Type I_{ca} detail located at Joint 6 on Girder 1. The process through which secondary fatigue crack growth initiated the premature failure of this detail is described in detail in Art. 6.2. The premature failure of this detail may reflect on the inadequate fatigue strength of the diaphragm configuration for severe torsional loadings, but it does not imply any inadequacy of the Type I_{ca} detail with regard to the AASHTO Category C design curve.

The eight Type I_{cb} details tested were subjected to stress ranges from 13.0 to 16.1 ksi. Four of these details exhibited fatigue strengths which exceed the AASHTO Category C design curve. Two Type I_{cb} details were not subjected to stress ranges high enough to evaluate their adequacy as Category C details. However, no visible cracks developed at these details prior to the end of the test. The two remaining Type I_{cb} details exhibited fatigue strengths that are significantly below the AASHTO Category C design curve.

Close inspection of these details showed that fatigue crack growth stemmed from regions marked by significant undercut at the weld toe. In addition, the detail that developed the through-thickness crack at 1.10 million cycles exhibited an extremely steep flank angle. This same detail forced the suspension of testing of Girder 2 at 1.47 million cycles when

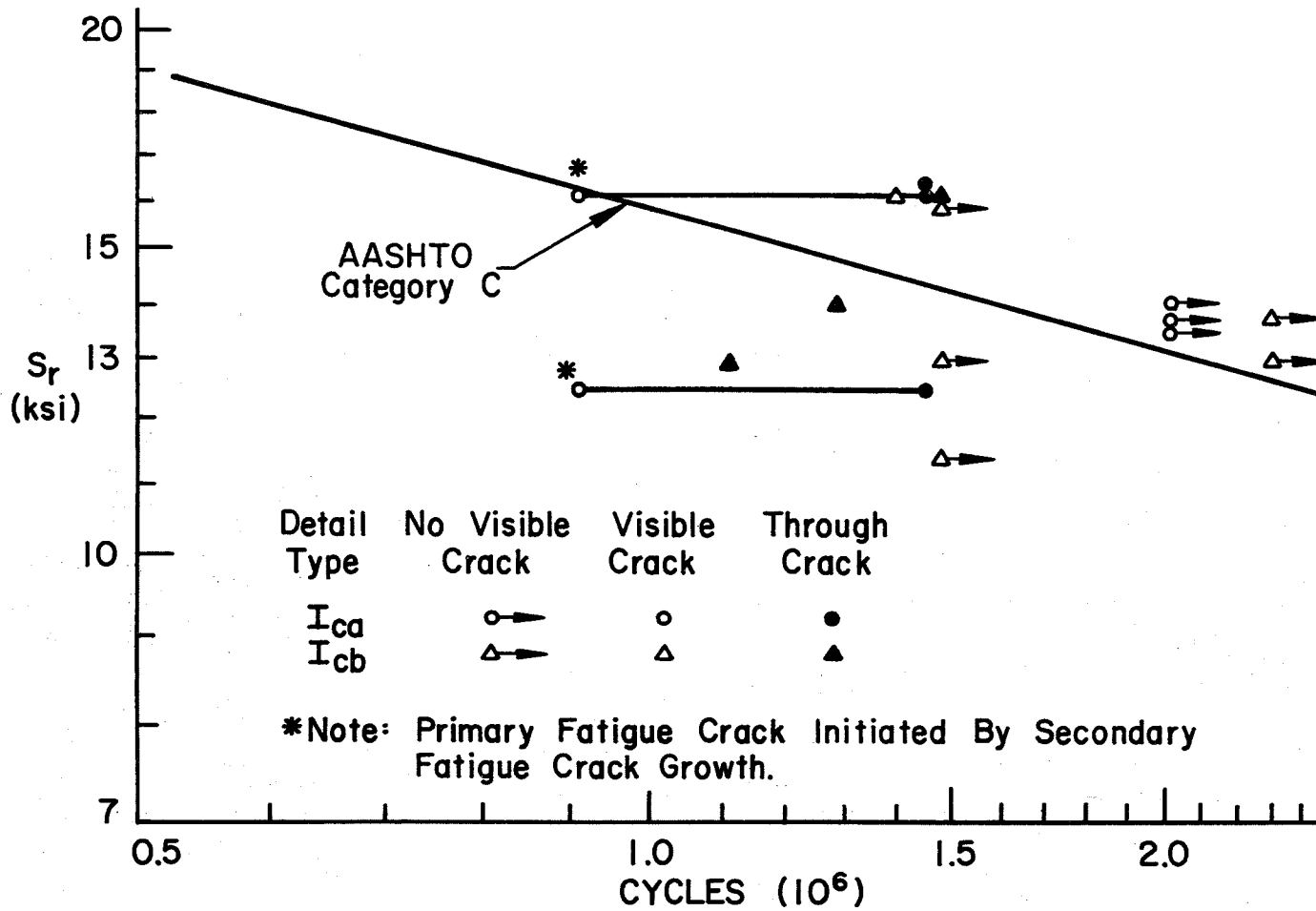


Fig. 68 Fatigue Results - Type I_{ca} and I_{cb} Details

fatigue cracks grew through the bottom flange at a number of points, rendering repair unfeasible. Although the poor fatigue strength of these details might be justified on the basis of abnormally large initial flaw sizes the question of possible size effects arises. With a fillet-welded stiffener traversing the entire width of the bottom flange, it is more likely that such otherwise abnormally large flaw sizes may occur. However, the performance of the majority of the Type I_{cb} details indicates that with careful welding procedures and proper inspection, Type I_{cb} details will achieve fatigue strengths exceeding the AASHTO Category C design curve.

7.1.2 Type II_c Details

The results of the fatigue tests of four Type II_c details are shown in Fig. 69.

Based on the original analysis and design of girder 3, two of these details were not expected to experience stress ranges high enough to cause significant fatigue crack growth. This expectation was borne out by the fatigue test results. However, two Type II_c details that were subject to sufficiently high stress ranges to produce significant fatigue crack growth were damaged by early secondary fatigue crack growth. In spite of this, one of the Type II_c details did exhibit a fatigue strength exceeding the AASHTO Category C design curve. However, the remaining Type II_c detail failed prematurely for an AASHTO Category C detail due to the secondary fatigue crack growth.

Although the results are not conclusive it is believed that AASHTO detail Category C is appropriate for Type II_c details.

7.1.3 Type III_{ca} and III_{cb} Details

The fatigue test results for all Type III_{ca} and III_{cb} details are shown in Fig. 70.

The Type III_{ca} details tested were subject to stress ranges from 9.2 to 12.6 ksi. Of the six Type III_{ca} details tested only two conclusively demonstrated the fatigue strength of an AASHTO Category C detail.

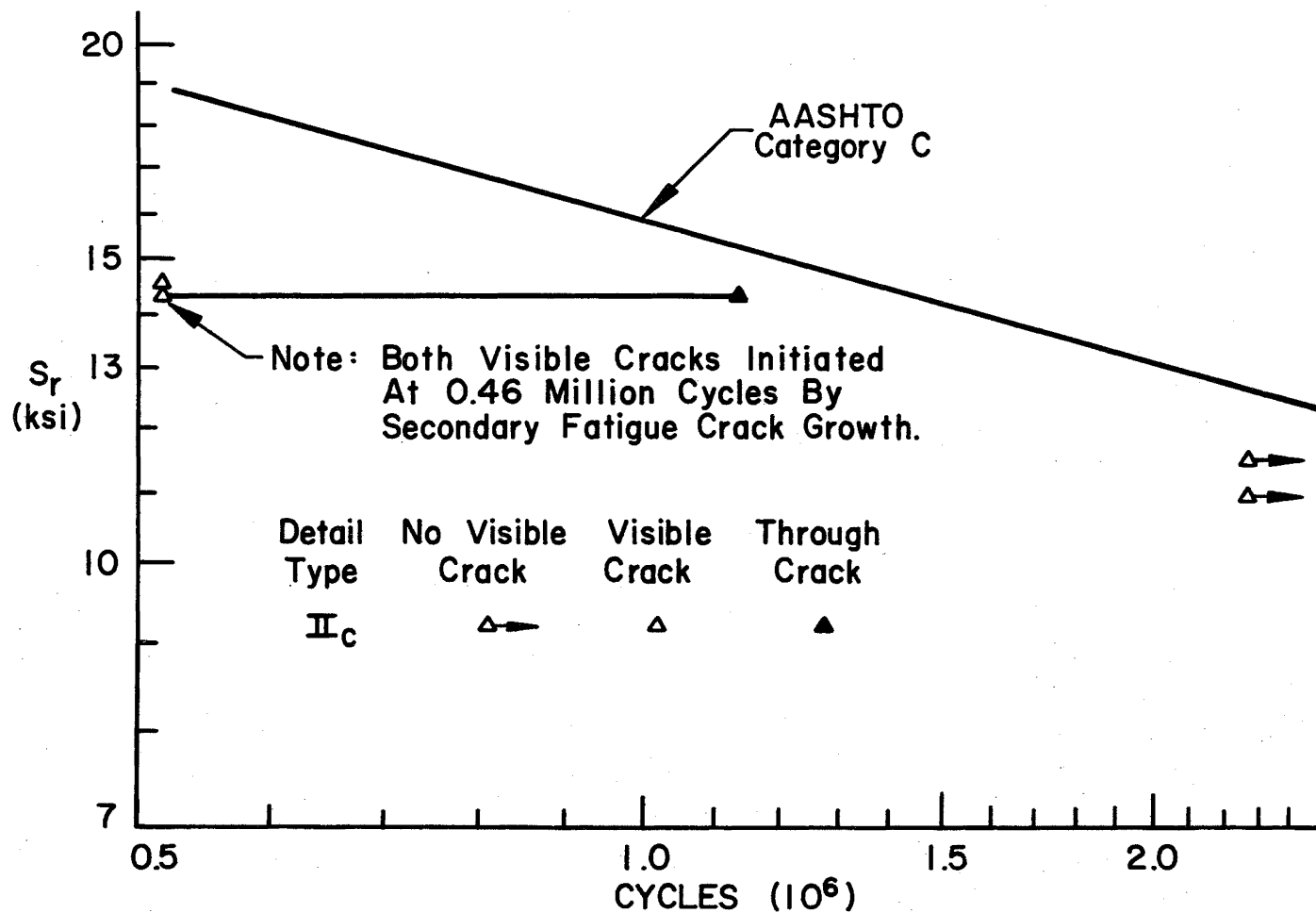


Fig. 69 Fatigue Results - Type II_c Details

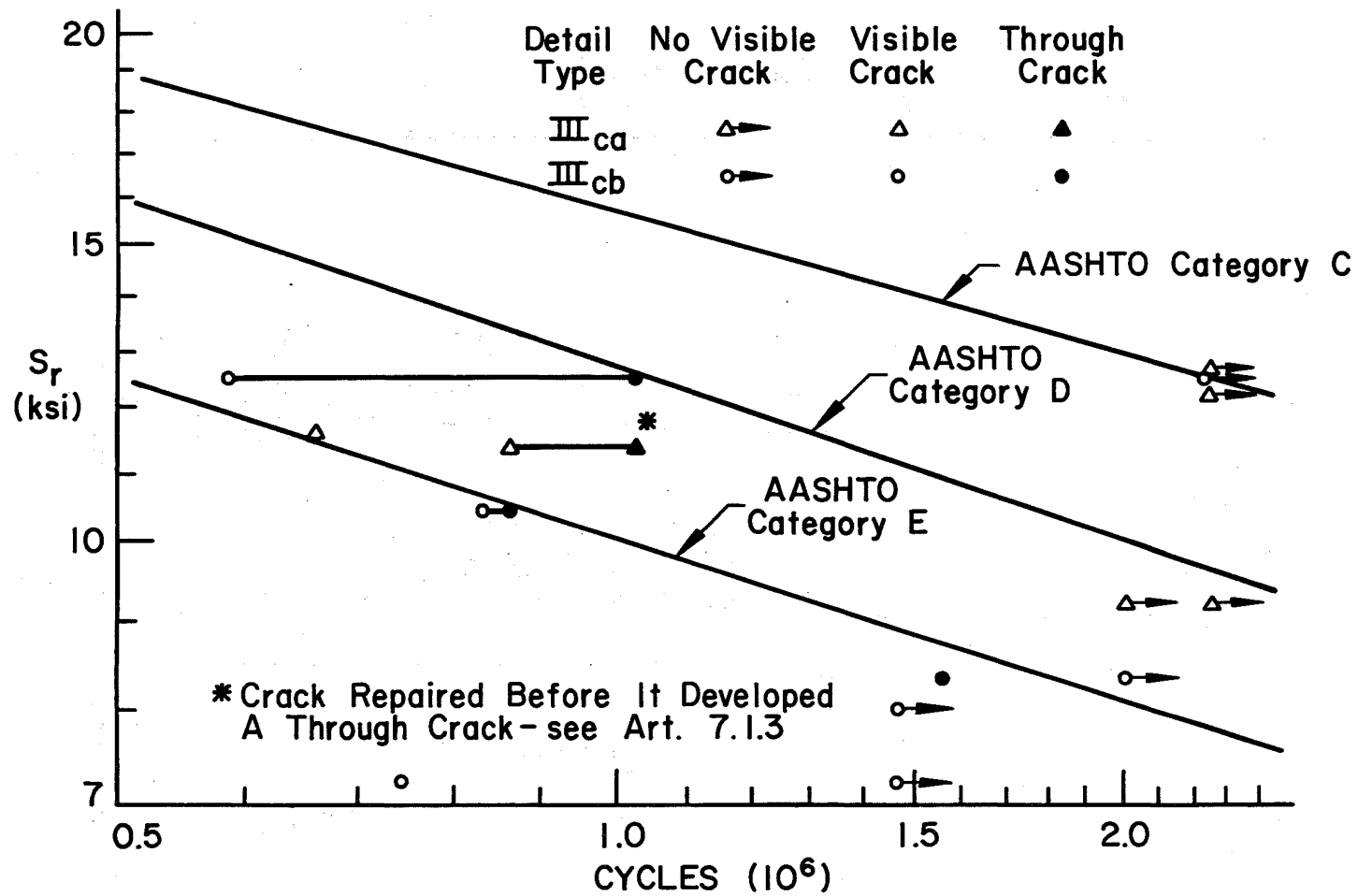


Fig. 70 Fatigue Results - Type III_{ca} and III_{cb} Details

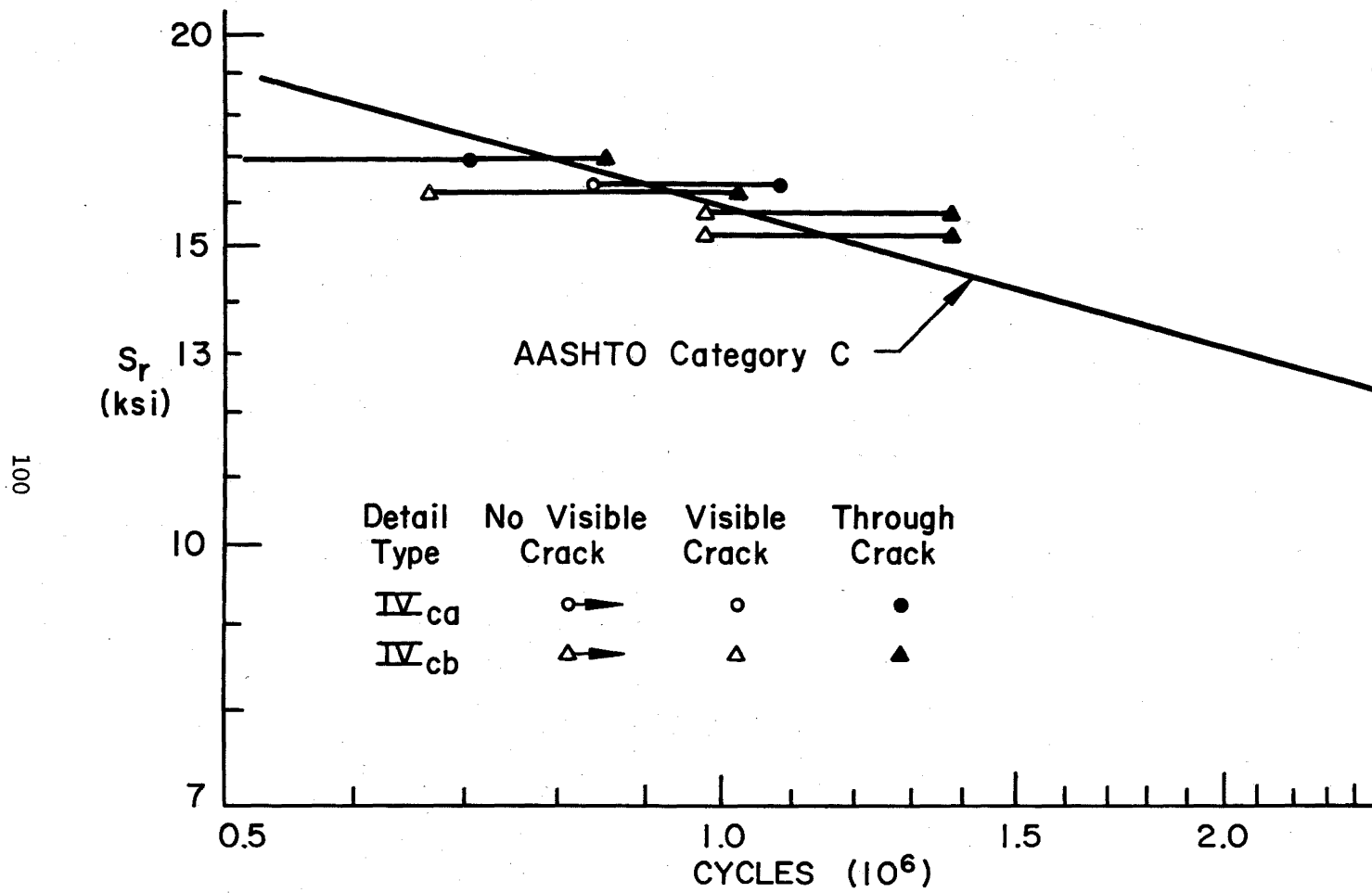


Fig. 71 Fatigue Results - Type IV_{ca} and IV_{cb} Details

Figure 70 also shows one Type III_{ca} detail as having developed a through-thickness crack at 1.02 million cycles. This detail actually never developed a through-thickness crack. It was repaired at 1.02 million cycles in order to permit continued fatigue testing over a weekend when a repair would have been impossible. The stress ranges at the three remaining Type III_{ca} details were not adequate to permit conclusive determination of their fatigue strengths. Further study of Type III_{ca} details is warranted before it can be considered an AASHTO Category C detail.

Four of the eight Type III_{cb} details tested demonstrated fatigue strengths comparable to AASHTO Category E details. The stress range at two Type III_{cb} details which showed no signs of fatigue crack growth were too low to evaluate their adequacy as AASHTO Category E details. The circumstances surrounding the development of fatigue cracks at two other Type III_{cb} details deserve elaboration. These details as well as other Type III_{ca}, and V_c details located on the webs of the box girders often showed significant cold lap and porosity at the weld termination. Although the reasons for these flaws are unclear, their effects on the fatigue strength of several of these details are detrimental. The visible and through-thickness cracks indicated at 0.74 and 1.56 million cycles, respectively, are believed to be due to the presence of abnormally large initial flaws. With careful welding procedures and strict quality control the deleterious presence of such initial flaws can be avoided. It is expected that the fatigue strength of Type III_{cb} details is adequately described by the AASHTO Category E design curve.

7.1.4 Type IV_{ca} and IV_{cb} Details

The fatigue test results for all Type IV_{ca} and IV_{cb} details tested are shown in Fig. 71.

Two Type IV_{ca} and four Type IV_{cb} details were included in the fatigue testing program. One Type IV_{ca} detail subject to a nominal stress range of 16.9 ksi developed a through crack at 0.70 million cycles which falls near but below the AASHTO Category C design curve. The other Type IV_{ca} detail and all four Type IV_{cb} details exhibited fatigue strengths which fall near but slightly above the AASHTO Category C design curve.

These results are important in two respects. First, all Type IV_{ca} and IV_{cb} details exhibited substantially improved fatigue strengths compared to the more common Type V_c detail (Art. 7.5), due to the circular or sloped transition at the end of the longitudinal stiffeners. Second, the fact that all Type IV_{ca} and IV_{cb} details fall so close to the AASHTO Category C design curve (with one Type IV_{ca} detail falling below) indicates that the beneficial effect of the curved or sloped transition may not be so great as might be predicted on a solely analytical basis.⁽¹⁴⁾ This is attributed to the sensitivity of the fatigue strength of these details to fabrication procedures and quality. In order to be totally effective the transition must be smooth. Any irregularities or flaws introduced by fabrication sharply reduce the beneficial effect of the transition on the fatigue strength of these details. A similar effect is noted in Ref. 15 with regard to groove-welded gusset plates with curved transitions.

It is important to note that all Type IV_{ca} and IV_{cb} details in this investigation were tested in the as-welded condition. The transition was not ground smooth after welding even though every effort was made to provide a smooth transition. Careful grinding of the transition after welding may significantly improve the fatigue strength of these details.

Both Type IV_{ca} and IV_{cb} details may be classified as Category C details provided that good fabrication and inspection practices are observed. Where the fatigue strength of these details is critical it is recommended that the transition be ground smooth after welding.

7.1.5 Type V_c Details

The fatigue test results for all Type V_c details tested are shown in Fig. 72.

The Type V_c details were subject to nominal stress ranges of 7.4 to 15.1 ksi. Although several Type V_c details did not experience stress ranges high enough to demonstrate their adequacy as Category E details, the fatigue tests constituted a valid test of fourteen Type V_c details. Of these details, only one demonstrated a fatigue strength below the Category E design curve. The premature failure of this detail may be explained in terms of the statistical nature of the detail category design

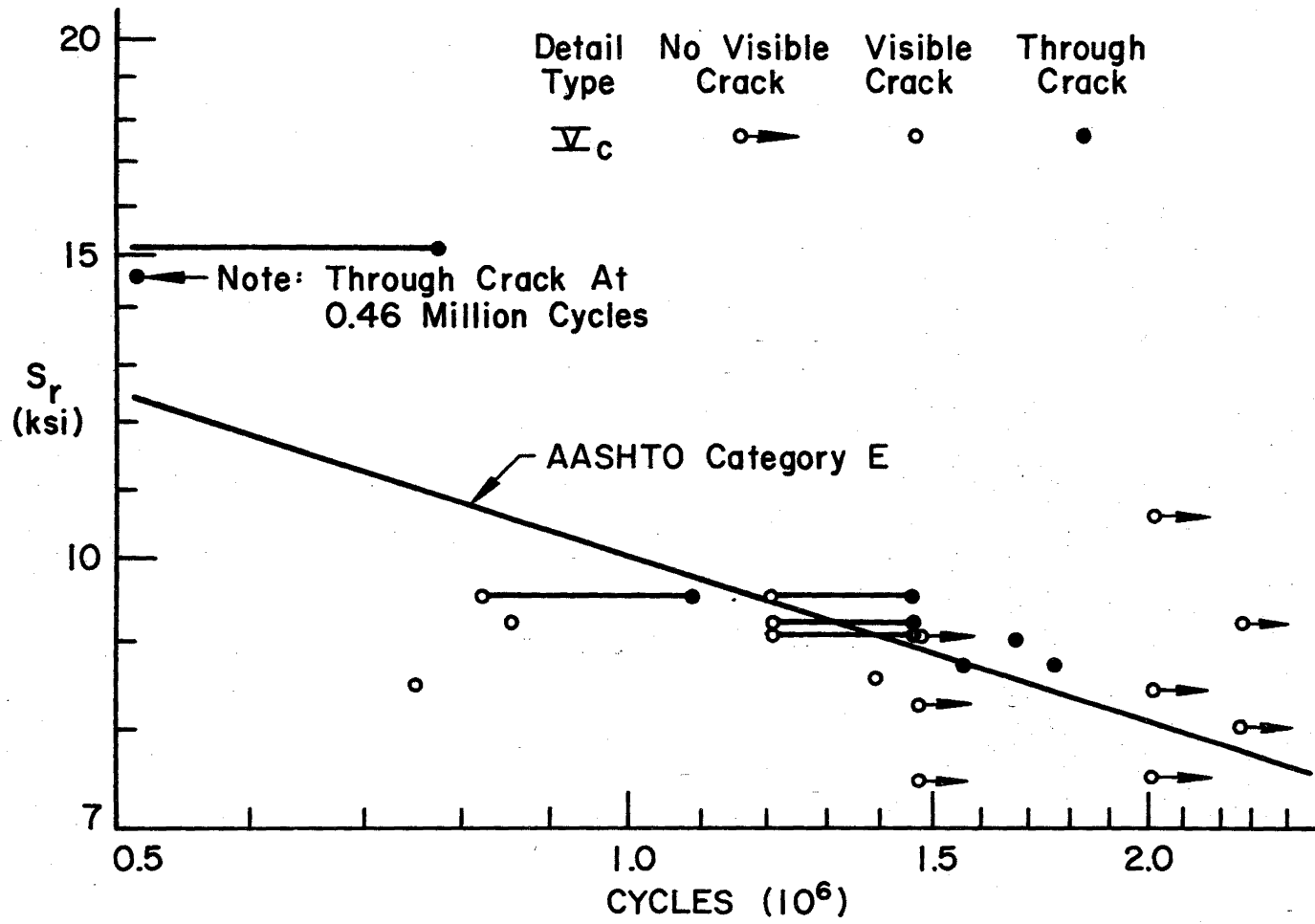


Fig. 72 Fatigue Results - Type V_c Details

curves. The AASHTO design curve (lower bound) is selected as the 95% confidence of 95% survival.⁽¹⁹⁾ On this basis then, the AASHTO detail Category E adequately describes the fatigue strength of the Type V_c details tested.

7.1.6 Type VI_{ca} and VI_{cb} Details

The fatigue test results for all Type VI_{ca} and VI_{cb} details tested are shown in Fig. 73.

Of the six Type VI_{ca} details tested three clearly demonstrated the adequacy of detail Category C to describe their fatigue strengths. Two more details did not develop any visible cracks prior to the end of the tests, but the nominal stress ranges were too low to permit a similar conclusion to be drawn about these details. The remaining Type VI_{ca} detail developed a visible crack at 1.10 million cycles under a stress range of 13.7 ksi, but showed no evidence of a through-thickness crack at the end of the test (1.47 million cycles). The high-strength bolts in this particular Type VI_{ca} detail were purposely not tightened to the level specified for a friction connection. The bolts were left in the "snug" condition in order to examine the effects of potential field installation errors. It is interesting to note that even this Type VI_{ca} detail demonstrated a fatigue strength at least equal to an AASHTO Category D detail.

None of the VI_{cb} details tested showed any visible fatigue crack growth. Due to the location of these details in the end span regions and the difference between the predicted and measured stress range profiles (Art. 4.2) these details were not subject to stress ranges high enough to evaluate their adequacy as AASHTO Category C details. However, the fatigue test results demonstrate that the Type VI_{cb} details are at least adequate with respect to the AASHTO Category D design curve.

7.1.7 Type VII_{ca} and VII_{cb} Details

The fatigue test results for the Type VII_{ca} and VII_{cb} details are shown in Fig. 74.

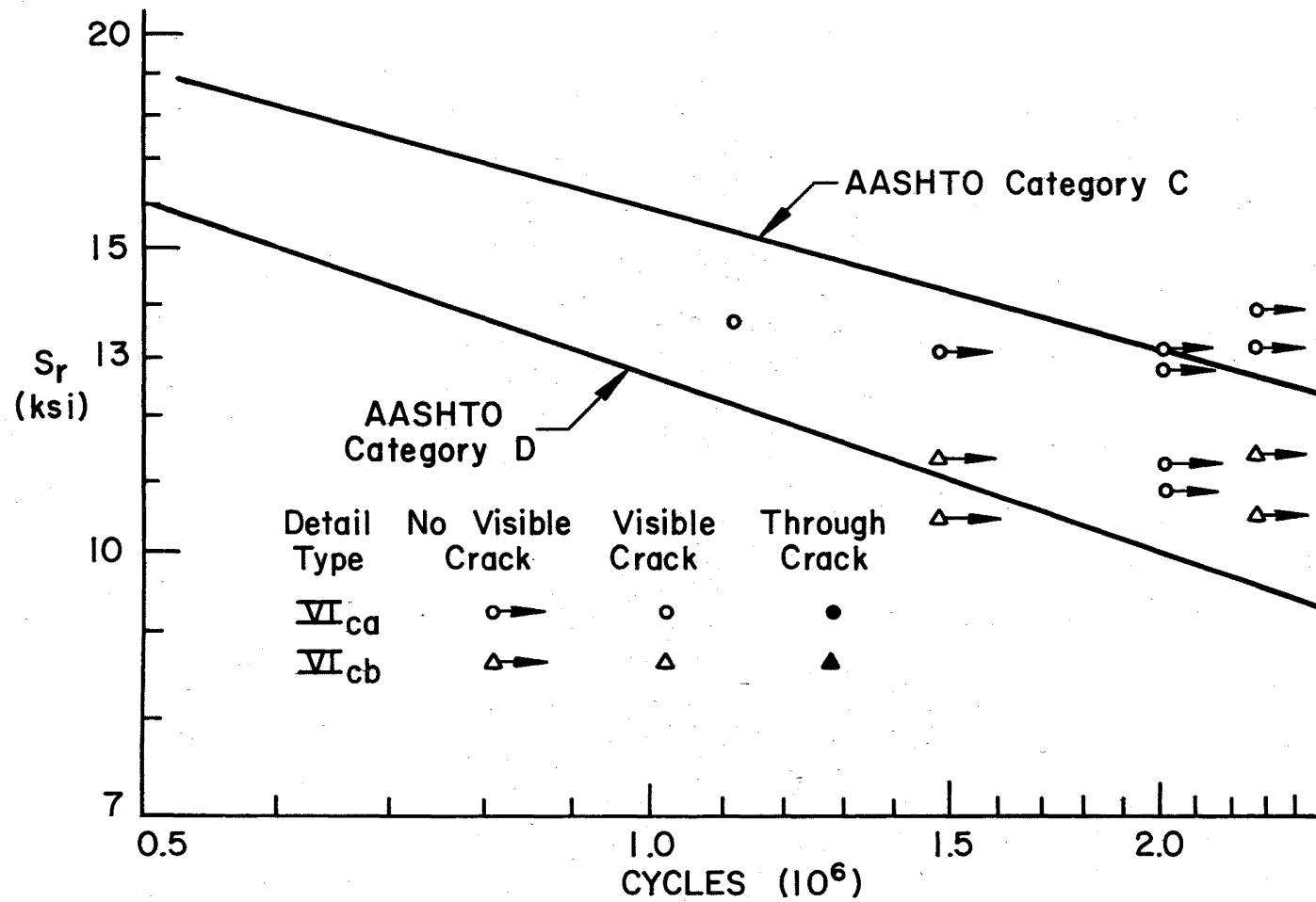


Fig. 73 Fatigue Results - Type VI_{ca} and VI_{cb} Details

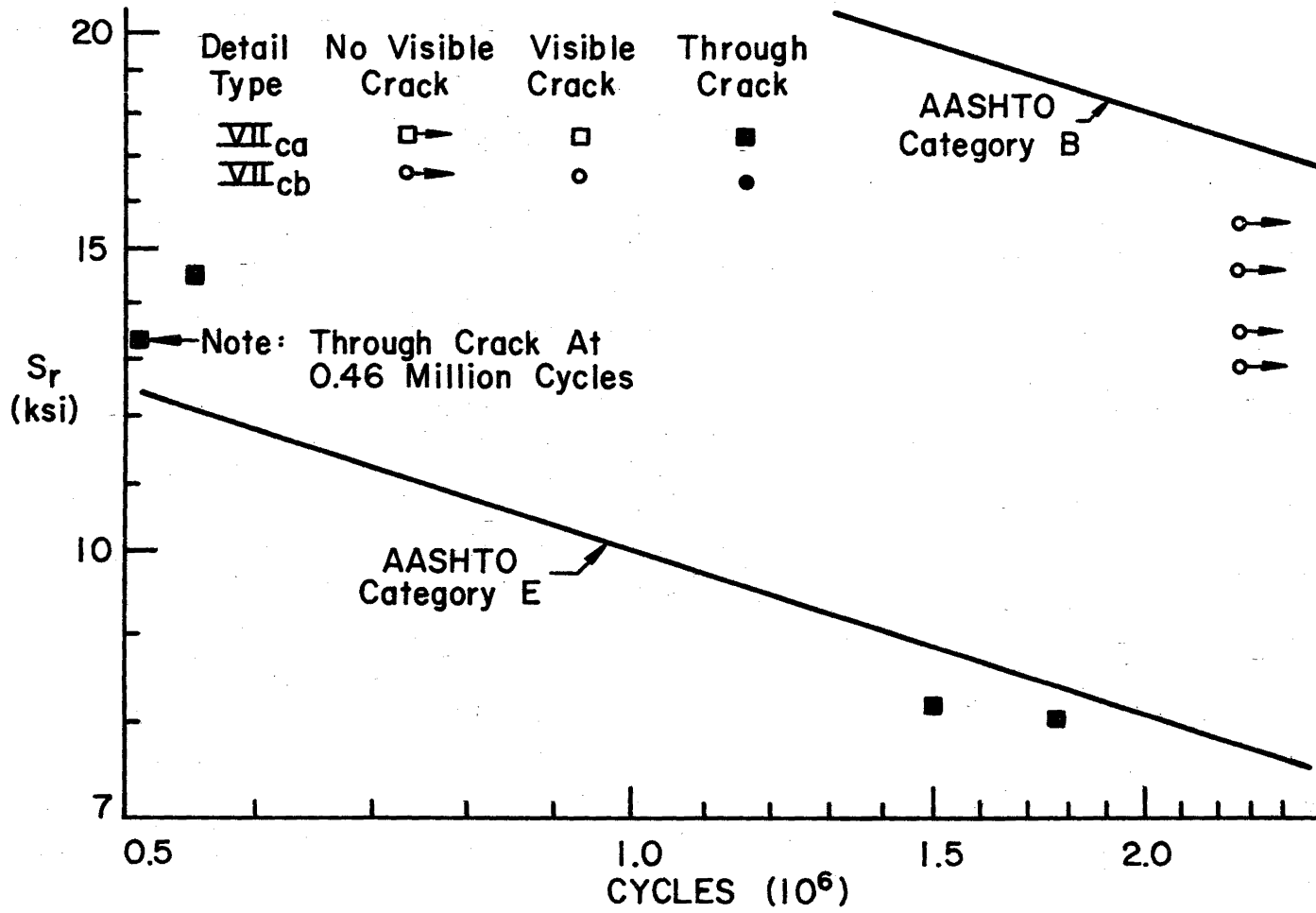


Fig. 74 Fatigue Results - Type VII_{ca} and VII_{cb} Details

All Type VII_{ca} details developed visible cracks prior to 83,400 cycles. These fatigue cracks began at the backup bar discontinuity. After growing through the tack weld across the backup bar discontinuity, the fatigue cracks progressed through the thickness of the flange as shallow surface flaws. Through cracks developed at 0.46 million to 1.76 million cycles due to nominal stress ranges from 14.5 to 8.0 ksi, respectively. As shown in Fig. 74 the observed fatigue strengths of two of the Type VII_{ca} details fall significantly below the AASHTO Category E design curve.

The results of the fatigue tests of the Type VII_{ca} details are consistent with the findings of a recent analytical study of the fatigue strength of discontinuous backup bar details.⁽¹⁶⁾ The backup bar discontinuity acts as a large initial flaw oriented perpendicular to the longitudinal tensile stress due to bending, thereby causing high stress concentration and sharply reducing the fatigue strength. Although further study is required to establish an appropriate lower-bound fatigue strength for discontinuous backup bar details, the information presently available indicates that such a lower bound falls significantly below the AASHTO Category E design curve. Classification of Type VII_{ca} details as a Category E detail is, therefore, inadequate. Until an appropriate detail classification can be established for discontinuous backup bar details, the most prudent approach is that adopted in the 1975 AWS Structural Welding Code which prohibits such details.⁽¹⁷⁾

None of the Type VII_{cb} details developed visible cracks after 2.27 million cycles under nominal stress ranges as high as 15.5 ksi. Because of the shift in the measured stress range profiles mentioned in Art. 4.2 none of the Type VII_{cb} details experienced stress ranges sufficiently high to reach the Category B design curve. However, all four Type VII_{cb} details exhibited fatigue strengths exceeding the AASHTO Category C design curve. The absence of any visible fatigue crack growth, coupled with the satisfactory performance of similar web-to-flange welds in previous tests on straight girders^(18,19) indicate that the Type VII_{cb} details would have demonstrated fatigue strengths comparable to the AASHTO Category B design curve.

7.1.8 Type VIII_c Details

The fatigue test results for six Type VIII_c details are shown in Fig. 75. The results for three other Type VIII_c details are not shown because the nominal stress ranges fall below 7.0 ksi. None of the Type VIII_c details tested developed visible or through-thickness cracks.

Due to the differences between the predicted and measured stress range profiles (Art. 4.2) the Type VIII_c details were subjected to low nominal stress ranges. Only one of the details tested experienced a stress range high enough to place the detail above the AASHTO Category D design curve. However, in view of the fact that none of the details tested exhibited any visible fatigue crack growth and considering the satisfactory performance of similar details in previous fatigue tests^(18,19) it is reasonable to assume that the Type VIII_c details tested meet the requirements for AASHTO Category D details.

7.2 Secondary Fatigue Crack Growth

The extensive damage sustained by Girder 3 after relatively few cycles points out the importance of secondary fatigue crack growth. Unfortunately, secondary fatigue crack growth is difficult to analyze or predict. However, several observations on the results of the fatigue tests can be made.

The severity of the secondary fatigue crack growth observed in the fatigue tests of Girder 3 can be attributed to three major factors: 1) the stiffness of the plate-type diaphragms relative to the distortional stiffness of the box girder, 2) the absence of welds connecting the diaphragms to the bottom flange at the load points and 3) inadequate provisions for developing the in-plane diaphragm forces so that these forces are not developed by web bending. With regard to cross-sectional distortion, the plate-type diaphragms are extremely stiff relative to the box girder cross section. Therefore, sizeable forces are generated in the diaphragms as the loads are distributed from the inner to the outer web. The magnitude of the forces in the diaphragms contributes to the formation of cracks in the diaphragm as well as in the web at the web-diaphragm connection. The absence of welds across the bottom of the diaphragms at the load points

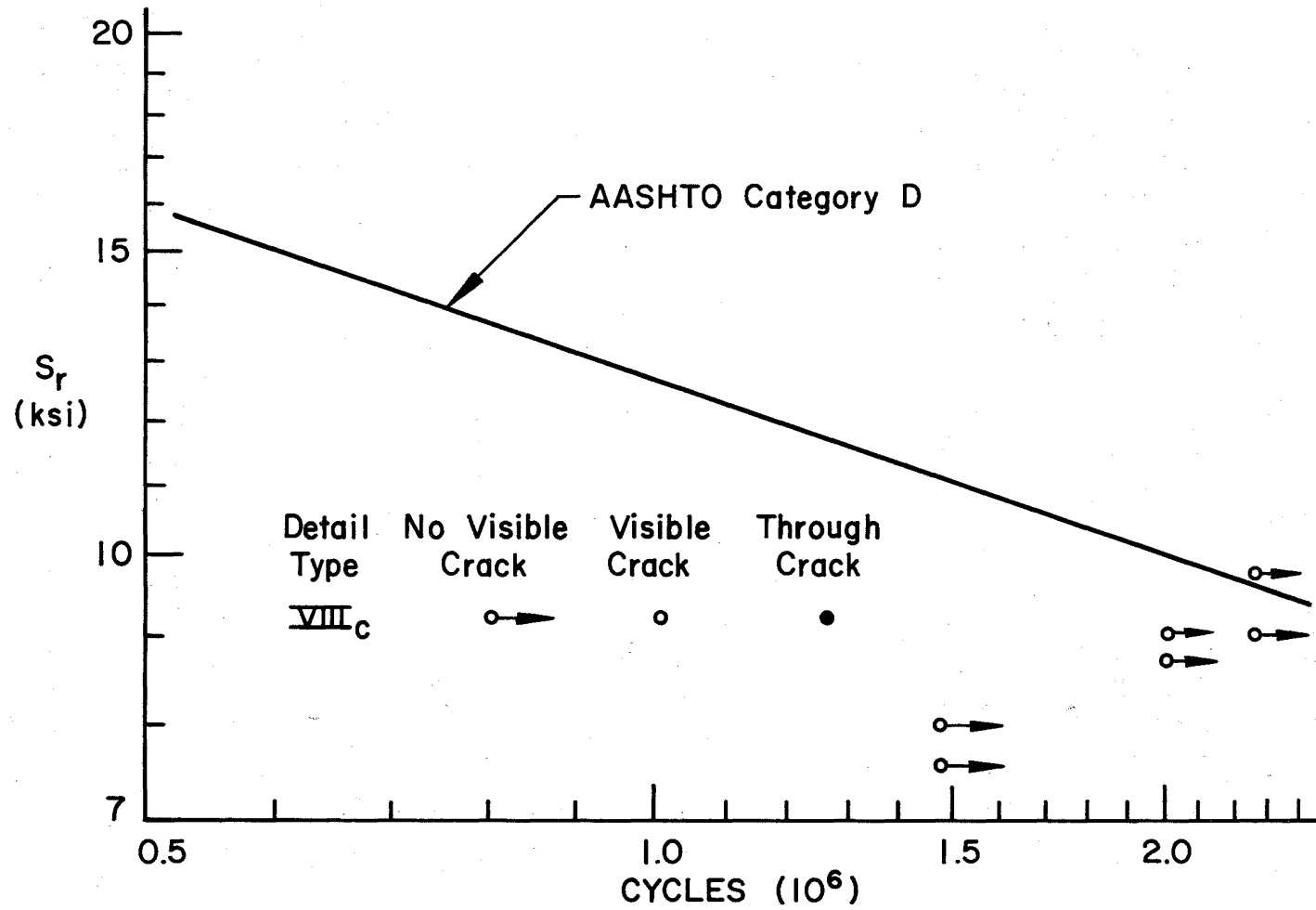


Fig. 75 Fatigue Results - Type VIII_c Details

aggravates the potential problem of fatigue crack growth from the cutout through which the longitudinal stiffener passes. If the diaphragm is welded to the bottom flange, forces can be transmitted across the cutout. Without the weld to the bottom flange, the diaphragm is inadequate in fatigue at the net section of the cutout. Also, if the transverse forces generated in the diaphragm are introduced into the top flange, the problem of the diaphragm punching through or tearing away from the web can be overcome as demonstrated by the modifications of Girders 1 and 2.

The damage done by secondary fatigue crack growth during the testing of Girders 1 and 3 demonstrates the difficulties of ensuring a fatigue resistant design of diaphragms. The manner in which the internal forces in the diaphragm are transmitted is difficult to analyze. The development of standard fatigue resistant diaphragm designs would be of great assistance.

It is important to note that the difficulties encountered with secondary fatigue crack growth are not due to the curvature of the girders per se. Secondary fatigue crack growth is an important consideration whenever transverse diaphragm forces and/or cross-sectional distortion are significant. Thus, these considerations apply to horizontally curved steel girder bridges as well as straight steel girder bridges under torsional loading.

8. SUMMARY AND CONCLUSIONS

The primary intent of this phase of the investigation of curved girder fatigue is to evaluate the fatigue performance of welded details on curved box girders. Eight types of AASHTO Category B, C, D and E welded details have been observed during the testing of three curved box girders. Each girder was subjected to approximately two million constant amplitude load cycles.

Based on the observation of primary and secondary fatigue crack growth the following conclusions are reached:

- (1) The fatigue behavior of AASHTO Category B, C, D, and E details, when placed on curved box girders, is adequately described by the present AASHTO design specifications for straight girders. Curvature, per se, does not significantly affect the applicability of these specifications.
- (2) The results of the fatigue testing program confirm the appropriateness of the classification of the following details in the AASHTO detail categories indicated:

- (a) Type I_{ca} and I_{cb} - Category C
- (b) Type II_c - Category C
- (c) Type III_{cb} - Category E
- (d) Type IV_{ca} and IV_{cb} - Category C
- (e) Type V_c - Category E
- (f) Type VI_{ca} - Category C
- (g) Type VII_{cb} - Category B
- (h) Type VIII_c - Category E

Detail Types III_{ca}, VI_{cb}, and VII_{ca} require further study as indicated in Chapter 9 to determine the appropriate detail categories.

- (3) The sensitivity of the fatigue strength of welded details to abnormally large initial flaw sizes was observed. Careful welding procedures and strict quality control are essential to the fabrication of fatigue-resistant steel bridges. Particular attention is required at Type IV_{ca} and IV_{cb} details if the transition is to be effective.
- (4) Special consideration needs to be given to the design of internal diaphragms. The manner in which in-plane diaphragm forces are transmitted to the box girder cross section determines the susceptibility of the girder to secondary displacement induced fatigue crack growth.

9. RECOMMENDATIONS FOR FURTHER STUDY

The results of the fatigue testing of three curved box girders indicates a need for additional study in the following areas:

- (1) Further study of detail Types III_{ca}, VI_{cb}, and VII_{ca} is required to firmly establish which detail categories are appropriate to these details.
- (2) The development of standard diaphragm designs or design guidelines which have a demonstrated resistance to secondary fatigue crack growth should be undertaken. Such a study should involve field studies of existing box girder bridges as well as extensive analytical and experimental study of the behavior of internal diaphragms in box girder bridges.

10. REFERENCES

1. Brennan, P. J.
ANALYSIS FOR STRESS AND DEFORMATION OF A HORIZONTALLY CURVED GIRDER BRIDGE THROUGH A GEOMETRIC STRUCTURAL MODEL, Syracuse University Report submitted to the New York State Department of Transportation, August 1970.
2. Culver, C.
DESIGN RECOMMENDATIONS FOR CURVED HIGHWAY BRIDGES, Carnegie-Mellon University Report submitted to the Pennsylvania Department of Transportation, June 1972.
3. Heins, C. P. and Siminou, J.
PRELIMINARY DESIGN OF CURVED GIRDER BRIDGES, AISC Engineering Journal, Vol. 7, No. 2, April 1970.
4. Heins, C. P.
DESIGN DATA FOR CURVED BRIDGES, C.E. Report No. 47, University of Maryland, March 1972.
5. U. S. Steel
ANALYSIS AND DESIGN OF HORIZONTALLY CURVED STEEL BRIDGE GIRDERS, United States Steel Structural Report ADUCO 91063, May 1963.
6. Colville, J.
SHEAR CONNECTOR STUDIES ON CURVED GIRDERS, C.E. Report No. 45, University of Maryland, February 1972.
7. CURT
TENTATIVE DESIGN SPECIFICATIONS FOR HORIZONTALLY CURVED HIGHWAY BRIDGES, Part of Final Report, Research Project HPR-2(111) "Horizontally Curved Highway Bridges," CURT, March 1975.
8. Daniels, J. Hartley, Zettlemoyer, N., Abraham, D. and Batcheler, R. P.
FATIGUE OF CURVED STEEL BRIDGE ELEMENTS - ANALYSIS AND DESIGN OF PLATE GIRDER AND BOX GIRDER TEST ASSEMBLIES, FHWA Report No. DOT-FH-11-8198.1, NTIS, Springfield, Va. 22161, August 1979.
9. AASHTO STANDARD SPECIFICATION FOR HIGHWAY BRIDGES, American Association of State Highway and Transportation Officials, Washington, D. C., 1977.
10. AASHTO INTERIM SPECIFICATIONS - BRIDGES, 1978 American Association of State Highway and Transportation Officials, Washington, D. C., 1978.
11. Bathe, K. J., Wilson, E. L. and Peterson, F. E.
SAP IV, A STRUCTURAL ANALYSIS PROGRAM FOR STATIC AND DYNAMIC RESPONSE OF LINEAR SYSTEMS, Earthquake Engineering Research Center Report No. EERC 73-11, University of California, Berkeley, Ca., June 1973, revised April 1974.

12. Kabir, A. F. and Scordelis, A. C.
COMPUTER PROGRAM FOR CURVED BRIDGES ON FLEXIBLE BENTS, Report No. UC SESM 74-10, University of California, Berkeley, Ca., September 1974.
13. Thurlimann, B. and Eney, W. J.
MODERN INSTALLATION FOR TESTING OF LARGE ASSEMBLIES UNDER STATIC AND FATIGUE LOADING, Proceedings, SESA, Vol. 16, No. 2, 1959.
14. Zettlemoyer, N.
STRESS CONCENTRATION AND FATIGUE OF WELDED DETAILS, Ph.D. Dissertation, Lehigh University, Bethlehem, Pa., October 1976.
15. Daniels, J. Hartley and Herbein, W. C.
FATIGUE OF CURVED STEEL BRIDGE ELEMENTS - FATIGUE TESTS OF CURVED PLATE GIRDER ASSEMBLIES, FHWA Report No. DOT-FH-11-8198.3, NTIS Springfield, Va. 22161, August 1979.
16. Batcheler, R. P.
THE FATIGUE STRENGTH OF DISCONTINUOUS BACKUP BAR DETAILS, M.S. Thesis, Lehigh University, Bethlehem, Pa., October 1977.
17. American Welding Society
AWS STRUCTURAL WELDING CODE, 1975.
18. Fisher, John W., Albrecht, P. A., Yen, B. T., Klingerman, D. T. and McNamee, B. M., FATIGUE STRENGTH OF STEEL BEAMS WITH WELDED STIFFENERS AND ATTACHMENTS, NCHRP Report No. 147, Transportation Research Board, National Research Council, Washington, D. C., 1974.
19. Fisher, John W., Frank, K. H., Hirt, M. A. and McNamee, B. M.
EFFECT OF WELDMENTS OF THE FATIGUE STRENGTH OF STEEL BEAMS, NCHRP Report No. 102, Highway Research Board, National Academy of Sciences, National Research Council, Washington, D. C., 1970.
20. Reemsnyder, H. S.
FATIGUE LIFE EXTENSION OF RIVETED CONNECTIONS, Journal of the Structural Division, ASCE, Vol. 101, No. ST12, December 1975.
21. Tada, H.
THE STRESS ANALYSIS OF CRACKS HANDBOOK, Del Research Corporation, Hellertown, Pa., 1973.

APPENDIX A: STATEMENT OF WORK

"Fatigue of Curved Steel Bridge Elements"

OBJECTIVE

The objectives of this investigation are: (1) to establish the fatigue behavior of horizontally curved steel plate and box girder highway bridges, (2) to develop fatigue design guides in the form of simplified equations or charts suitable for inclusion in the AASHTO Bridge Specifications, and (3) to establish the ultimate strength behavior of curved steel plate and box girder highway bridges.

DELINEATION OF TASKS

Task 1 - Analysis and Design of Large Scale Plate Girder and Box Girder Test Assemblies

Horizontally curved steel plate and box girder bridge designs will be classified on the basis of geometry (radius of curvature, span length, number of span, girders per span, diaphragm spacing, types of stiffener details, type of diaphragm, web slenderness ratios and loading conditions). This will be accomplished through available information from existing literature and other sources, as required.

Current research on the fatigue strength of straight girders has identified and classified those welded details susceptible to fatigue crack growth. This classification shall be extended to include critical welded details peculiar to curved open and closed girder bridges. These welded details shall be examined with respect to their susceptibility to fatigue crack growth and analyses shall be made to estimate the conditions for fatigue crack growth.

Based on the analyses described above, a selected number of representative open and closed section curved bridge girders shall be defined for purposes of performing in-depth analyses, design, and laboratory fatigue tests of large scale test assemblies. These girders shall be typical and will characterize commonly used girders, to include the use of welded details. The assemblies shall be analyzed and designed using currently available design guides, methods, and/or computer programs. Each test assembly shall be designed to incorporate the maximum number of

welded details susceptible to fatigue crack growth. Stresses in all components of the cross section shall be examined so that the significance of each stress condition can be evaluated. An assessment of the significance of flexural stress, principal stress, stress range and stress range gradient shall be determined at each welded detail. The significance of curved boundaries on the stresses shall be examined. Stress states in welded details equivalent to those used in straight girders shall be examined.

Curved plate and box girder test assemblies shall be designed so that ultimate strength tests can be carried out following the planned fatigue tests, with a minimum of modification.

Task 2 - Special Studies

In addition to but independent of the analyses and designs described in Task 1, certain other special studies shall be performed. These special studies are specifically directed towards those problems peculiar to curved girder bridges, as follows: (1) the significance of a fatigue crack growing across the width of a flange in the presence of a stress range gradient shall be studied, (2) the effect of heat curving on the residual stresses and fatigue strength of welded details shall be examined, (3) newly suggested web slenderness ratios for curved girder webs reduce present slenderness ratios of unstiffened webs. These slenderness ratios shall be examined in terms of fatigue performance of curved webs, and (4) the effect of internal diaphragms in box beam structures will be examined with regard to fatigue behavior.

Task 3 - Fatigue Tests of Curved Plate Girder and Box Girder Test Assemblies

The plate and box girder test assemblies designed in Task 1 shall be tested in fatigue. Emphasis shall be placed on simulating full-scale test conditions. The test results shall be correlated with the analyses made in Task 1 and the results of the special studies performed in Task 2.

Task 4 - Ultimate Load Tests of Curved Plate and Box Girder Assemblies

Following the fatigue tests of Task 3, each plate and box girder test assembly shall be tested statically to determine its ultimate strength

and mode of behavior. Fatigue cracks shall be repaired, where necessary, prior to the static tests. Consideration shall be given to providing a composite reinforced concrete slab on each test girder prior to the static tests.

Task 5 - Design Recommendations

Design recommendations for fatigue based on the analytical and experimental work shall be formulated in a manner consistent with that for straight girders. Specification provisions shall be formulated for presentation to the AASHTO Bridge Committee.

APPENDIX B: LIST OF REPORTS PRODUCED UNDER DOT-FH-11-8198

"Fatigue of Curved Steel Bridge Elements"

- Daniels, J. Hartley, Zettlemoyer, N., Abraham, D. and Batcheler, R. P.
ANALYSIS AND DESIGN OF PLATE GIRDER AND BOX GIRDER TEST ASSEMBLIES,
DOT-FH-11-8198.1, August 1979.
- Zettlemoyer, N., Fisher, John W., and Daniels, J. Hartley.
STRESS CONCENTRATION, STRESS RANGE GRADIENT AND PRINCIPAL STRESS
EFFECTS ON FATIGUE LIFE, DOT-FH-11-8198.2, August 1979.
- Daniels, J. Hartley and Herbein, W. D.
FATIGUE TESTS OF CURVED PLATE GIRDER ASSEMBLIES, DOT-FH-11-8198.3,
August 1979.
- Daniels, J. Hartley and Batcheler, R. P.
FATIGUE TESTS OF CURVED BOX GIRDERS, DOT-FH-11-8198.4, August 1979.
- Daniels, J. Hartley and Batcheler, R. P.
EFFECT OF HEAT CURVING ON THE FATIGUE STRENGTH OF PLATE GIRDERS,
DOT-FH-11-8198.5, August 1979.
- Daniels, J. Hartley, Abraham, D., and Yen, B. T.
EFFECT OF INTERNAL DIAPHRAGMS ON THE FATIGUE STRENGTH OF CURVED
BOX GIRDERS, DOT-FH-11-8198.6, August 1979.
- Daniels, J. Hartley, Fisher, T. A., Batcheler, R. P. and Maurer, J. K.
ULTIMATE STRENGTH TESTS OF CURVED PLATE AND BOX GIRDERS, DOT-FH-
11-8198.7, August 1979.
- Daniels, J. Hartley, Fisher, John W., and Yen, B. T.
DESIGN RECOMMENDATIONS FOR FATIGUE OF CURVED PLATE GIRDER AND BOX
GIRDER BRIDGES, DOT-FH-11 8198.8, August 1979.

APPENDIX C: FATIGUE CRACK REPAIR

The relationship of the fatigue life, N , of a given detail to the nominal stress range, S_r , can be written as:

$$N = A S_r^{-n}$$

where A = a coefficient which reflects the effects of material properties, detail geometry, expected initial flaw sizes, etc., and
 n = an exponent which is constant for the given material and environmental conditions.

Since n is generally taken as 3.0 for structural steels, the fatigue life, N , of a given detail is observed to be very sensitive to the nominal stress range, S_r .⁽¹⁹⁾

As explained in Art. 4.2, some welded details on the box girders experienced higher nominal stress ranges than anticipated. As a result, some details failed prior to the end of fatigue testing at approximately two million cycles. In order to permit continued fatigue testing to obtain fatigue data on all the other details on each girder it was necessary to repair the details that failed and ensure the integrity of each girder throughout the fatigue tests. Thus the authors had an excellent opportunity to study fatigue crack repair first-hand.

Most fatigue cracks that required repair developed as through-thickness cracks due to primary fatigue crack growth (see Art. 6.1). Although the repair of these cracks was complicated by the difficulty of access to the interior of the box girder, several methods were used to repair these cracks as described below.

One of the first methods used was to drill $\frac{1}{2}$ inch to $\frac{3}{4}$ inch holes at the crack tips and weld a small coverplate over the cracked section. Such repairs can be difficult because of the necessity of making overhead welds on the bottom flange of the girders. However, weld quality was not observed to be a problem. Cracks at the weld toe of the coverplate were observed to occur after less than 150,000 cycles at a nominal stress range

of 14.6 ksi. The fatigue strength of the coverplate repairs, thus fell far below the fatigue strength of a Category E detail. The poor performance of this repair method is attributed primarily to the increased compliance of the cracked flange section beneath the coverplate. In a normal coverplated detail, the flange and coverplate "share" the stresses at the coverplated section. However, at the coverplated repair, the coverplate carries virtually all of the stresses at the section due to the presence of the fatigue crack in the flange. The increased stress transfer into the coverplate therefore causes increased stress concentration at the toe of the transverse weld, leading to premature failure of the repair. Thus, the welded coverplate repair was observed to be essentially ineffective.

Another method of fatigue crack repair consisted merely of drilling $\frac{1}{2}$ inch to $\frac{3}{4}$ inch holes at the crack tips as shown in Fig. 41. This method was employed in the final stages of a fatigue test when it was only necessary to prevent a through crack from growing larger for an additional 100,000 to 200,000 cycles under relatively low stress ranges. The effectiveness of this method is very sensitive to the care with which the holes are drilled. Nicks or burrs on the drilled surface often provide a site for renewed fatigue crack growth, rendering the repair useless. Careful grinding and polishing of the drilled surface improves the effectiveness of this repair method. Premature failures of repairs made in this manner were most often attributed to drilling the holes behind the crack tip. Recommended procedure is to drill the holes slightly ahead of the crack tips. Due to back-surface and stress concentration effects at the hole, the fatigue crack will generally grow into the hole. In spite of these precautions, this method is unreliable in arresting a through-thickness crack, and virtually useless in arresting large fatigue cracks subject to high stress ranges.

An improvement on the preceding method provides one of the simplest and most effective repair procedures. In this method $1-1/16$ " diameter holes were drilled at the crack tips which were found using the cleaning fluid and 10X magnifying glass as described in Art. 5.2. Then 1" diameter high-strength A325 bolts were installed in the holes and tightened $\frac{1}{2}$ turn past the snug condition. The local influence of the bolt prevents renewed

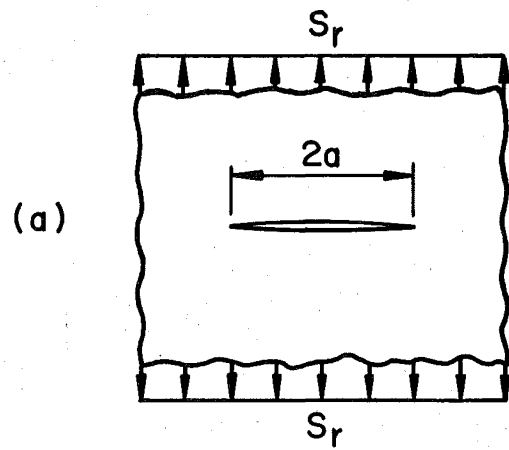
fatigue crack growth past the hole. The effectiveness of a similar procedure was demonstrated by Reemsnyder in Ref. 20.

This procedure was used extensively to repair through-thickness cracks in the webs and bottom flange of the box girders. None of the fatigue cracks repaired in this manner exhibited renewed fatigue crack growth prior to the end of testing. An example of the effectiveness of this procedure is the Type IV_{ca} detail at location i on Girder 1 (Fig. 44). A through-thickness crack was discovered at 701,000 cycles due to a measured nominal stress range of 16.9 ksi. The crack was repaired by drilling and bolting the crack tips which occurred on each side of the stiffener. The crack was arrested under the bolt heads and no renewed fatigue crack growth was observed even at 2.02 million cycles, the end of testing.

The effectiveness of installing high-strength bolts at the crack tips can be demonstrated by reference to available analytical solutions for the range of the stress intensity, ΔK . An approximate analytical solution for ΔK can be obtained by superposition of the crack tip stress solutions shown in Fig. C1. Figure C1(a) shows a through-thickness crack in an infinite plate subjected to a uniform stress and the corresponding solution for ΔK . Figure C1(b) shows a through-thickness crack with a uniform crack surface traction, p , distributed over a portion of the crack length.⁽²¹⁾ By superposition of these two solutions the reduced range of the stress intensity can be approximated as shown in Fig. C1(c).

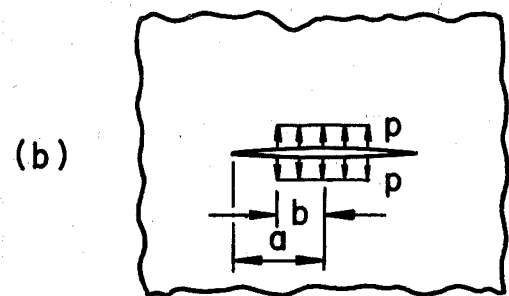
For example, consider a through-thickness crack, 3 inches long ($a = 1.5$ in), in an infinite plate subjected to a stress range of 15 ksi. The corresponding range of the stress intensity is 32.6 ksi/ $\sqrt{\text{in}}$. The suggested repair of this fatigue crack consists of drilling 13/16 inch diameter holes located as shown in Fig. C2 and installing 3/4" diameter A325 high strength bolts. Locating the edge of the holes at the crack tips as shown, ensures that the bolts will be fully effective in reducing ΔK . The bolts are installed by the turn-of-the-nut procedure.

Friction beneath the head and nut of the high-strength bolts generates the normal and friction forces shown in Fig. C3. These forces



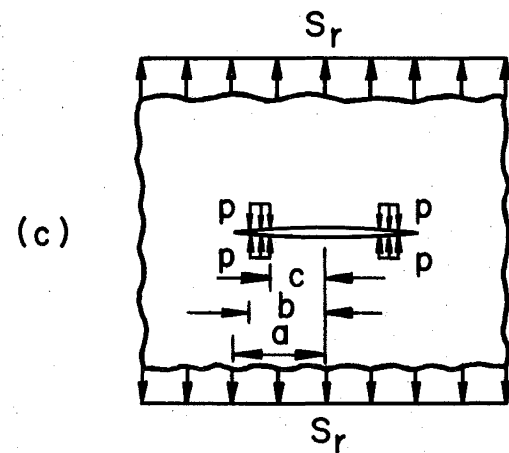
$$\Delta K = S_r \sqrt{\pi a}$$

From Ref. 21



$$K = 2/\pi p (\sin^{-1} b/a) \sqrt{\pi a}$$

From Ref. 21



$$\Delta K = \left[S_r + 2p/\pi (\sin^{-1} c/a - \sin^{-1} b/a) \right] \sqrt{\pi a}$$

Fig. C1 Crack Tip Stress Solutions

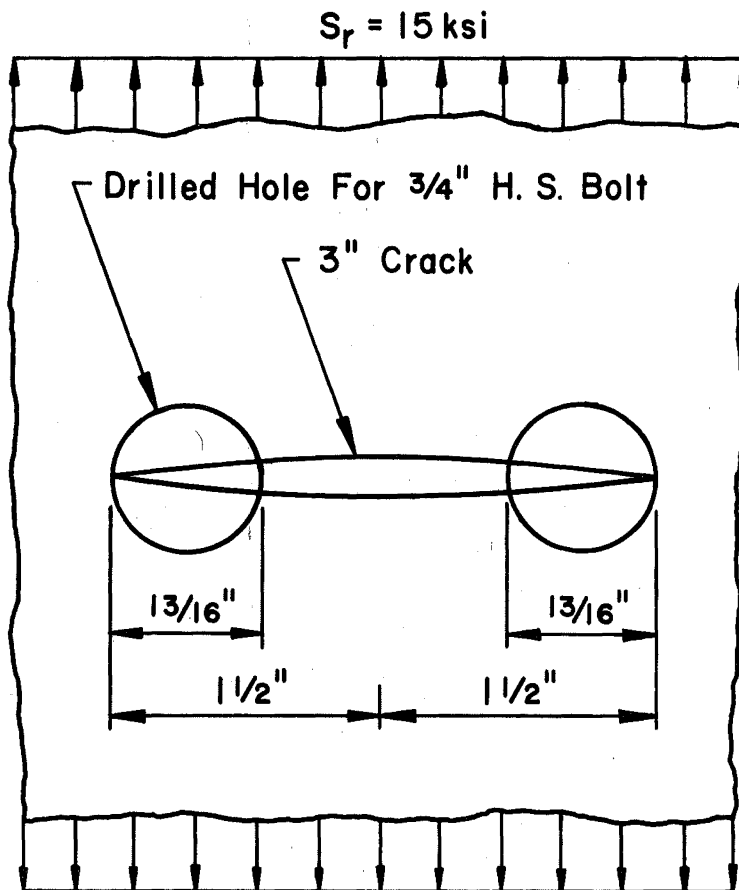


Fig. C2 Fatigue Crack Repair by Drilling Holes at Ends of Fatigue Crack and Bolting

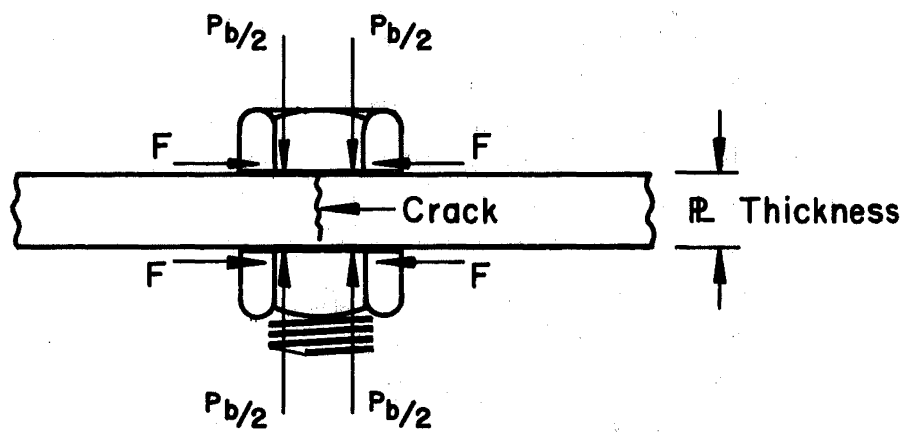


Fig. C3 Normal and Frictional Forces Developed
Beneath the Head and Nut of a Bolt

tend to resist the crack opening displacements. For a 3/4" diameter A325 bolt, the crack closing force, P, is equal to 6.63 K/Bolt. Distributing the crack closing force, P, over the width of the bolt head across the flats and the thickness of the plate, t, results in a uniform crack surface traction, p, equal to 14.1 ksi. The solution for the range of the stress intensity shown in Fig. C1(c) then yields a ΔK equal to 8.5 ksi $\sqrt{\text{in}}$. Thus, the repair of the fatigue crack results in a 74% reduction in the range of the stress intensity for the given fatigue crack and stress conditions.

Consideration of the approximate analytical solution shown in Fig. C1(c) provides insight into the effect of various parameters on the effectiveness of the above repair procedure. Bolt diameter, grade of bolt, plate thickness, and the nominal stress range at the fatigue crack are factors which must be considered in the development of proper repair procedures based on this method.

The final repair procedure that was used consisted of drilling 1/2" to 3/4" holes at the crack tips and also installing a bolted splice plate across the fatigue crack (Fig. 42). The splice plate was sized several inches wider than the length of the fatigue crack and was of similar thickness to the flange. The bolted connection was designed to develop the maximum dead load plus live load stresses as a friction connection. Thus, the stress range acting on the crack surface is transferred through the splice plate, allowing the holes drilled at the crack tips to arrest the fatigue crack. This procedure was used extensively to repair through-thickness cracks in the bottom flange near interior diaphragms. Only one of these repairs exhibited renewed fatigue crack growth prior to the end of testing. The failure of that particular repair was attributed to cutting oil that was inadvertently left on the faying surfaces of the bolted splice, demonstrating the need for careful supervision and inspection of repair procedures. If properly designed and installed, bolted splice repairs can be counted upon to develop fatigue strengths equivalent to AASHTO Category B. (19)

The complexity of secondary fatigue crack growth makes it possible to prescribe specific repair procedures. Effective repair of secondary

fatigue crack growth can only be achieved through experience, intuition and careful analysis. The repairs described in Art. 6.2 and 7.2 were effective in maintaining the integrity of the box girders. From these results a few general conclusions can be drawn. First, extreme caution must be exercised in the introduction of out-of-plane forces into thin plates. Second, careful analysis of the diaphragm members themselves for their adequacy under the transverse forces generated by torsional loadings is required.

FEDERALLY COORDINATED PROGRAM OF HIGHWAY RESEARCH AND DEVELOPMENT (FCP)

The Offices of Research and Development of the Federal Highway Administration are responsible for a broad program of research with resources including its own staff, contract programs, and a Federal-Aid program which is conducted by or through the State highway departments and which also finances the National Cooperative Highway Research Program managed by the Transportation Research Board. The Federally Coordinated Program of Highway Research and Development (FCP) is a carefully selected group of projects aimed at urgent, national problems, which concentrates these resources on these problems to obtain timely solutions. Virtually all of the available funds and staff resources are a part of the FCP, together with as much of the Federal-aid research funds of the States and the NCHRP resources as the States agree to devote to these projects.*

FCP Category Descriptions

1. Improved Highway Design and Operation for Safety

Safety R&D addresses problems connected with the responsibilities of the Federal Highway Administration under the Highway Safety Act and includes investigation of appropriate design standards, roadside hardware, signing, and physical and scientific data for the formulation of improved safety regulations.

2. Reduction of Traffic Congestion and Improved Operational Efficiency

Traffic R&D is concerned with increasing the operational efficiency of existing highways by advancing technology, by improving designs for existing as well as new facilities, and by keeping the demand-capacity relationship in better balance through traffic management techniques such as bus and carpool preferential treatment, motorist information, and rerouting of traffic.

3. Environmental Considerations in Highway Design, Location, Construction, and Operation

Environmental R&D is directed toward identifying and evaluating highway elements which affect the quality of the human environment. The ultimate goals are reduction of adverse highway and traffic impacts, and protection and enhancement of the environment.

4. Improved Materials Utilization and Durability

Materials R&D is concerned with expanding the knowledge of materials properties and technology to fully utilize available naturally occurring materials, to develop extender or substitute materials for materials in short supply, and to devise procedures for converting industrial and other wastes into useful highway products. These activities are all directed toward the common goals of lowering the cost of highway construction and extending the period of maintenance-free operation.

5. Improved Design to Reduce Costs, Extend Life Expectancy, and Insure Structural Safety

Structural R&D is concerned with furthering the latest technological advances in structural designs, fabrication processes, and construction techniques, to provide safe, efficient highways at reasonable cost.

6. Prototype Development and Implementation of Research

This category is concerned with developing and transferring research and technology into practice, or, as it has been commonly identified, "technology transfer."

7. Improved Technology for Highway Maintenance

Maintenance R&D objectives include the development and application of new technology to improve management, to augment the utilization of resources, and to increase operational efficiency and safety in the maintenance of highway facilities.

* The complete 7-volume official statement of the FCP is available from the National Technical Information Service (NTIS), Springfield, Virginia 22161 (Order No. PB 242057, price \$45 postpaid). Single copies of the introductory volume are obtainable without charge from Program Analysis (HRD-2), Offices of Research and Development, Federal Highway Administration, Washington, D.C. 20590.

